A Thesis Submitted for the Degree of PhD at the University of Warwick

http://go.warwick.ac.uk/wrap/35750

Zirconia Toughened Ceramics

by

Markys G. Cain, B.Sc.

For submission to the

degree of Doctor of Philosophy

University of Warwick

Department of Physics

October 1990

I would like to dedicate this thesis
to my mother and father & wltrlsfmgc

ABSTRACT

The objectives for the thesis were to generate tough ceramics utilising the toughening mechanisms inherent to zirconia materials. The aims have been realised with the successful fabrication of hot pressed silicon nitride / zirconia composite ceramics. The zirconia was prestabilised with two different types of dopant additives, yttria and ceria, with the intention of understanding the chemical compatibility with the silicon nitride matrix and the overall effect on the subsequent mechanical properties. The volume fraction of added zirconia was also varied. The increased toughness over silicon nitride materials alone was attributed to the toughening agents inherent to zirconia which existed either in the form of the tetragonal polymorph or the monoclinic variant. The toughening modes were dependent on initial chemistry of the composite system. When the zirconia was prestabilised with yttria the tetragonal polymorph was retained within the composite. The enhanced toughness was attributed to a transformation toughening mechanism. However, when the zirconia was prestabilised with ceria the depletion of Ce from solid solution with the zirconia during processing resulted in the formation of the unstabilised monoclinic variant. The enhanced toughness was attributed, in this case, to a microcrack type energy absorption mechanism, similar to several ZTA composite ceramics.

Additionally, an experiment using ultrasound non-destructive testing, indicated that Tetragonal Zirconia Polycrystals (TZP) is ferroelastic and, as such, can provide a significant contribution to enhanced levels of fracture toughness in these materials or composites containing the same. Further work has been conducted to actually observe, as a function of applied uniaxial stress, the crystallographic changes occurring within the *bulk* of a 3Y-TZP ceramic via neutron elastic scattering at the ILL, Grenoble, France. This experiment has provided clear direct proof of the ferroelastic nature of zirconia. A similar experiment will be carried out at the Rutherford Laboratory, though with significantly improved statistics.

An approach to improve the high temperature properties of TZP via the chemical alteration of the grain boundary phase was also considered. As a preliminary step the grain boundary volume was increased through controlled additions of the grain boundary composition in the form of both a premilled and a premelted glass. Poor fired densities were attained, however, due to the solute additive partitioning from the generation of an enhanced grain boundary phase to overstabilisation of the zirconia resulting in the formation of cubic stabilised zirconia. Furthermore, the incorporation of nitrogen within the grain boundary phase, via sintering TZP with sole additions of AlN, resulted in the attainment of poor fired densities and hence was not considered a suitable method for grain boundary modification.

Contents

Acknowledgements

Although many people were involved in the completion of this thesis, it remains for me to thank those who contributed a great amount, either professionally or personally. Much thanks are due to Mike Lewis who has provided some clear and professional help and who has also become a good working colleague. As much thanks are clearly due to many of the research technicians, notably Gerald Smith and Steve York for their continuing help, encouragement and skill in electron microscopy and much more. Similarly, the help given by Pat Beecraft in his workshop has been invaluable as have Danny Lee, Bob Lamb and Harold Mathers. Many good times were had with my working friends, notably Ian Tuersley and John Fernie and it would be most improper not to thank Paul Thompson for the pipe soldering and computing help! I would also like to acknowledge the help given by Stan Jones and Colin Norman of Alcan Chemicals Ltd throughout the duration of this research and to the Science and Engineering Research Council who helped to fund the programme.

During the completion of the thesis my mother tragically died and I thank Rebecca Stewart for her incredible support through the most difficult times. Her love, compassion and drive has helped me more than she thinks. I finally thank my mother and father, brothers and sister for their immense encouragement always given. My mother was perhaps the single most person who gave me such optimism and willpower to succeed, which I hope I have done.

DECLARATION

This dissertation is submitted to the University of Warwick in support of my application for admission to the degree of Doctor of Philosophy. It is an account of my work carried out in the Department of Physics, University of Warwick during the period October 1986 to November 1989 and, except where specifically acknowledged in the text, is a result of my own independent research. No part of this thesis has been submitted in respect of a degree to this or any other university.

Markys G Cain

OCTOBER 1990 Markys G Cain

Chapter 1

Introduction and Objectives

1.1 Materials Selection for High Temperature Application

The requirement for advanced materials, with particular applications within the aerospace and automotive industry, has provided the research impetus for advanced ceramic materials during the past twenty or so years .

Ceramics can be classified within three categories; Traditional Ceramics, Structural Engineering Ceramics and Electro-Ceramics. The first group are commonly formed from 'fired' and glazed natural silicate minerals and form the oldest known class of materials. The second category, the subject of this thesis, constitutes a class of materials that may possess a combination of properties which include high strength up to elevated temperatures, dimensional stability and good erosion and corrosion behaviour, high hardness, high elastic modulus, low density and generally a low coefficient of friction. The third category form a family of electronic materials, which possess novel electronic, piezoelectric, dielectric, ionic, ferroelectric and ferromagnetic properties, e.g. materials such as Strontium Titanate and Barium Titanate typify ferroic ceramic materials which find many applications within the electronics industry.

Presently, one of the key objectives in advanced structural ceramic research is in the deployment of the materials within energy - conversion systems, such as the Advanced Gas Turbine (AGT) or the Turbo Compound Diesel Engine [1,2] and the turbo-petrol engine. Such applications are considered because of unique properties possessed by certain ceramics. For instance, the ability of ceramic materials to operate at much higher temperatures than metals eliminates the forced cooling necessary in conventional metal or superalloy engines currently operating at between 900-1000°C. The use of ceramics translates into a greater engine thermodynamic efficiency with a resultant decrease in specific fuel consumption. Research indicates [3] that engines fabricated with major ceramic components can be as much as 50% more efficient compared with present engine technology . Further advantages, attributable to increases in operating temperature, are a progressively lower exhaust emission, through burning the fuel more efficiently, and additional benefits afforded by multifuel engines [2,4].

Many ceramics have a lower density than most metals which confers a lower moment of inertia. This is an important factor in material selection for high performance, high rotational speed engines e.g. automotive turbochargers. In contrast to metals, the increased resistance at high temperatures to creep, oxidation, corrosion, erosion and wear, as well as being better thermal insulators, are further attributes considered to be of crucial importance to heat engine and other applications.

An equally important application for which ceramic materials are ideally suited in the much higher general temperatures envisaged is that required for wear parts; e.g. within engines, bearings, pumps etc. The specific properties required for such applications may include high hardness, high toughness, low coefficient of friction, chemical inertness, high strength and low thermal expansion coefficient. Lubrication media required for ceramic wear components, however, has received little attention [5] and the tribological properties possessed by ceramics are not yet fully understood.

Further examples of possible applications for ceramic components include heat exchangers, for which long term high temperature corrosion resistant materials are needed, preferably in the form of an open cell honeycomb structure (e.g. aerogels) and as coatings, whereby some of the advantages conferred by ceramics are used to provide barriers to either high temperatures or chemical attack or both. In the latter example, the key properties which would dictate the success of coatings are the interfacial bonding strength, the coefficient of linear thermal expansion and adhesive qualities between coating and substrate. The use of ceramics within the medical field has steadily increased over the past 15 years [5]. Clearly the important properties required for applications such as hip-joint prostheses, bone plates, artificial tendons etc. are chemical compatibility, long wear life and high strength.

1.2 Contenders for High Stress/High Temperature Applications and High Temperature Limitations

Ceramic materials which offer the most promise for incorporation within gas turbine, jet, rocket and automobile engines are based on SiC, Si_3N_4 and ZrO_2 monolithics and more recently on dispersion and fibre reinforced composite structures based on the same materials.

Table 1 : Monolithic Ceramic Comparison Table

MAX. OP. TEMP./°C	TYPE	COMPOSITION	MICROSTRUCTURE	MECH. PROP.'S		SOME COMMERCIAL APPLICATIONS
				MOR MPa	K_{1C} MPam$^{1/2}$	
1300	1) Si_3N_4 SSN (Sintered Silicon Nitride)	6% Y_2O_3 + variable $Al_2O_3 + AlN$. 6%Y_2O_3	5-10% crystalline matrix + β'"SYALON" β' Si_3N_4 + glass	500 - 800	5-8	Tool Tips Heat engine components. Wear parts Seals, bearings.
> 1500	2)SiC SSiC (Sintered SiC)	0.5-1% B + C or Al + C additives	αSiC + up to 30% Intergranular residue with Al/Al_2O_3 additions or βSiC.	400 - 600	3-5	Engine Rotors/ turbines (as for Si_3N_4). Heating elements.
	3)ZrO_2					
800	a) TZP (Tetragonal Zirconia Polycrystal)	2-4% Y_2O_3 Sintered 1350-1500°C	Fine Grained, fully tetragonal polycrystal.	1000 - 2500	7-12	Valve faces/seats Liners,Piston caps.Refrac.'s Heat eng. components.
900	b)PSZ (Partially Stabilised	8-10%MgO/CeO/Y_2O_3 Sintered 1650-1850°C Ht. Treat. 1100-1450°C	Tet. ZrO_2 precipitates in Cubic matrix.	600-800	6-8	Thermal barriers solid Elect. Oxy. sensors
1000	c)ZTA (Zirconia Toughened Alumina)	$Al_2O_3 + ZrO_2$ (tet. or mono.) Composite	Dispersed Tet. ZrO_2 in Al_2O_3 matrix Or Duplex Structures	500 - 2500	5-8	As TZP/PSZ
2100	d)CSZ (Cubic Stabilised Zirconia)	Fully Stabilised Cubic Zirconia	Coarse Grained cubic ZrO_2 10-100μm	200	3	Ceramic glazes colours Gemstones

Examples of advanced structural engineering ceramics are found in Table 1, together with some relevant microstructural features and a number of possible commercial applications [6,7].

It is unfortunate that, within the 1000-1400°C operating regime, severe problems are encountered in using ceramic components under stress, especially in oxidising or corrosive environments. The discovery that zirconia can exhibit strengths and values of fracture toughness at low to intermediate temperatures (<1000°C), which were far superior to any known ceramic material led to them being labelled as the ceramic analogue of steel [8]. The mechanisms responsible for the impressive properties are based on a phenomenon known as transformation toughening. Essentially, this involves the ability of a particular metastable crystalline phase of zirconia to transform to a stable phase in the vicinity of a propagating crack. This action absorbs energy from the crack front thereby contributing to the materials toughness (see chapter 3). There is an intrinsic limit, however, set by the temperature, at which transformation toughening will no longer contribute to the materials' toughness. Typically, this temperature is about 900°C, (see chapter 3). In addition to an enhanced toughness, zirconia based ceramics also possess a low thermal conductivity and have a similar thermal expansion coefficient with metallic alloys. These properties are presently being exploited in advanced adiabatic engines (engines with minimal heat loss during the thermodynamic process) where coatings of zirconia have been successfully applied onto cylinder walls, exhaust manifolds etc., acting as thermal insulating barriers.

Monolithic ceramics based on silicon nitride and silicon carbide are presently the main contenders for high temperature applications (>1000°C). In many ways this is due to a combination of properties including high modulus, hardness, resistance to time dependent deformation when stressed at high temperature (creep deformation resistance), low thermal expansion and hence a good thermal shock resistance and an inherent oxidation resistance (see chapter 4). These properties are intrinsic to the major phases βSi_3N_4 or the substituted 'Sialon' derivatives ($\beta' Si_{3-x}Al_xO_xN_{4-x}$) and either the hexagonal α SiC or cubic β SiC. Basically, silicon nitride is di-phasic, consisting of silicon nitride crystalline grains surrounded by an intergranular bonding phase. It is generally accepted that the limitations for high temperature use are dictated by the quantity and type of this intergranular second phase [9,1,6] which softens at high temperatures and contributes to the deformation processes observed in these and also in certain zirconia toughened ceramics. Currently, research is directed towards either the elimination of this second phase or devitrification of the intergranular glassy phase via a chemical alloying approach typified by the β' sialons (see chapter 4).

The mechanical properties of the above monolithic ceramics can be enhanced through the incorporation of particulate, fibrous or whisker second phase reinforcements. This set of ceramics are known generally as composite ceramics. The fundamental reasoning behind these materials is based on the premise that one or more components may be incorporated within a matrix to realise a synergistic improvement in properties, thereby creating an improved material. In many instances, the incorporation of fibres or whiskers within a matrix has yielded composites with enhanced values of fracture toughness compared to the matrix alone. The mechanisms responsible for the observed properties are dependent on the type of reinforcement. For example, in fibre reinforced composites, crack deflection around the high modulus fibre and fibre pull-out at the onset of composite failure, are considered to be mainly responsible for the increased levels of fracture toughness. The long term high temperature stability of this class of material and, additionally, the difficulty in material consolidation (or densification) represents some of the major limitations presently encountered.

1.3 Research Objectives

A broad objective of the research described here has been to design, fabricate and evaluate Advanced Structural Engineering Ceramics, ultimately for high temperature application, incorporating the toughening concepts inherent to many zirconia ceramics.

To fulfill this general aim, outlined above, two different approaches have been adopted. It will become clear that both strategies are complementary each possessing the same ultimate aims, that is; the attainment of a tough high temperature material possessing high strength, resistance to corrosion and long term stability coupled with an ease of fabrication. To meet these aims the following two strategies represent the majority of the work conducted in this thesis, and are further exemplified at the end of chapter 3:

1 . to improve the fracture toughness of a silicon nitride ceramic monolith (with inherently good high temperature properties) via the incorporation of zirconia toughening agents.

2. to improve the properties of transformation toughened zirconia ceramic monolith to higher temperatures, via modifications to its grain boundary intergranular phase.

Additionally, the objectives of the thesis embody: the correlation of microstructural analysis with mechanical properties; to understand any toughening mechanisms applicable to either strategies outlined above; to determine the stability of the systems at high temperatures and the limiting factors with regard to high temperature application. Furthermore, the physics and crystallography of a ferroic transition particular to zirconia, are investigated in a novel way arising from concurrent observations of the crystallography and mechanical properties of both TZP monolithic ceramics and the composite systems studied.

The following two chapters will survey the development of the silicon nitride and zirconia family of ceramics and will expand on and clarify the limitations observed in these materials. The detailed design strategies will be set out at the end of chapter 3, with subsequent chapters concerned with the experimental techniques, results and discussion.

Chapter 2

Silicon Nitride Based Ceramics

The monolithic ceramics based on the silicon nitride family are presently the major contenders for high temperature (> 1000°C) applications. The crystal structure and covalent bonding of the 'silicon' based ceramics confers a combination of properties including hardness, good creep resistance, high modulus, low thermal expansion and so a high thermal shock resistance. Additionally, the protective SiO_2 surface film that forms on the ceramic whilst in an oxidising environment, confers a good resistance to oxidation. The above properties are realised by the major phases βSi_3N_4 or the 'substituted' Sialon derivatives. The precise material properties are dictated by the differences in the microstructures, which is governed by the fabrication processes. Table 2.1 illustrates the range of Si_3N_4 - based ceramics, identified by acronyms frequently used in the literature [6].

Table 2.1: Si_3N_4 - based Ceramics

Major phase : normally βSi_3N_4 or substituted-derivative
β' ($Si_{3-x}Al_xO_xN_{4-x}$)

TYPE	COMPOSITION	SOURCES	MICROSTRUCTURE
HPSN or HIPSN	1% MgO additive 2-5% Y_2O_3 additive	Norton NC132 Battelle - USA	0-3% mainly glassy intergranular residue
SSN	5% MgO + 9% Al_2O_3 6% Y_2O_3 + variable Al_2O_3/AlN 6% Y_2O_3	Kyocera SN205 Lucas-Cookson-Syalon 101/102 GTE PY6	5-10 % glassy or crystalline matrix + β' β Si_3N_4 + glass
RBSN	Nitriding of Si during sintering without additives	Norton NC350 AED "Nitrasil"	60-90% αSi_3N_4 10-40% βSi_3N_4 5% Si 15-30% porosity
SRBSN	Similar to RBSN, followed by high temperature sinter (with additives)		Similar to SSN

2.1 Material Consolidation - Sintering

A major microstructural problem exists, however, in the development of a fully dense polycrystalline solid with strong intergranular bonding. The relatively slow solid state self-diffusion rates in covalent solids, such as Si_3N_4, dictates that full density must be obtained via an alternative densification mechanism. In Si_3N_4 the mechanism hinges on a minor silicate liquid phase, present at the sintering temperature, which surrounds the silicon nitride grains. The liquid sintering catalyst is generated by a reaction of an added impurity metallic oxide (e.g. MgO, Y_2O_3) with an accidental surface (SiO_2) layer present on the precursor $\alpha - Si_3N_4$ grains, from which the final $\beta - Si_3N_4$ grains evolve.

α and $\beta - Si_3N_4$ have similar crystal structures based on SiN_4 tetrahedral units, both having hexagonal symmetry with similar unit cell **a** parameters but with $c_\alpha \sim 2c_\beta$ [10]. The liquid phase sintering mechanism can be summarised by the following three stages of densification;

(i) particle rearrangement in the presence of the first formed liquid with relatively rapid kinetics, dependent on liquid volume, viscosity, particle size, etc.

(ii) solution of α with the simultaneous reprecipitation of $\beta - Si_3N_4$ which is diffusion or reaction controlled.

(iii) solid state diffusion to remove remaining closed porosity and any remaining liquid.

The above three stages of densification should not be confused with the classical Kingery formulation [11] which described the second stage as a solution and reprecipitation occurring at the point of contact between two crystallites with no subsequent change in the crystal polymorph. The situation is very different in the case of silicon nitride. The mechanism responsible for the attainment of densification is due to the chemical driving force between α and β and not the contact dissolution arising from contact stresses between two crystallites [12].

The sintering reaction and microstructural evolution is shown schematically in figure 2.1 [13]. The hot pressed silicon nitride is a monophase ceramic with a small residual liquid volume. The pressureless sintered ceramic has a larger liquid volume cooling to the glassy state as a semicontinuous matrix for the β' crystals.

The application of stress to achieve full density (e.g. hot pressing) coupled with the presence of the residual silicate grain boundary phases imposes severe fabri-

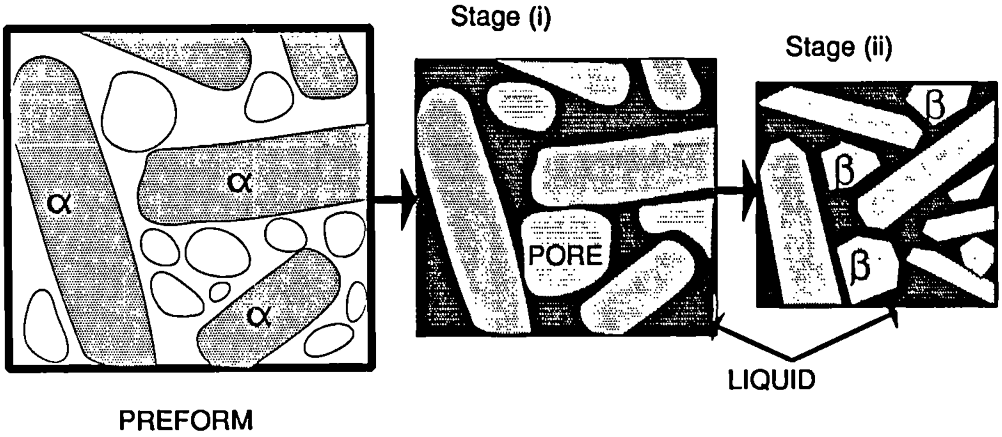

Figure 2.1: Schematic illustrating the idealised liquid phase sintering mechanism proposed by Lewis via particle rearrangement with accompanying $\alpha - \beta$ solution-reprecipitation

cation disadvantages and inevitable high temperature property degradation. This dichotomy in the requirement of a liquid phase to promote densification and in the restriction imposed by the residual grain boundary phase on the high temperature properties has been, to a large extent, resolved using the sialon ceramic alloying concept.

2.2 The development of Si-Al-O-N alloys

Several routes to improve the high temperature properties have been studied. Richerson [14] determined the detrimental effects of impurity atoms (such as calcium) within the ceramic on the fracture strength at elevated temperatures. The strength decreased as a function of impurity concentration at a temperature of 1375°C. The most dramatic change in high temperature properties, however, has been achieved by controlling the amount of impurity surface SiO_2 available for liquid formation. This is based on the joint discovery by Jack and Wilson [15] and Oyama and Kamigaito [16] that O^{2-} may be substituted for N^{3-} in the $\beta - Si_3N_4$ structure providing that Al^{3+} is simultaneously substituted for Si^{4+} to maintain charge neutrality. The solid solution, β', has the general composition $Si_{3-x}Al_xO_xN_{4-x}$ with $x \geq 2$. The further addition of MgO as a sintering aid has resulted in a ceramic with a density approaching that of the theoretical limit. A transient liquid formed during the sintering, based on a Mg-Si-Al-oxynitride has been successfully removed by the addition of AlN which has the effect of 'balancing' any excess SiO_2 present on the surface of the Si_3N_4.

Yttria has been shown to be an ideal hot pressing additive [9,17] for silicon nitride, since it forms a liquid phase below the hot pressing temperature which allows rapid sintering and, as the pressing temperature increases, when densification is complete, these phases react with more silicon nitride to produce a highly refractory bonding phase. A β' 'SYALON' ceramic is fabricated from mixtures of the terminal components via an overall reaction : [18]

$$\alpha Si_3N_4 + SiO_2(surface) + Y_2O_3 + (Al_2O_3 + AlN) \rightarrow \beta' Si_{3-x}Al_xO_xN_{4-x}$$
$$+ Y - Si - Al - O - N(liquid)$$

The AlN is normally added as one of *the near-neighbour polytypoids* [13,18] *and* is used as a sensitive control of O/N ratio, substitution level (x) in β' and hence of the O/N ratio in the final liquid phase [18]. Lewis reasons [18] that the key to a successful high temperature silicon nitride ceramic is to maximise the N/O ratio in the final liquid. This has the overall effect of increasing the liquid viscosity and, more importantly, controls the liquid crystallisation products. If a high nitrogen AlN polytypoid is used in the sintering process, partial matrix crystallisation may occur during normal process cooling, otherwise the matrix remains in its glassy state. The primary crystallisation product is based on the compound Yttrium Aluminium Garnet $(3Y_2O_3 - 5Al_2O_3)$ - YAG. Crystallisation is promoted by an increased polytypoid content [13] and full matrix crystallisation may be induced by heat treatments at between 1200°C and 1400°C [19]. Syalons with a lower polytypoid content either do not crystallise their matrix phase at all during heat treatment, or contain additional phases such as yttrium-disilicate [13]. The attainment of a bi-phase β' + YAG Syalon ceramic is therefore dependent on both a high nitrogen content and high purity of the interstitial sintering liquid [18].

2.3 Property Limitations

2.3.1 High Temperature Mechanical Limitations

Engineering applications of the Si-based ceramics are limited by their relatively low fracture toughness (typically $K_{1c} \sim 3-8MPam^{1/2}$) and modulus of rupture (MOR). Additionally, the large spread in the absolute values of measured properties such as fracture toughness and MOR (e.g. synonymous with a low Weibull modulus) associated with failure from the dominant flaw, dictates the maximum applied stress that these materials should encounter, which is well below their mean values. High temperature mechanical properties are dependent on the choice of terminal components, the particular fabrication route and resulting microstructure of the material. For the hot pressed Sialons, the high temperature ceiling is limited by creep deformation processes occurring at ~1100°C. The creep damage proceeds via the nucleation of cavities within the intergranular phase followed by the subsequent growth and coalescence to form critical cracks which ultimately lead to specimen failure [20]. The cavities are almost invariably nucleated within glassy pockets located at triple grain junctions and form by the process of grain boundary sliding [21]. The cavities nucleate at sites within the grain boundary phase such as impurities, dislocations and ledges, vapour bubbles etc. It follows that cavitation increases with an increase in volume fraction of intergranular glassy phase, with a decrease in glass viscosity and with increasing glass impurity concentration.

The absence of creep cavitation (≤1500°C) in thermally treated hot pressed sialons was directly linked to the successful removal of these triple junction glass residues [10]. The pressureless sintered β'-YAG Syalons, distinguished by their enhanced liquid volume and fully crystalline second phase, do not exhibit creep cavitation. The mechanism responsible for the creep deformation of these ceramics is considered to arise from the high temperature diffusional transport of matter along grain boundaries acting in parallel with $\beta - \beta$ grain boundary sliding, the rate controlling mechanism being diffusional (Coble) creep. This deformation process ($\beta' - \beta'$ grain boundary sliding) is synonomous to the superplastic flow deformation in metallic alloys and Tetragonal Zirconia Polycrystalline ceramics, chapter 3.

In summary, the particular creep mechanism in β' ceramics will depend on applied stress, temperature and residual glass volume. However, three main regions of creep behaviour have been identified: [18]

1. In bi-phase β' / glass ceramics, at high temperatures and low stresses, there is a free viscous flow of the grain boundary glass phase, without cavity nucleation.

2. In hot-pressed monophase ceramics with grain boundary residues or where

matrix crystallisation is incomplete in β' ceramics, the hydrostatic stresses in assymetric glassy pockets, due to β'-β' grain boundary sliding, initiates cavity nucleation. The coalescence of such cavities along with grain boundary sliding contributes to the creep strain.

3. Ceramics having complete matrix crystallisation, or in ideally monophase materials, exhibit Coble creep; that is interfacial or grain boundary diffusion being the dominant rate-controlling mechanism.

An additional and equally inhibiting high temperature degradation, exhibited by all the silicon nitride range of alloys, is sub-critical crack growth. At stress intensities, K_1, which are less than the critical stress intensity, K_{1c}, sub-critical crack growth can occur, whereby flaws present within the material may extend at applied stress levels below the materials fracture strength. Several mechanisms responsible for such failure in ceramics include dominant crack extension via coupled diffusion of material away from the crack tip when the material is stressed to relatively high levels, or at high temperatures and low stresses, the material can fail by sub-critical flaws extending into damaged regions of the ceramic. These damaged zones typically consist of an accumulation of cavities generated via a stress induced grain boundary sliding mechanism, described above.

2.3.2 High Temperature Environmental Limitations

The oxidation of single phase sialon alloys is comparatively slow and is controlled by the viscosity of the silicate residues which, in turn, is controlled by the out-diffusion of impurity metallic ions from grain boundaries to the oxidation film [18]. The oxidation rate, therefore, becomes self-limiting when the grain boundaries have been depleted of impurities. Clearly, materials with a larger grain boundary glass volume, which provide a large reservoir and easy path for metallic ions, will exhibit comparatively large oxidation rates [19]. The bi-phase Syalons exhibit low oxidation rates at temperatures below ~1300°C comparable with hot pressed β' ceramics, but at higher temperatures exhibit comparatively short term failure in an oxidising environment due to a reversion of the near-surface YAG to the liquid state assisted by SiO_2 enrichment. The development of bi-phase β'-YAG ceramics, with the YAG sited in isolation rather than forming a semi-continuous matrix, has resulted in enhanced oxidation properties up to temperatures of ~1400°C [23].

2.4 Limitations and Solutions

The most significant problems affecting the silicon nitride range of alloys, outlined above, are their low levels of fracture toughness and limited thermal stability at high temperatures. A promising solution to the former is one of particulate reinforcement using the toughening modes attributable to the zirconia range of alloys, but without loss of the inherent high temperature properties characteristic of the nitride. Furthermore, it has been shown that additions of zirconia to silicon nitride improves high temperature stability by creating a more refractory grain boundary phase (see chapter 5), and additionally the zirconia-silicon nitride couple can exist in thermodynamic equilibrium by judicious control of the chemistry. The following chapter reviews the zirconia family of materials, the toughening modes characteristic of zirconia and finally an outline of the objectives of the research is given in more detail.

Chapter 3

Zirconia Based Ceramics

The toughening mechanisms responsible for the impressive strengths and fracture toughness of zirconia ceramics represents one of the most active areas of ceramic research currently undertaken, and has been labelled a major 'scientific revolution' [24]. The following sections present a survey of the crystallography and the toughening mechanisms applicable to this class of ceramic.

3.1 Crystal structure and Polymorphism

Zirconia (ZrO_2) is polymorphic and exhibits three well defined crystallographic phases [25], monoclinic, tetragonal and cubic. (A high pressure orthorhombic form has also been shown to exist [26]). Figure 3.1 identifies the three polymorphic stability temperatures and Table 3.1 summarises the crystallographic data for

CRYSTAL STRUCTURE	Monoclinic		Tetragonal		Cubic
SPACE GROUP	$P2_1/c$ C_{2h}^5		$P4_2/nmc$ D_{4h}^{15}		Fm3m O_h^5
LATTICE PARAMETERS	a=5.142Å b=5.206Å β=99°18' (30°C)		a_t=3.653Å c=5.293Å (1393°C)		a=5.272Å (2400°C)
ORDER (No. of molecules in unit cell)	4		2		1
T_c (heating) (cooling)		1150°C 900°C		2370°C 2355°C	
DENSITY	5830kgm^{-3}		6100kgm^{-3}		6090kgm^{-3}

Table 3.1: Crystal Structure Data for Zirconia [32,37,38,112,113,114]

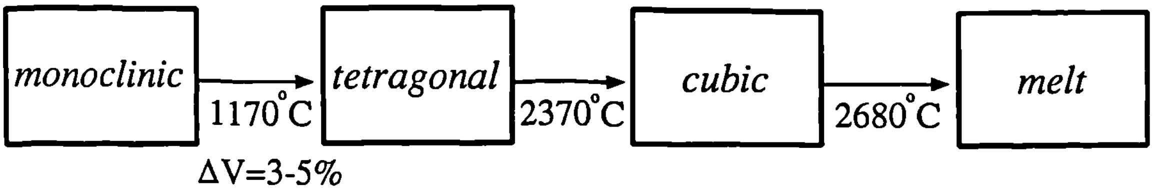

Figure 3.1: Polymorphic Transitions in Zirconia

the three structures. (N.B. the data in Table 3.1 is representative only for the un-alloyed ZrO_2; when alloyed - e.g. with Yttria or Magnesia - then the lattice dimensions will change according to the concentration and type of doping).

The large volume change associated with the tetragonal to monoclinic transformation, indicated in figure 3.1, prohibits the refractory properties of pure Zirconia from being used in structural applications. Complete 'stabilisation' can be accomplished, however, with the addition of an appropriate additive such as Calcia, Yttria, Ceria or Magnesia acting as solid-solution dopants. If sufficient stabilising additive is used then the cubic form of Zirconia (CSZ - Cubic Stabilised Zirconia) can be retained indefinitely at room temperature. This 'subset' of Zirconia ceramics is generally referred to as 'Fully Stabilised Zirconia'. If less stabilising oxide is added then a 'Partially Stabilised Zirconia' (PSZ) is the result. PSZ consists of two or more intimately mixed phases, usually the cubic major dispersed phase and tetragonal minor dispersed phase which represent the toughest of the PSZ materials. Finally, if the precise amount of stabilising additive is used and, furthermore, the zirconia grain size is of a sufficiently small and critical size, then a 100% tetragonal (TZP - Tetragonal Zirconia Polycrystalline) zirconia ceramic can be produced, existing in a metastable state at room temperature. The phase diagram reproduced in Figure 3.2 (a) further clarifies these microstructural distinctions [27]; the dopant levels required for different oxide additives being determined using the phase diagrams in figures 3.2 (b) & 3.2 (c).

3.2 Polymorph Stabilisation

Two types of transformation occur in zirconia, depending on the temperature [28];

- @ T>1500K ionic diffusion of O^{2-} and Zr^{4+} allows diffusion controlled transformations, the normal phase equilibria being functions of temperature and composition as in the phase diagram.
- @ T<1500K cationic diffusion is sluggish and transformations occur via a diffusionless route or in a martensitic fashion. i.e., parent and product have the same composition.

The stabilisation mechanisms pertaining to zirconia can be best rationalised by the defect structure of doped zirconia. In cubic zirconia, the dopant ions (M^{2+} or

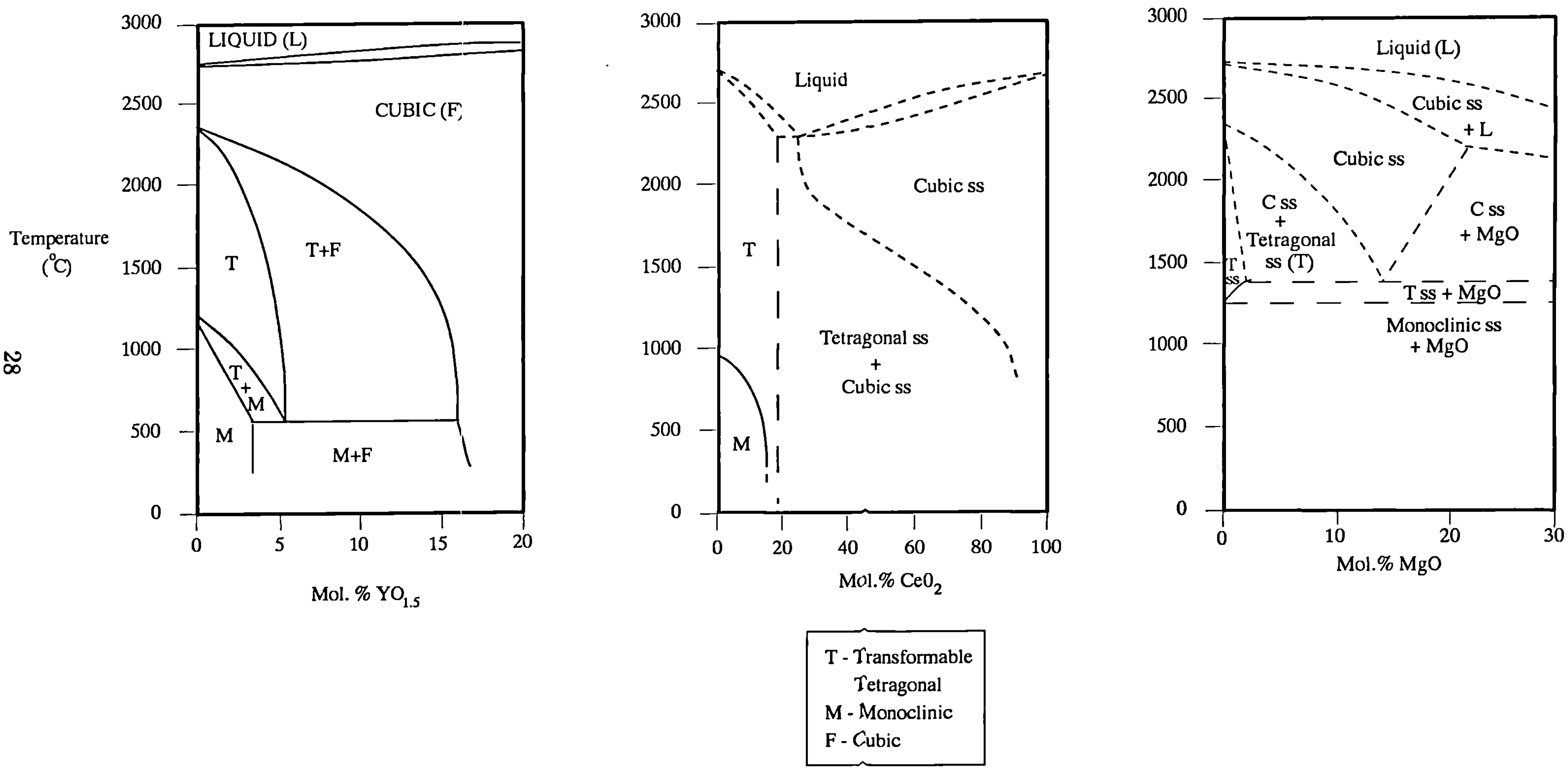

Figure 3.2: Phase Diagram[27] of (a) Yttria-, (b) Ceria- and (c) Magnesia-Zirconia System

M^{3+}) replace Zr^{4+} ions with the simultaneous generation of O^{2-} ion vacancies (V_o''), [1] e.g.;

$$MO \rightarrow M_{Zr}'' + V_o'' + O_o \tag{3.1}$$

$$M_2O_3 \rightarrow 2M_{Zr}''' + V_o'' + 3O_o \tag{3.2}$$

The dopant ions and O vacancies are randomly distributed on the crystal lattice sites, e.g. on the sub fcc lattice of Zr ions and on the sub cubic (tetrahedral sites in fcc) lattice of O ions respectively. The mechanisms responsible for the successive stability of the cubic and tetragonal ZrO_2 are, however, not clearly understood and a very brief review now follows, highlighting the essential features of the instabilities and the resulting phase transitions observed.

On simple thermodynamic arguments the cubic phase is stabilised by the extension of its transformation temperature to lower temperatures via the addition of certain oxide dopants. When the dopant concentration within the zirconia is low ($x < x_c$, where x_c is the critical amount to fully stabilise the cubic phase) the dopant ions are isolated from one another or they form discrete finite clusters, thereby stabilising only small regions of the volume. When the dopant amount exceeds the

---

[1] Using the standard Kroger-Vink notation

critical value x_c then the dopant ions can form an 'infinite cluster' in the fcc lattice and hence fully stabilise the volume. Percolation theory (the theory of species moving through another - e.g. transport theory) has shown [29] that the critical value x_c is mainly dependent on the lattice constant and ionic radii for a certain dopant. The resulting volume fraction v_{cp} of stabilised cubic phase *for a given dopant level* was found to depend on geometrical parameters such as the variance and the mean of the grain size, i.e. a fine and uniform grain size assisted in the formation of the stabilised cubic ZrO_2 phase (this follows from observing that a grain will fall within the stabilised cubic phase field when the spatial extent of the stabilising clusters exceeds that grain size). The stabilisation of tetragonal ZrO_2 is also dependent on mean grain size and amount and type of dopant (see following section).

The electronic structures of c- and t- zirconia have recently been calculated [30]. During the c-t transformation, displacements of the O anions from their ideal fluorite positions were observed to induce large changes in the subsequent electronic structure. This led to a resulting decrease in the ionicity of the tetragonal structure with respect to the cubic phase. Morinaga concluded that the tetragonal polymorph was more stable than the cubic phase due to the increased covalency of the tetragonal bonding between the shorter of the 2 Zr-O bonds. The anion displacements associated with the cubic-tetragonal transformation resulted in an *increase* in the band gap energy between the Zr-4d and O-2p bands further substantiating the overall enhanced stability of the tetragonal phase compared with the cubic polymorph. It was argued that cubic zirconia was not a particularly stable crystalline form (probably due to the small cation/anion ionic radius ratio [31]) and hence will readily react with other certain elements (oxide dopants) thereby inducing stability.

3.2.1 Cubic-Tetragonal Transformation

The cubic - tetragonal (c-t) transition has recently been theoretically investigated by Negita [32] and can be summarised as follows:

- O^{2-} ion displacements from their ideal fluorite position (as in the case of cubic doped zirconia).
- occurrence of cell doubling - (the c-axis of the tetragonal cell is parallel to the c-axis of the c-polymorph but the periodicity changes from a/2 in the cubic case to a in the tetragonal).
- the tetragonal transformation is improper ferroelastic, i.e. the c-t transformation is accompanied by spontaneous volume and shear strains.

Negita concluded that the condensation of a particular phonon mode at the cubic Brillouin zone boundary was responsible for the change of space group, primitive cell and atomic positions associated with the cubic-tetragonal phase transition.

The ferroelastic nature of tetragonal zirconia has been the subject of much debate very recently [33,32,Chapter7] and will be introduced in this section. Ferroic transitions can best be described with reference to the change in symmetry between the parent phase and product phase. For a transition to be ferroic there must be a change in the point group symmetry and, possibly, an accompanying change in translation. Additionally, the transition is accompanied by a spontaneous component for polar tensors of different ranks, e.g. strain (a tensor of rank2). A pure ferroelastic material will thus be characterised by (1) a change in the crystal system and (2) the generation of a spontaneous macroscopic strain. The ferroelastic transition can be considered to be the mechanical analogue of the ferromagnetic transition, since it is possible to generate in it a stress-strain hysteresis loop, see Chapter 7 [34]. Other characteristic properties of ferroelastic transitions are the appearance of a domain structure within the transformed crystals and the occurrence of a pronounced anomaly, at the transition, in certain elastic constants of the material [34]. The latter characteristic, i.e. the anomalous behaviour in certain elastic constants at the transition, subdivides ferroelastic materials into two further sub-groups. The two situations encountered are described by either a *vanishing* of an elastic constant, proper ferroic transitions, or a *moderate discontinuity* of this quantity where the transition is known as improper ferroic. During a proper ferroic transition each unit cell undergoes identical atomic displacements which results in the onset of a non-zero spontaneous polarization.

There is clearly only one type of cooperative displacive movement of ions, all in the same direction and all having identical values. The case for improper ferroics is distinguished by the occurrence, at the transition, of 2 or more energetically equivalent displacement states. In all cases of improper ferroelastic materials studied to date, the transition has resulted in a doubling of the unit cell and the generation of a spontaneous polarization/orientation through an indirect coupling of the atomic displacements (arising from the ferroic transformation) with the rest of the unit cell. Furthermore, the equivalence of the stable displacement states, should give rise to the formation of anti-phase domain boundaries [34] within the grains of the material; e.g. in ferroelectric materials the equivalent boundaries are the familiar domains. The displacive cubic-tetragonal transformation in zirconia has been investigated [35,36] and was characterised by the observation of anti-phase domain boundaries in the transformed phase, which is compatible with an improper ferroelastic transition in zirconia. The ferroelastic nature of zirconia is experimentally investigated and discussed in relation to its possible beneficial effects on certain mechanical properties in Chapter 7 and additionally in the paper affixed in the rear of the thesis.

3.2.2 The Martensitic Tetragonal-Monoclinic Phase Transformation

Many of the characteristics of martensitic transformations in metallic alloys can be applied to the tetragonal-monoclinic transformation in zirconia [37,28,38,39,40].

- the transformation is military, i.e. the tetragonal-monoclinic transition is diffusionless and takes place via a cooperative movement of many atoms by a shear mechanism, with a velocity approaching that of sound through the material. The transformation is not associated with any compositional change.
- the martensitic transformation is a first order transition (i.e. the parent and product coexist as the transformation proceeds) and is generally accompanied by a shape change with a definite orientation relationship (frequently with non-rational indices) between the parent phase and the product. Presence of a habit plane, common to both parent and product, is a feature associated with any transformation including the martensitic transformations and is observed in the t-m transformation in zirconia. Structural accommodation between the parent and product occurs via twinning of the martensite whilst maintaining an undistorted habit plane.
- the shear component of the transformation and the associated dilation are accompanied by an overall increase in the strain energy of the system.

- the transformation is athermal in nature (e.g. independent of time, cf. isothermal), this means that a further change of temperature is required to advance the transformation. The strain energy so produced inhibits further transformation (or via additional restraining factors such as grain boundaries, other martensite plates etc.) until a further change of temperature occurs.

- a temperature hysteresis is observed between the martensite start and reverse transformation. This can be explained by assuming that the strain involved in accommodating a monoclinic domain in a tetragonal matrix is not the same as that for a tetragonal domain in a monoclinic matrix [41,42].

Further characteristics of the tetragonal - monoclinic transformation in bulk zirconia include the effect of the particle size on the probability of transformation and on the control of solid solution alloying oxide level on the transformation temperature. The transformation is retarded by reducing the grain size (see section 3.3), and the t-m transformation temperature reduced with increasing alloying level. Furthermore the *stability* at any particular temperature is sensitive to the height of the activation hill separating the two polymorphs which is determined by factors such as stabilisation content in solid solution with the zirconia. The retention of the metastable tetragonal polymorph contained within a polycrystalline body is classically described by analysing the magnitude of the *strain energy* arising from the elastic *constraint* imposed by the surrounding grains on shape and volume changes associated with the t-m transition. The constraint can arise from the anisotropic strain fields of surrounding grains in a polycrystalline material or similarly by a second phase material, such as alumina in Zirconia Toughened Alumina (see section 3.4.2). Mechanisms which can relieve some of this strain energy such as microcracking or twinning can affect the overall retention of the metastable tetragonal zirconia. The grain size effect on the thermodynamics of transformation has been successfully described [43] by analysing the changes in surface energy as the transformation proceeds. The three surface related mechanisms - twinning, microcracking and a combination of these two - which can relieve some of the strain energy associated with the t-m transformation, introduces a size dependent energy term into the total free-energy change associated with the tetragonal and monoclinic transformation. This describes the grain size effect for the retention of metastable tetragonal zirconia.

The *transformation kinetics* of the t-m transformation has also been described by the growth of pre-existing, precursor nuclei [28]. It was postulated that, for a given driving force, the probability of a grain transforming was dependent on the probability that it contained an <u>effective</u> nucleus. It was assumed that a statistical number of nuclei were distributed within a volume of the material and that the probability that a grain contained an effective nucleus was, thus, dependent on its volume and hence particle size. Therefore, grains below a critical size which do not contain an effective nucleus retained the tetragonal structure. This result leads to the particle size effect, as described above, for the retention of the high temperature tetragonal polymorph at successively lower temperatures. Although the exact nature of these nuclei is unknown, it was considered to consist of an intermediate structure of the two phases (t & m) formed by dislocation arrays, stacking faults or other faulted structures [44]. The transformation to the less coherent monoclinic stable polymorph results in a higher surface energy but a lower strain energy thereby reducing the overall strain energy of the system.

3.3 Transformation Toughening

The common feature that ceramic materials exhibit is their brittle behaviour. When presented with a particular design requirement, engineers must, above all, be able to rely on their choice of material, such that, the finished product has a well defined reliability. The **distribution** of fracture stresses, around the mean fracture stress, gives information about the reliability of the material, which is characterised by the dimensionless Weibull modulus eg. see reference 45 for critical analysis. It follows from the Weibull expressions, that an increasing Weibull modulus signifies a decrease in the dispersion of the fracture stress about the mean value. This then, translates into a higher reliability for the material. With these values concerning material reliability available, the engineer can design with the confidence that the materials he will choose will not fail under the stresses that his design will impose. Typical values of the Weibull modulus for Si_3N_4 ceramics are about 10 - 15, whereas, for some zirconia ceramics values in excess of 30 have been reported [46]. This seemingly excellent reliability, is directly linked to the toughening phenomena associated with Zirconia ceramics, due to the materials' inherent flaw tolerance.

In an article entitled 'Ceramic Steel' [8], Garvie, Hannink and Pascoe described a new ceramic consisting of a dispersion of *metastable* tetragonal precipitates in a matrix of cubic zirconia. They found that the strength of such a material was approximately three times that of the monoclinic - cubic zirconias. The increase in the strength was attributed to an increase in the work of fracture. This was believed to be a result of the martensitic (change in volume) transformation of zirconia from tetragonal to monoclinic symmetry in the stress field of a propagating crack. The change in volume of the zirconia precipitates, due to the transformation, will absorb some of the strain energy associated with the stress field surrounding the crack tip. The toughness of the material is, therefore, increased since additional energy would be required for the crack to propagate. The authors considered the tough PSZ's to be a ceramic analogue of steel due to the many features common to both systems - i.e. three allotropes, martensitic transformations and metastable phases..

It is now relatively clear what mechanisms are responsible for the increase in the strength and the fracture toughness of the ceramics. Depending on the particular type of zirconia (e.g. PSZ, TZP, ZTA) one or more of the following Transformation - Toughening mechanisms are considered responsible for the enhanced mechanical properties.

3.3.1 Microcrack Toughening

This form of toughening can be induced through either a stress-induced microcracking mechanism or via microcracking during a stress induced t-m transformation. The distinction is clear: the former situation occurs when, following sintering a zirconia material in the appropriate phase field, subsequent cooling through the transformation temperature (T_{t-m}) initiates the martensitic tetragonal - monoclinic phase transformation with its associated volume expansion of 3-5% (section 3.1), (Figure 3.3a,b) [7].

The tangential stresses formed around the particle, due to the matrix constraint, induce microcracks in the surrounding matrix. It is the ability of these microcracks to either extend in the stress field of a propagating crack or to deflect the propagating crack (and so to absorb or dissipate the cracks energy), that yields the increased fracture resistance afforded by these ceramics.

The latter situation, i.e. microcracking during a stress-induced transformation, is a process initiated by the constrained transformation from t-m symmetry of a grain which has been subjected to the stress field of a propagating crack. Both mechanisms

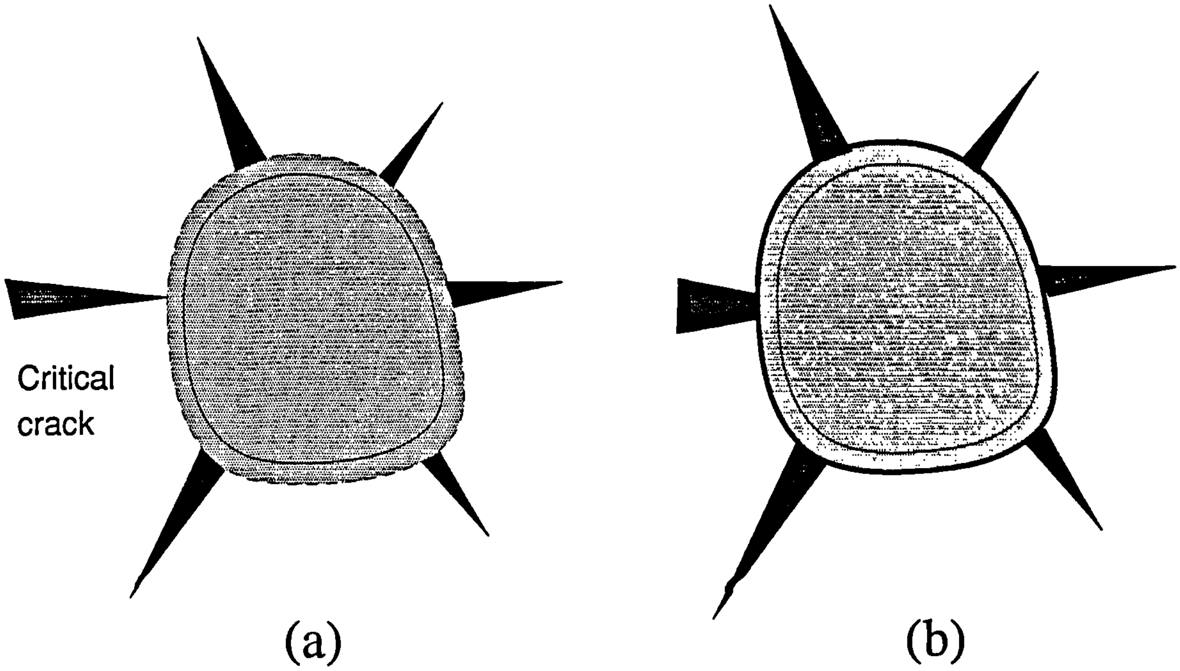

Figure 3.3: The Martensitic Reaction occurring in ZrO_2 (tet. - mono.) with its 3-5% volume increase initiates a series of microcracks around the ZrO_2 particles (a). A crack propagating in the ceramic becomes ‘blunted‘ by the inclusion (b), thus increasing the fracture toughness.[7]

rely on a wake effect for toughening enhancement, where the increment in toughness is directly linked to the increase in permanent strain due to the microcrack opening. The microcrack extension, however, will have the overall effect of reducing the matrix modulus, which, in turn, has the effect of reducing the fracture toughness. Clearly an optimum situation exists such that the microcracked process zone is minimized (and hence the modulus change minimised) but the change in the permanent strain is maximised (and hence as much energy as possible is absorbed by microcrack extension). However, since large increases in strain are not normally associated with small process zones [47] it is likely that microcracking *during* a stress induced transformation would not contribute significantly to the overall fracture toughness.

Stress-induced microcracking, however, has been shown to provide a significant toughening effect, both theoretically [47] and experimentally [48]. An optimum condition exists for such a stress-induced microcracked system. The transformable tetragonal particles must be sufficiently large such that the tetragonal to monoclinic transformation can occur on cooling but must be small enough so that the microcracks developed do not overlap to form a continuous microcrack network. It has been shown [43] that the critical grain size for the retention of the tetragonal structure of ZrO_2 could be increased by increasing the elastic modulus of the matrix, and by increasing the level of the stabilising oxide additive. (Increasing the oxide additive concentration reduces the chemical free energy change between the

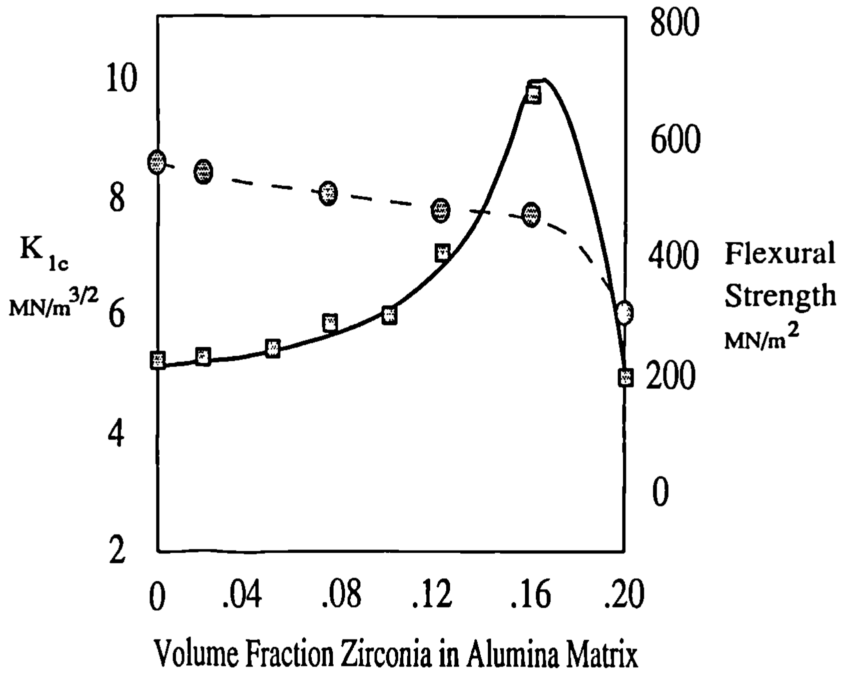

Figure 3.4: Fracture toughness and flexural strength as functions of the volume fraction of Zirconia [49].

tetragonal and monoclinic structures).

In order to obtain maximum toughness, the volume fraction of the ZrO_2 particles must be set at an optimum level [49]; this is illustrated in figure 3.4. The abrupt drop off in strength at higher volume fractions of Zirconia is due to the interaction between the microcracks associated with neighbouring ZrO_2 particles.

The theoretical approach based on a continuum model adopted by Faber [47] led to the following expression for toughening enhancement equation 3.3:

$$K_c^{\infty}/K_c = Q[\theta(h)^{1/2}E_1/K_c, f_s] \tag{3.3}$$

where

K_c^{∞}/K_c = the relative toughness increment

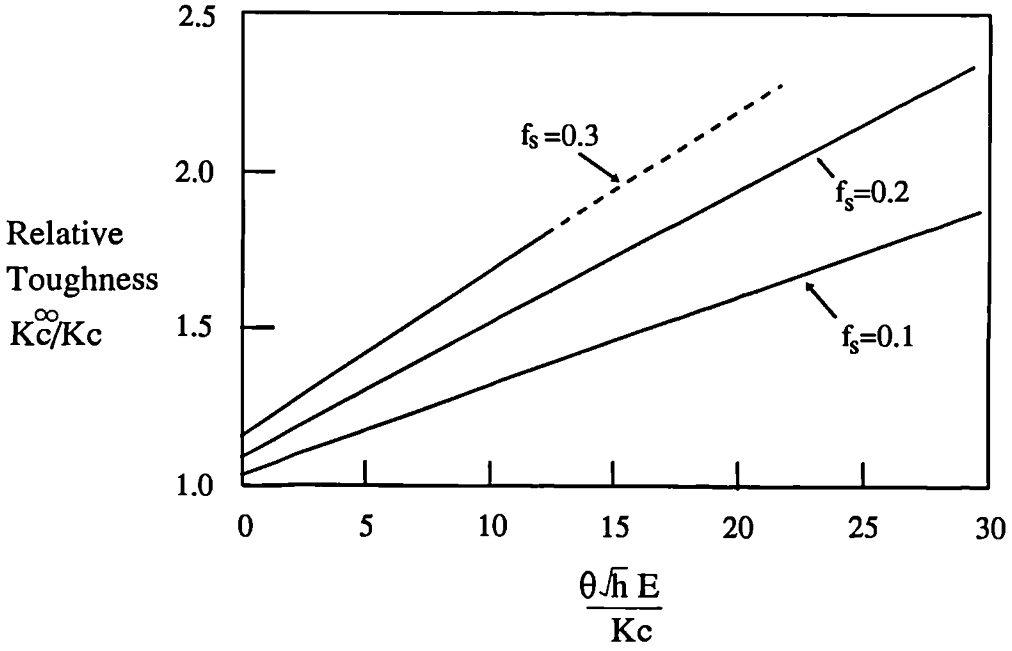

Figure 3.5: Relative Toughness Increments vs the Dimensionless Stress Intensity parameter for a Variety of Microcrack Densities, f_s.

θ =permanent strain

h = process zone size

E_1 = elastic modulus

f_s = microcrack density.

Q is a function plotted in figure 3.5 and relates the relative toughness increments to the physical parameters set out in equation 3.3. It is clear that substantial toughness increments are possible. Furthermore, the predictions lie well within the experimental observations of Claussen et al [50].

3.3.2 Stress-Induced Transformation Toughening

If the metastable tetragonal form of zirconia is retained at room temperature, then a phenomenon known as stress-induced transformation toughening can occur.

Metastable tetragonal ZrO_2 is attained at room temperature by :

(i) Maintaining a uniform distribution of a critically fine grain sized ZrO_2 powder.

(ii) Imposing a constraining pressure on the Zirconia particles exerted by the matrix.

The critical grain size to produce the spontaneous tetragonal - monoclinic transformation can be controlled, to a large extent, by the concentration of stabilising additive (Figure 3.6 [43]). Clearly the grain size, stabilising content and tetragonal retention are all interrelated parameters.

The toughening mechanism is considered to be a stress induced transformation of the metastable tetragonal particles to the monoclinic form. Consider a dispersion of metastable tetragonal ZrO_2 particles constrained within a matrix (Figure 3.7 [7]).

If a crack were to extend under stress through the matrix, then a stress field will be set up around the crack tip [51,52]. This stress field will relax the matrix

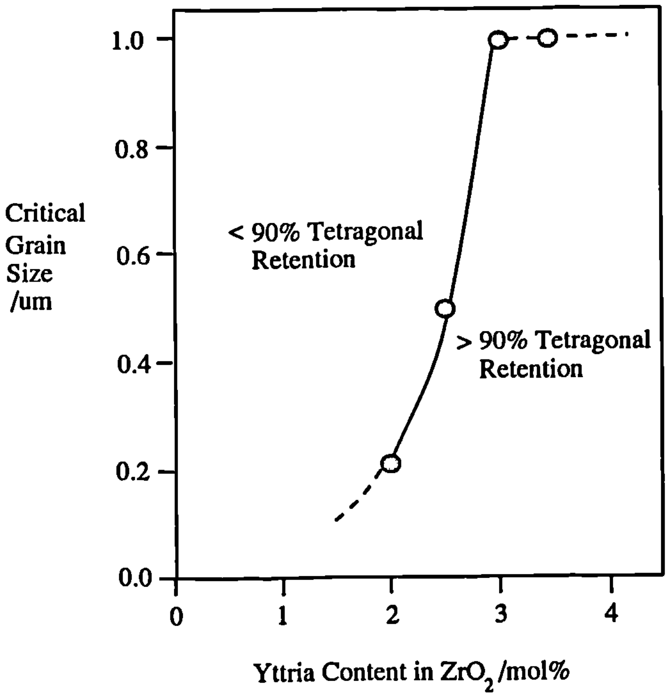

Figure 3.6: Dependence of the critical grain size on the Yttria content in a Y-TZP ceramic.[43]

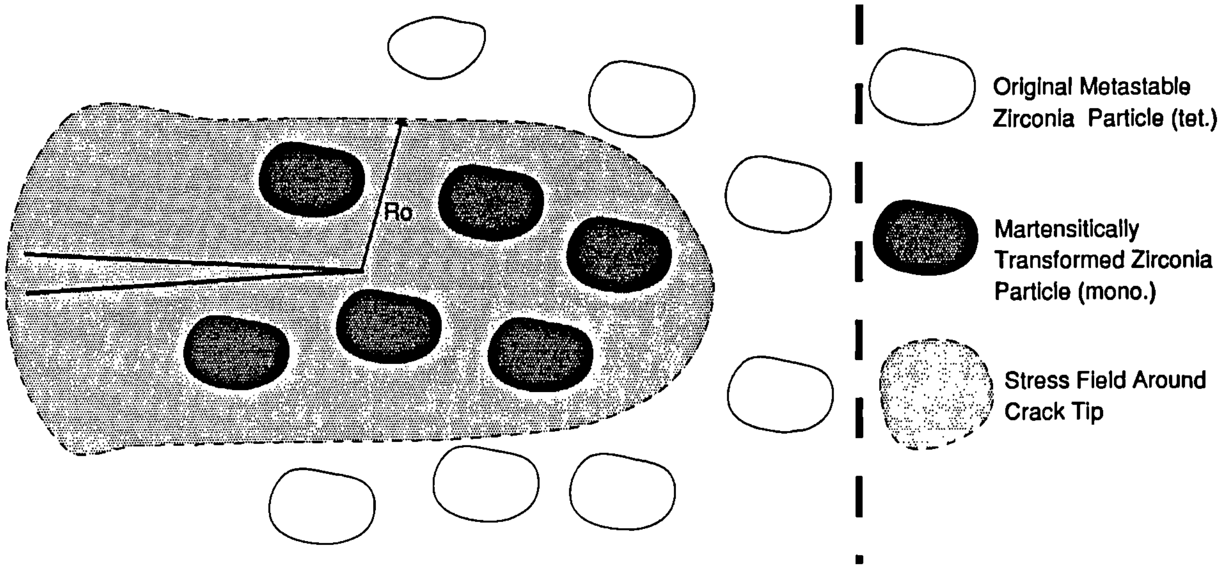

Figure 3.7: Stress induced transformation of ZrO_2 particle in presence of stress field of a propagating crack.[7]

constraint imposed on the tetragonal particles and, if the stress is high enough, the net resultant tensile stress on the particle will enable it to transform to the stable monoclinic form. The volume expansion (3-5%) and shear strain (1-7%) associated with the martensitic transformation will lead to a resultant compressive strain within the matrix. Since this occurs within the vicinity of the crack then extra work would be required to propagate the crack through the ceramic. This accounts for the increase in toughness and hence strength.

A theoretical approach to the contribution to fracture toughness from the martensitic t-m transformation [43] led to the following expression for the critical stress intensity factor, K_c, of

$$K_c = \left(K_0^2 + \frac{2RE_cV_i(|\Delta G^c| - \Delta U_{sef})}{(1-\nu_c^2)}\right)^{1/2} \tag{3.4}$$

where

K_0 = Critical stress intensity without transformation toughening.

$(|\Delta G^c|$-$U_{sef})$ = Work done/unit volume by stress field to induce transformation.

E_c = Youngs Modulus, ν_c = Poissons ratio,

V_i = Volume fraction of retained tetragonal phase,

R = transformed zone (approx. inclusion size)

The equation shows that the contribution to fracture toughness can be maximised by maximising (a) the volume fraction of transformable phase, (b) the elastic modulus of the composite, (c) the factor $|\Delta G^c|$-U_{sef} and (d) the transformation zone, R.

Clearly, maximising the volume fraction would result in a single phase tetragonal zirconia polycrystalline material (TZP). The overall elastic modulus can be enhanced by chosing a suitable composite phase with a modulus higher than tetragonal zirconia such as alumina. A conflict now arises though, since if a second phase is introduced then the volume fraction of transformable phase will be reduced. A compromise situation exists which is dependent on the ratio of the modulii of zirconia to second phase [43]. The factor $|\Delta G^c|$-U_{sef} governs the dependence of fracture toughness on alloy chemistry and temperature. The tetragonal - monoclinic reaction proceeds with a decrease in $|\Delta G^c|$ with increasing temperature and increasing alloy content. Therefore, the fracture toughness is expected to decrease with an increase in both these parameters, i.e. the fracture toughness will be optimised at the lower temperatures and minimal alloy contents. The final parameter which was shown to affect the contribution to the fracture toughness was the size of the transformation zone, R. A major assumption made, when deriving the above expression, was that the transformations occurring in the wake of the propagating crack were irreversible; that is, most of the matrix constraint was lost during crack extension. This assumption led to the hypothesis that the zone size would be directly linked

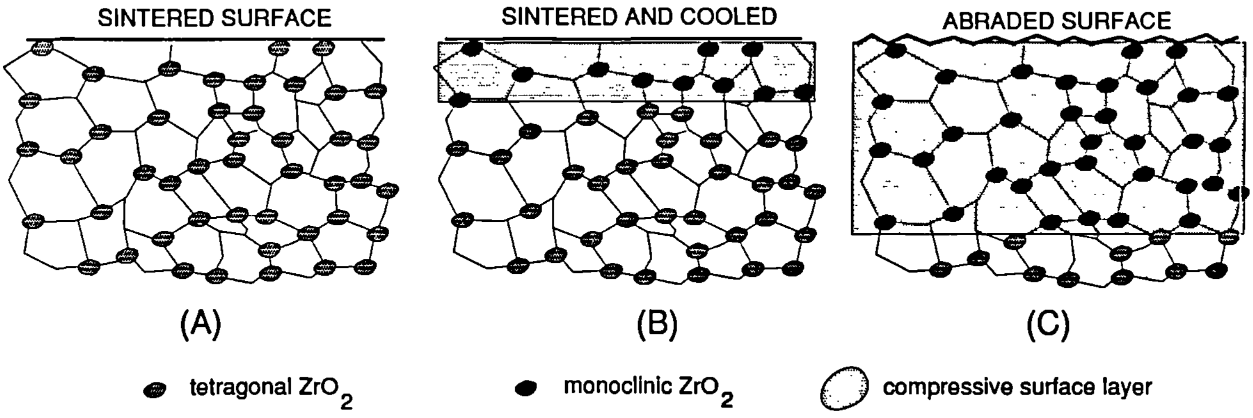

Figure 3.8: Compressive surface layers generated in the surface of a Zirconia ceramic. Note the increased depth of transformation by abrasion or grinding.[53]

to the inclusion or grain size, D i.e. R $\sim$ D, and that the fracture toughness would increase with increasing grain size [43].

3.3.3 Compressive Surface Layers

This form of strengthening is understood [53] to arise from the spontaneous transformation from tetragonal symmetry to monoclinic occurring in the surface layers of the ceramic when subjected to surface grinding for example. The transformation is spontaneous because of the lack of matrix constraint at the surface (Figure 3.8 [53]).

The resultant compressive stress developed in the surface layer of the ceramic inhibits any subsequent growth of flaws introduced through handling or machining. A critical layer thickness exists such that the thickness is greater than the critical flaw size, but small in comparison to the cross section of the ceramic.

3.4 Fabrication of Toughened Ceramics

3.4.1 Partially Stabilised Zirconia - PSZ

The microstructure of a typical PSZ is sketched in the phase diagram of Figure 3.9 [6].

The essential feature of all PSZ ceramics is the two phase C + T field in which they are sintered. Alloying ZrO_2 with solute oxides such as Y_2O_3, MgO and CaO stabilise the cubic polymorph by the extension of its transformation temperature to lower temperatures. Sintering in the C + T phase field produces a ceramic consisting of large cubic grains (about 100 μm). Following a suitable heat treatment in the 1100 - 1450°C interval, coherent tetragonal precipitates are nucleated, the morphology being dependent upon the solute oxide used (e.g. lenticular for MgO, cuboid for CaO and platelet for Y_2O_3). The precipitate particle size is critically controlled by the heat treatment to produce metastable tetragonal ZrO_2 at room temperature, which will transform to monoclinic symmetry in the presence of a stress field of a crack [54].

3.4.2 Zirconia Toughened Ceramics - ZTC

The dispersion of tetragonal stabilised ZrO_2 within other ceramic matrices forms the basis for Zirconia Toughened Ceramics (ZTC). Both intra- and inter-granular

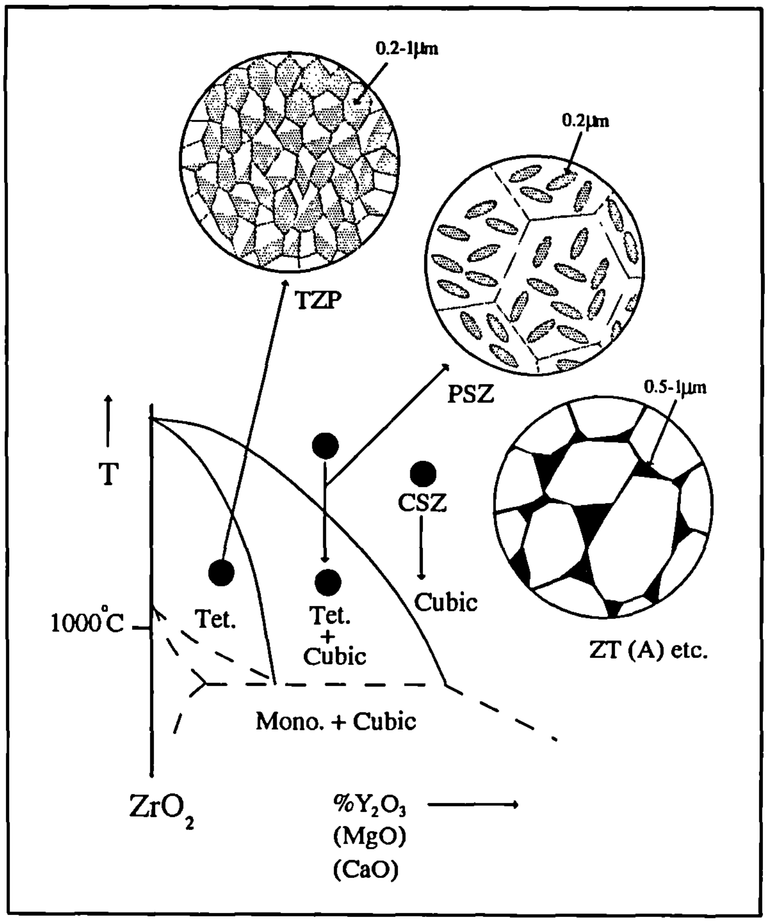

Figure 3.9: Phase Equilibria and Related Microstructure for PSZ ceramics

dispersions are desirable, the latter being the most effective and most simple to fabricate using conventional ceramic processing [55]. Zirconia Toughened Alumina - ZTA - typifies this type of ceramic, where strengths in excess of 2500 MPa have been reported. The increased mechanical properties have been attributed to microcrack development surrounding a dispersion of unstabilised zirconia particles within the alumina matrix. The extension of such microcracks when subjugated to the stress field of a propagating crack absorbs energy from the crack front thereby conferring an increased resistance to crack growth.

The addition of alumina particles to zirconia forms the basis of another set of toughened ceramics. The addition of alumina (20% typically) is considered to serve two purposes. The first is the increased elastic modulus the composite acquires which has only a minor effect on the strength. More importantly, the alumina acts as grain boundary pinning points, thus preventing the development of the large, unwanted, cubic grains of zirconia. The final microstructure is a homogeneously distributed zirconia/alumina fine grained ceramic, the grain size being optimised in relation to thermal stability and crack induced transformation (typically the zirconia grain size is in the 0.2 - 1 μm range).

3.4.3 Duplex Structures

By careful design and the use of a multiphase system, ceramics with a high fracture strength and toughness can be realised [7]. A microstructure based on large agglomerates of metastable tetragonal polycrystals in a matrix of fine grained alumina has been developed [56] and further improved to yield fracture strengths in excess of 700 MPa and fracture toughness values > 12MPam$^{1/2}$. In common with all toughened ceramics, the toughness is a result of the interaction between a crack front and a combination of the microcracking and transformation toughening mechanisms. The cracks will tend to move towards the zirconia agglomerates (since the matrix has a higher elastic modulus than zirconia), the energy associated with the crack front being absorbed by the toughening mechanisms discussed in section 1.5.

3.4.4 Tetragonal Zirconia Polycrystals - TZP

TZP ceramics are *fully tetragonal fine grained polycrystalline ceramics. They* exhibit the highest reported strengths and fracture toughness of any other monolithic ceramic. Strengths up to 2500 MPa and values of fracture toughness of 17 $MPam^{1/2}$ have been attained [57] at room temperatures.

The retention of the tetragonal form of ZrO_2 is accomplished by critical control of particle size and stabilising additive. This sets a limit on the sintering temperature if the tetragonal phase field is to be adhered to, figure 3.10 [27].

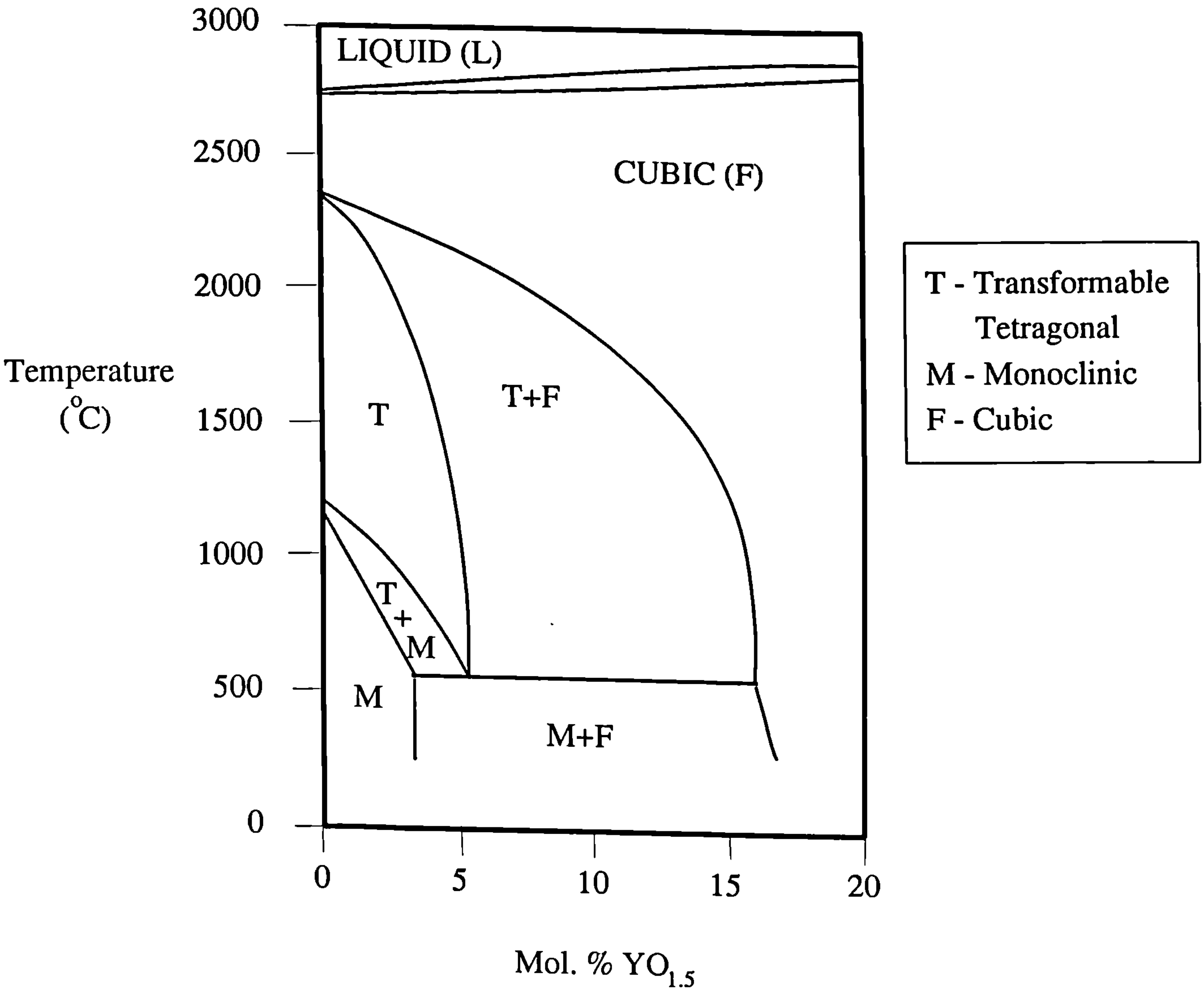

Figure 3.10: Y_2O_3 - ZrO_2 phase equilibrium diagram.[27]

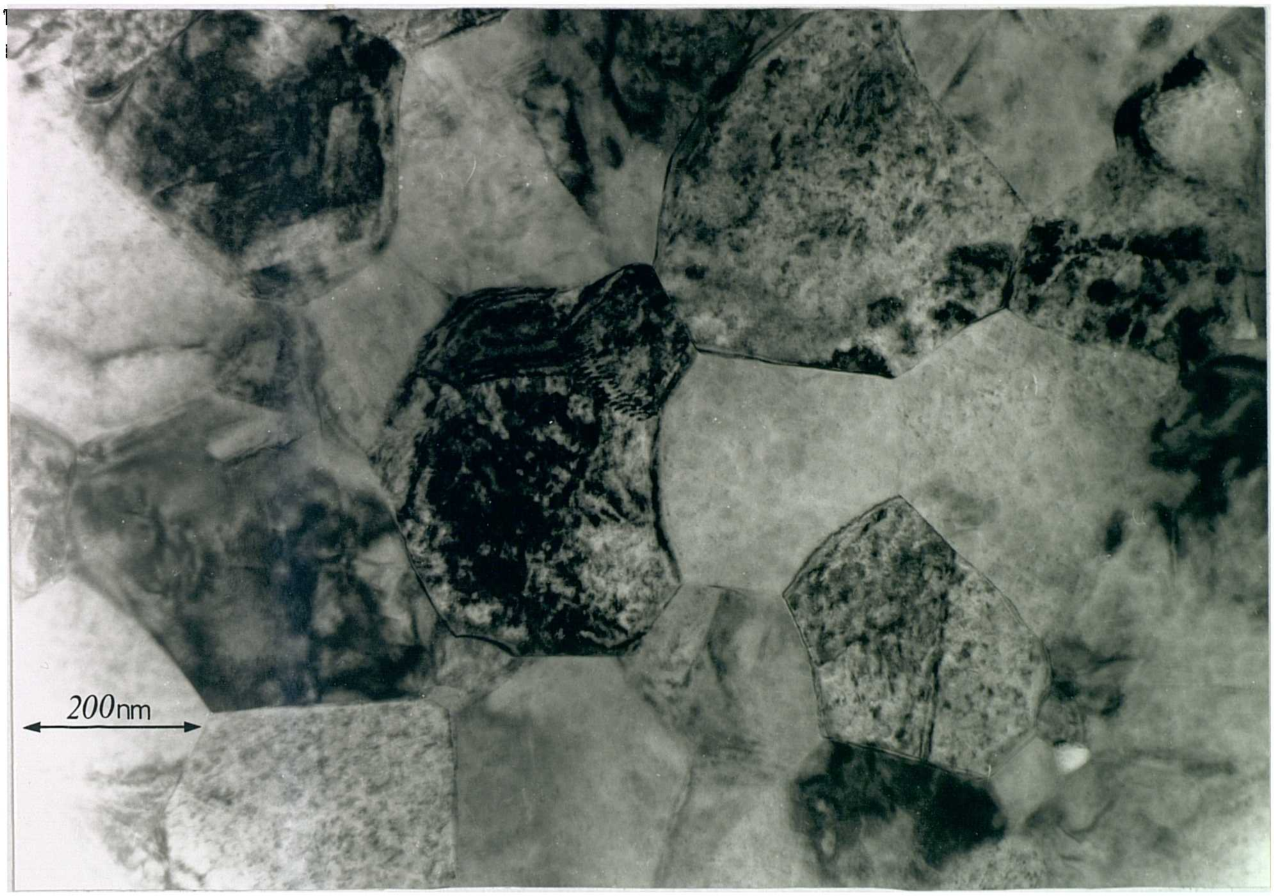

Figure 3.11: Transmission Electron Micrograph of TZP ceramic.

It is possible to sinter commercially available powders to theoretical densities at about 1400°C, to yield a fine grained wholly tetragonal ceramic, (Figure 3.11).

To eliminate the possibility of minor phases such as cubic or monoclinic zirconia it is necessary to use a chemically homogeneous starting powder and to maintain a high degree of cleanliness during the preparation. Typically the grain size is less than $0.8 \mu m$, the highest strengths requiring a grain size of 0.3 - 0.4 μm. For Y -

TZP ceramics the highest strengths are achieved using approximately 3 mol.% Y_2O_3 stabilising concentration.

The sintering temperature is set by the solute oxide content and the need to sinter within the single phase tetragonal phase field (Fig. 3.10). At the low sintering temperatures encountered, the attainment of full theoretical density has to be accomplished via Liquid Phase Sintering (LPS) rather than the less rapid, and essentially inoperative, solid state densification route. The transient liquid acts as a high diffusivity medium for cation transport - primarily Zr - thus enabling rapid densification to occur [11,58]. The liquid phase, which surrounds the zirconia grains at the sintering temperature, is thought to be a low viscosity liquid in the $M - Al_2O_3 - SiO_2$ ternary, where M is the solute oxide additive and Al_2O_3 and SiO_2 are impurities present in the starting powders. Transmission Electron Microscopy clearly reveals this glassy grain boundary phase (figure 3.12).

A consequence of the fine grain size and the presence of the grain boundary phase is the superplasticity TZP ceramics exhibit at 1200°C, with extensions of 100% being measured in tension [59].

3.5 Property Limitations

Although it is clear that TZP ceramics exhibit excellent mechanical properties at ambient temperatures, there is a severe degradation in strength and creep resistance

Figure 3.12: Medium resolution Transmission Electron Micrograph of TZP revealing amorphous grain boundary phase.

at temperatures above about 800°C (figure 3.13).

The loss in strength can be considered to arise from two microstructural reasons :

(1) It has been shown [43] that the contribution to fracture toughness, K_{1c}, by a stress induced transformation is proportional to the chemical free energy change, ΔG_c, associated with the transformation. $|\Delta G_c|$ is known to decrease with increasing temperature and with alloying content. i.e. the transformation toughening contribution will decrease as the tetragonal to monoclinic transformation 'driving force' is reduced. The temperature where the contribution of the stress induced toughness disappears, will depend on the magnitude of the change in the strain energy associated with the transformation [43], $|\Delta U_{sef}|$ (f in the subscript is a constant dependent on the size of the arrested crack). Phenomena that can help relieve the

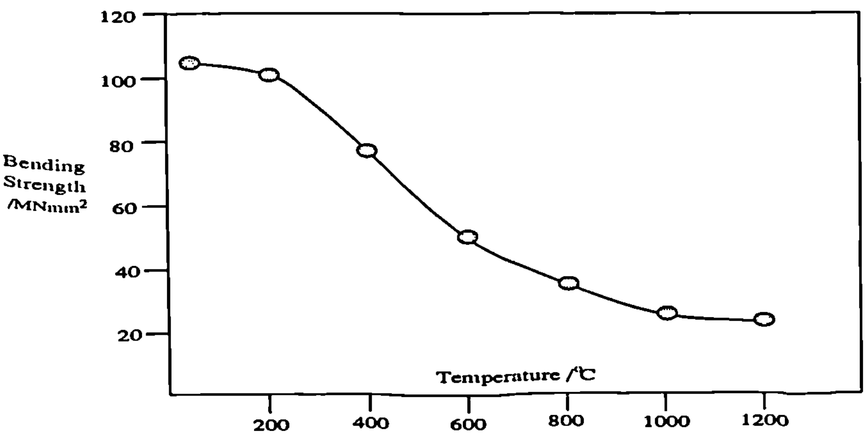

Figure 3.13: Reduction in strength of TZP ceramics with increasing temperature.

strain energy during the crack propagation, e.g. twinning, will decrease the value of f and thus increase the temperature at which the contribution from the stress induced toughening disappears [43].

(2) The small grain size and softening of the amorphous grain boundary phase at high temperatures severely impairs the creep resistance of the ceramic. Microstructural analysis [60] of the grain boundary phase identifies Y_2O_3, SiO_2 and Al_2O_3 to be the major materials present. Whether there is any dissolution of ZrO_2 in the glassy phase has yet to be, unambiguously, determined.

The specific creep mechanism will depend on glass composition and the applied stress [61,62], but it is generally applicable that grain boundary sliding and viscous crack nucleation and growth, (e.g. particle rearrangement initiating crack development due to the softening of the glassy grain boundary phase), represent the main contributions to the deformation process. For superplastic materials, at low stresses it is anticipated that classical diffusional creep (both lattice diffusion - Nabarro-Herring - and grain boundary diffusion - Coble) will be the rate controlling mechanism [62]. The high stress rate controlling mechanism is dislocation creep [62]. It is important to realise that the three types of creep deformation processes are inter-related; it is the relationship obtained between the speed of deformation of a particular rate controlling process and the applied stress that clarifies which mode of operation is dominant at any particular stress level.

A further degradation in the strength of TZP is found in the temperature range 150 - 300°C. This is due to a transformation from tetragonal to monoclinic symmetry starting at the surface and is reported to be particularly enhanced in humid atmospheres [60,63]. The destabilisation mechanisms are not yet fully understood, but may be associated with hydrothermally induced surface nucleation of m-ZrO_2 [64]. It appears, however, that the extent of surface transformation is critically dependent on yttria stabilisation content and the grain size. For instance, a 3mol.% Y-TZP with a grain size of 0.4 μm exhibits no significant surface transformation after a 50h anneal at 200°C, while the same material with a grain size of 0.64 μm had transformed to about 70% monoclinic zirconia [65]. The degradation can be eliminated by increasing the yttria content and reducing the grain size. This, inevitably, leads to some loss in toughness. A Y-TZP with a highly inhomogeneous distribution of yttria has been found to be particularly stable [60] . The stability is attributed to the generation of surface compressive layers due to the understabilised ZrO_2 grains in the surface layers, thus inhibiting surface crack propagation.

3.6 High Temperature Design Strategies For Zirconia Toughened Ceramics

The fundamental research objectives were set out in chapter 1. The following reiterates the main aims and describes the strategies in a little more detail. Each strategy provides the focus for separate chapters found later in the thesis.

3.6.1 Zirconia Toughened Silicon Nitride

Presently, one of the main candidates for high temperature applications, is based on the silicon nitride range of alloys (Chapter 2). A feature common to most ceramic materials, however, is their low resistance to fracture. The fracture toughness of silicon nitride can be enhanced by additions of particulate zirconia, if the zirconia is retained either in the tetragonal or monoclinic structure [66,67,68]. The increased toughness can be linked to the martensitic tetragonal-monoclinic transformation or by the extension of pre-existing microcracks, respectively, in the vicinity of a propagating crack. The incorporation of transformation toughened zirconia within

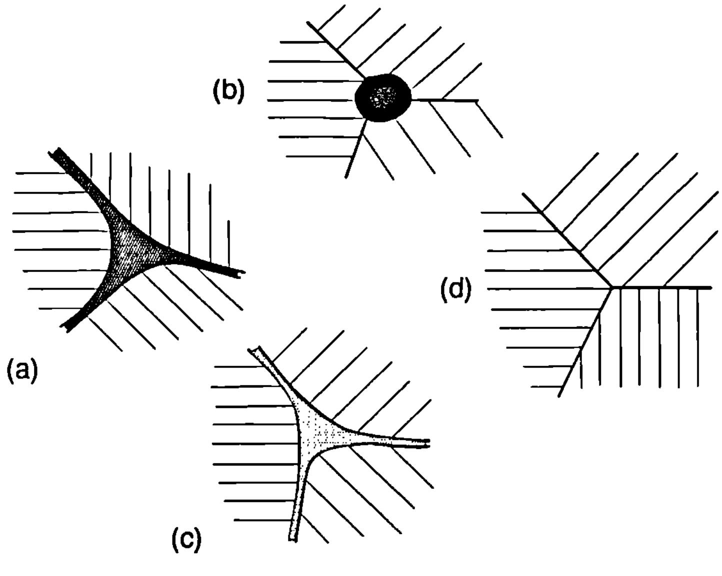

Figure 3.14: Grain boundary modifications applicable to TZP ceramics:(a) amorphous phase wetting the grain boundaries; (b) non-wetting grain boundary; (c) crystallised grain boundary and (d) clean grain boundary

a silicon nitride matrix forms the basis for the first strategy and is presented in chapter 5.

3.6.2 TZP Grain Boundary Modification

The high temperature limitations for TZP ceramics are predominantly set by grain boundary chemistry. Several strategies for the improvement of the high temperature properties, via modifications to the grain boundary phase, are outlined below and in figure 3.14, [61].

The amorphous phase surrounding the TZP grains, figure3.14(a), is characteristic of the microstructure of most TZP ceramics. The three main strategies are:

total elimination of the glassy intergranular phase (d); to reduce the wetting of the grain boundaries by appropriate compositional changes, (b); modifications to the glass composition to realise a more refractory phase (c), either in the form of a completely crystalline grain boundary phase or, at least, an increase in the original grain boundary glass viscosity.

The final approach has been successfully applied to the silicon nitride range of alloys where grain boundary modifications have incremented the useful operating temperature to about 1300°C (chapter 2). Grain boundary refinement via chemical modification forms the basis for the second strategy and is presented in chapter 6.

Chapter 4

Experimental Techniques

This chapter will detail the standard experimental apparatus and techniques that were repeatedly used throughout the research. Specific details pertaining to certain aspects of experimental procedure will be described where necessary in subsequent chapters.

4.1 Powder Preparation

The precursor powders used throughout the research are listed in table 4.1 together with the manufacturer, chemical purity and particle size.

POWDER	MANUFACTURER	COMPOSITION	PURITY							AVERAGE PARTICLE SIZE/μm	SPECIFIC SURFACE AREA
			SiO_2	Y_2O_3	Al_2O_3	Fe_2O_3	Na_2O	$I_g loss$	-		
3Y TZP '3Y PSZ'	TOYA SODA Manuf.Co.Ltd Tokyo.Japan	3mol%Y_2O_3 5.03wt%Y_2O_3	.005	5.03	.092	.006	.005	.6		0.3	17
12CE TZP 'PSZ - CE14'	UNITEC CERAMICS. UK	Sample Ref: 12mol.%CeO_2	.16	-	.04	.06	-	-	-	95%~ 1.1μm 50%~ .45μm	7
			N	O	C	Cl	Fe	Ca	Al		
αSi_3N_4	UBE Industries Ltd., Tokyo Japan	SNE 10 100%Silicon NItride 95%α + 5%β	39	1.3	<0.2	50ppm	50ppm	<10ppm	22ppm	0.2	10 - 12
αAl_2O_3	ALCOA	99.9%Al_2O_3									
SiO_2	VENTRON	99.9%SiO_2									
			ErO_2	GdO_3	Al	Ca	Fe	Mg	Si		
Y_2O_3	Johnson Matthey	Yttrium Oxide	5ppm	3ppm	10pm	10ppm	<1ppm	<1ppm	30ppm		

Table 4.1 : Precursor powders used throughout the research, with indicated compositions, purities and particle size information

The required compositions, detailed elsewhere, were dry mixed, dispersed in distilled and deionised water and attrition milled using zirconia milling media [1] in a rotary attrition miller[2] operated at 2000rpm for 25 minutes. The homogeneous slurry was carefully extracted from the mill, using additional water to purge remaining powder, and spray dried using a mini-spray drier.[3] The spray drying process is a convenient and rapid method for producing powders having a high resultant homogeneity and which are largely free of agglomerates. The powder, having been heated to ~ 200°C during the process, is also completely dehydrated. The whole process can be completed within approximately 1 hour, depending on initial slurry viscosity, amount of slurry and certain powder characteristics.

4.2 Powder Compaction and Densification

Samples to be pressureless sintered were uniaxially die pressed in a rectangular steel die/punch set, lubricated with a mould release agent (PTFE), to a pressure of ~8 MPa. The fragile billets were then sealed in polythene envelopes and cold

---

[1] 3Y-TZP balls, 3mm in diameter, TSK Ltd. Japan

[2] Eiger 250ml Mini Motormill Attrition Miller.

[3] Buchi 190 Mini Spray Drier.

isostatically pressed [4] in oil at a mean pressure of ~170 MPa. Pressureless sintering was conducted in a vertical tube high temperature furnace capable of maintaining temperatures in excess of 1700°C. The furnace was fitted with a sophisticated electronic PID time-temperature controller, $MoSi_2$ heating elements and facilities for gaseous/vacuum environmental control, figure 4.1.

The heating/cooling ramp rate was fixed at 5°C/minute in order to reduce the probability of thermally shocking the alumina tube and crucible support structure. Crucibles were either zirconia or alumina and were lightly packed with a bed of powder of the same composition as the samples to be sintered.

Samples to be uniaxially hot-pressed were prepared in the following manner, using the set-up outlined in figure 4.2.

The hot pressing furnace[5] used Radio Frequency (R.F.) induction to heat a graphite susceptor which contained the sample. An alternating R.F. field was coupled to a small coiled copper tube, through which cooling water passed. The graphite susceptor, placed concentrically inside the copper coil, absorbed energy from the localised electromagnetic field, with a subsequent increase in its temperature. This heat energy was transmitted to the sample via conduction, and some lost to the surroundings via radiation and convection. Heat loss was minimised by the use of thermally insulating 'bubble alumina' powder which surrounded the susceptor

---

[4] Stansted Isostatic Press

[5] The R.F. furnace was a 'Radyne' 30kW power induction furnace, Wokingham, England

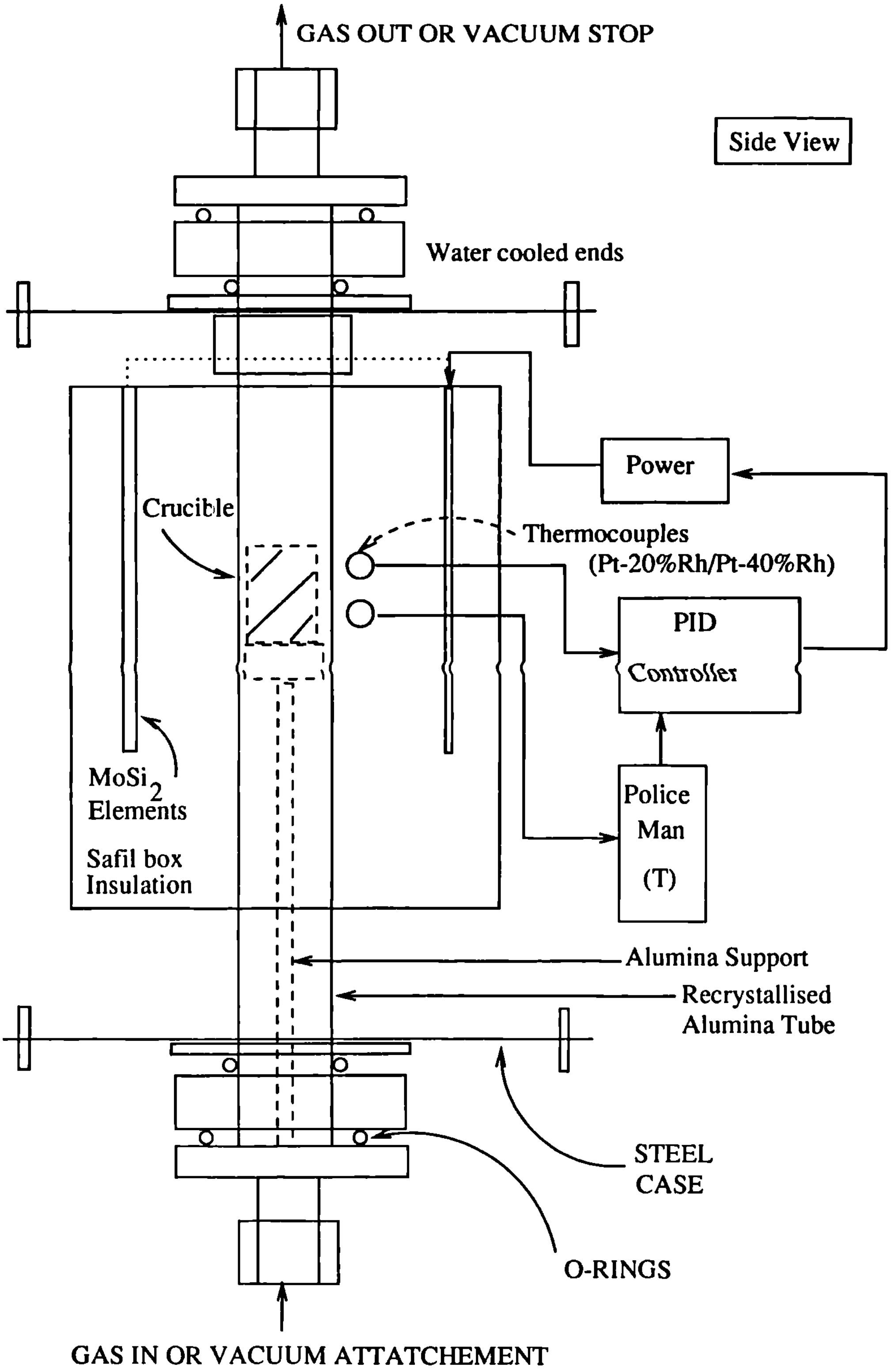

Figure 4.1: Vertical alumina tube high temperature furnace used to pressureless sinter the compositions described in subsequent chapters

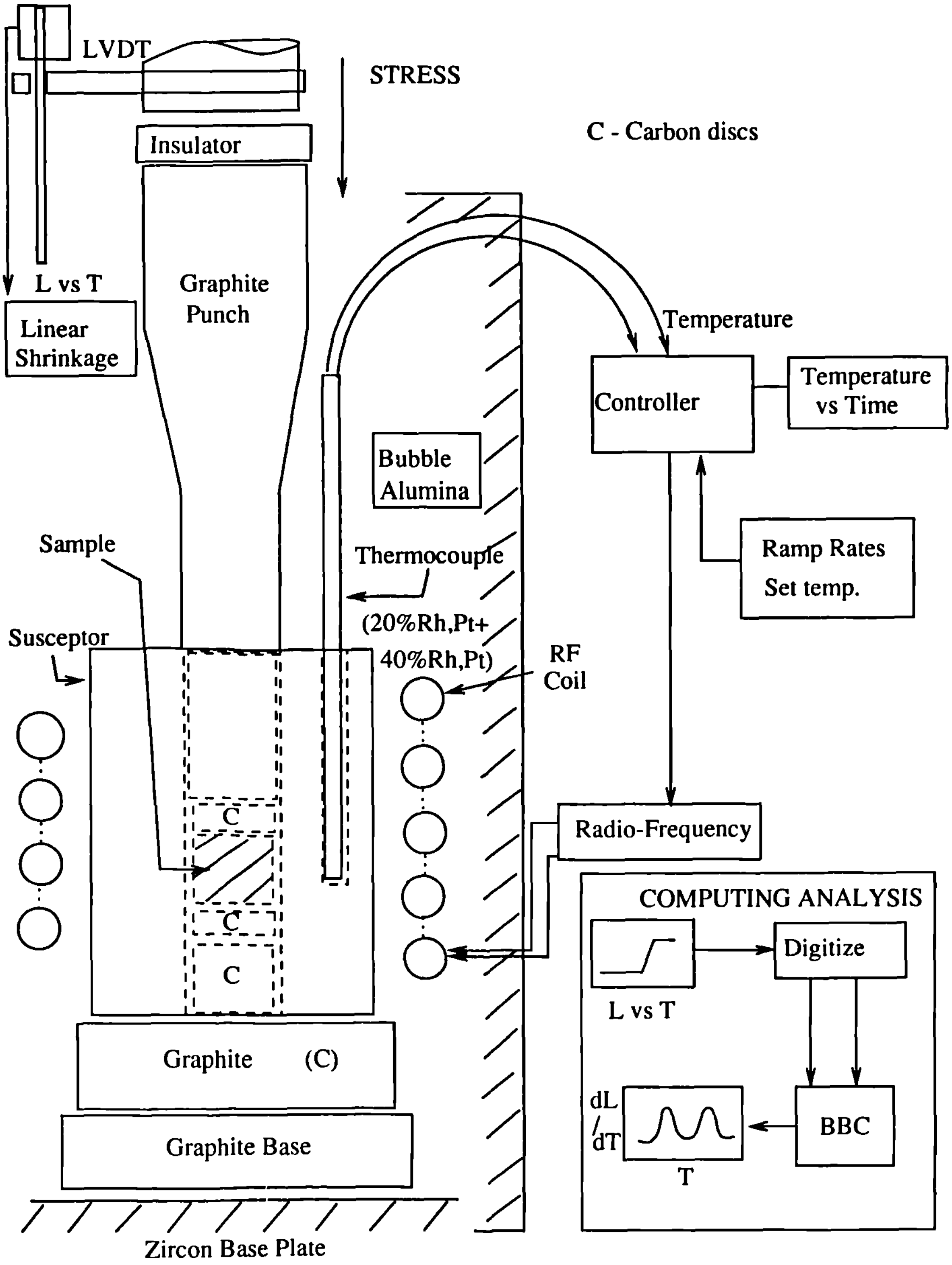

Figure 4.2: Hot-Press apparatus and electronic/computing flow diagram

during the hot pressing cycle.

The bore of the graphite susceptor was rinsed in an acetone/boron nitride powder suspension leaving a thin deposited BN layer. This coating minimised reactions between the graphite and sample and aided the removal of the sample following hot pressing. A small graphite end punch, also coated in BN, was inserted into the susceptor which was then charged with ~10g of the sample powder. A thin graphite disc coated in an identical manner to the above, was next placed in the bore of the susceptor and pressure was applied to compact the dry powder. The top punch was next inserted and the entire punch/susceptor arrangement carefully aligned with the hydraulically operated steel ram, see figure 4.2. A disc, made of porous SiC, was placed between the graphite punch and steel ram to provide additional thermal insulation. A Pt-20%Rh/Pt-40%Rh thermocouple, sheathed in a closed end alumina tube was positioned into a hole predrilled in the body of the susceptor. The pressure was increased to ~10MPa whilst the bubble alumina was poured into the chamber. 'Saffil' boards were placed over the enclosure and any small remaining gaps plugged with 'Saffil' wool. The R.F. power was applied in two stages. For the first 20 minutes the maximum suggested initial power rating, corresponding to a coil current of ~0.9Amps, was adhered to, followed by steady increments up to the operating power of ~4kW. The R.F. generator was monitored and controlled by an electronic PID controller capable of maintaining the set temperature to ±1°C. All hot pressing runs were carried out in air at $1700 \pm 5°C$ at a pressure of $22 \pm 2MPa$. The strength of graphite is known to increase with an increase in temperature. The pressure was, therefore, slowly increased to its maximum set value during the first 1200 degrees, to reduce the risk of fracture.

A Linear Variable Displacement Transducer (LVDT), attached to the hot press and moving ram, was coupled to an X-t chart recorder giving an accurate linear displacement, or shrinkage, versus time plot. This plot was later digitised and processed using purpose written software[6] to generate information on the rate of shrinkage versus temperature for any particular hot pressing run. The digitisation of the X-t plot was carried out using an X-Y plotter reconfigured such that the original plot could be 'traced' out using the X-Y pen, converting the X-Y points to X-Y voltages. The voltages were conditioned before being sent to the analogue input of the BBC Master microcomputer, where the data was stored. The 1000 X-Y data points were processed using a three point average differentiation program, with the simultaneous transpose of time, t, for temperature, T, and the resulting $\delta L/\delta T$ data plotted as a function of temperature. *Peaks in the graph thus corresponded* to maxima in the rate of densification of the compacts. In this way, the kinetics of sintering could be correlated with temperature and composition.

---

[6] BBC Masterseries computer, software-M G Cain

4.3 Measurement of Density

The surface layer of sintered and hot pressed samples was ground away using diamond grinding paste on cast iron lapping plates. Samples were suspended in fine (36 swg) copper wire cradles, suitably attatched to a ±1mg pan balance. The cradle/sample arrangement was weighed in air and also when immersed in distilled and deionised water. The measured weight loss was used to determine the density of the sample by applying Archimedes principle and equation 4.1.

$$\rho_s = \rho_f \left(\frac{W_a}{W_a - W_f} \right) \tag{4.1}$$

where:

ρ_s - density of sample

ρ_f - density of immersion fluid (water)

W_a - weight in air W_f - weight in fluid

During immersion in water, ~5 minutes, any change in weight was noted, indicative of water absorption resulting from open connected porosity within the sample.

The theoretical densities were calculated using a simple rule of mixtures[7] of the density (ρ) and volume fraction (x_i) of constituent phases.

---

[7] $1/\rho = \Sigma \frac{x_i}{\rho_i} : (\rho Si_3N_4 = 3.14gcm^{-3}, \rho(t)ZrO_2 = 6.1gcm^{-3})$

4.4 X-Ray Diffraction

X-ray diffraction (XRD) techniques were used extensively to study the crystalline phases present within the surface of the material[8]using a Philips type PW 1130/00 X-ray powder diffractometer[9]. A copper monochromator produced the characteristic $K_{\alpha_1 \alpha_2}$ and K_β energies which were filtered using a nickel window to remove the K_β peak. The interplanar dimensions were calculated using the standard equation of Bragg diffraction, equation 4.2.

$$\lambda = 2d sin\theta \tag{4.2}$$

where:

λ= Characteristic X-ray wavelength = 1.5405Å

d=interplanar spacing

θ=diffracted beam angle

The diffracted peaks corresponding to the K_{α_2} energy could not be distinguished from those arising from the K_{α_1} X-ray line, except at very high diffracting angles or when analysed at higher than normal resolution. Crystalline phases were identified from the trace using the J.C.P.D.S. powder diffraction files.

---

[8] For Cu K_α X-Rays the depth for 90% loss of beam intensity in zirconia is typically $40\mu m$.

[9] Operated at 40kV and 35mA.

The relative proportions of phases present within the sample were determined from peak height analysis of the X-ray trace. X-ray quantitative analysis, however, is dramatically affected by crystallite shape, size and orientation. Furthermore, preferential alignment of grains within a material also affects the relative intensities of the diffraction peaks. It is clear that several diffraction peaks must be analysed and averaged in order to yield an accurate value for the volume composition of any particular phase. The α/β silicon nitride ratio was determined by measuring the intensities of the following diffraction peaks;

$\alpha - Si_3N_4$: (101), (110), (200), (201), (102), (210), (301)

$\beta - Si_3N_4$: (110), (200), (101), (210)

and using the calibration curves produced by Gazza et al [69], which have been subsequently fitted to a quadratic function and incorporated into a computer program[10]. Errors associated with this procedure were typically less than 10%.

Quantitative analysis of the monoclinic content of zirconia was determined from measurements of the peak heights of the monoclinic (111) and ($11\bar{1}$) reflections and the tetragonal (111) reflection, figure 4.3.

Substitution of these values into equation 4.3 [70] yields the volume fraction of the monoclinic phase.

---

[10] BBC Master series microcomputer, software M G Cain

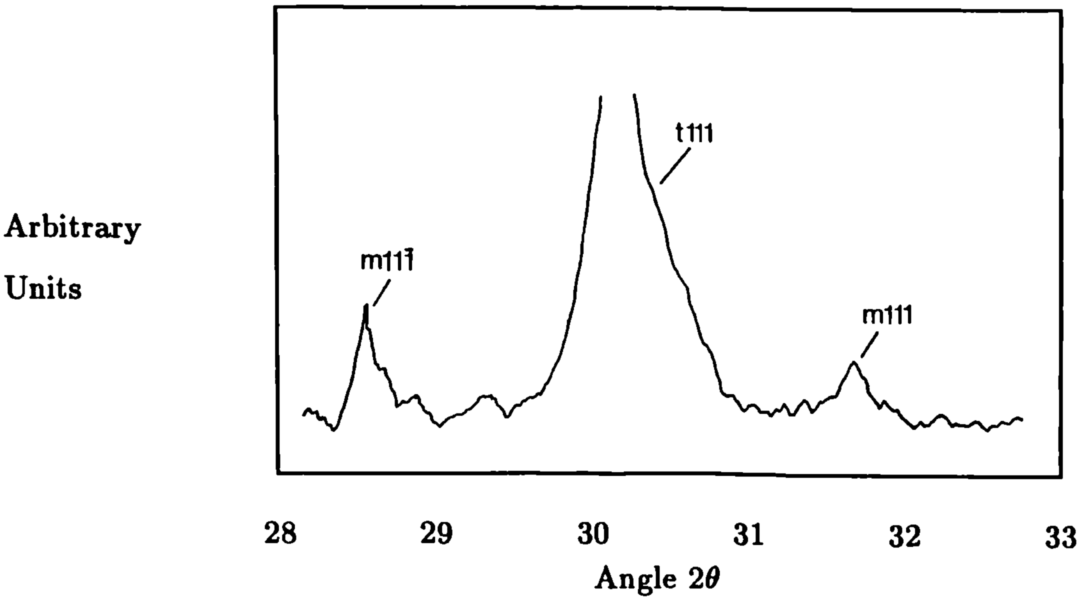

Figure 4.3: Tetragonal/Monoclinic zirconia ratio

$$\%mono = \left(\frac{m(111) + m(11\bar{1})}{t(111) + m(111) + m(11\bar{1})}\right) \times 100\% \qquad (4.3)$$

Tetragonal and cubic zirconia can be differentiated by high angle X-ray diffraction analysis. In the region $2\theta = 72^\circ - 76^\circ$ cubic zirconia exhibits a diffraction peak at 73.7° (d=1.28Å) corresponding to the (400) set of planes. In tetragonal zirconia, this peak splits into the corresponding (004) and (400) tetragonal peaks, figure 4.4.

The cubic to tetragonal ratio can be approximately determined using equation 4.4 [71].

$$\frac{M_c}{M_t} = 0.88 \times \frac{I_{(400)c}}{I_{(400)t} + I_{(004)t}} \qquad (4.4)$$

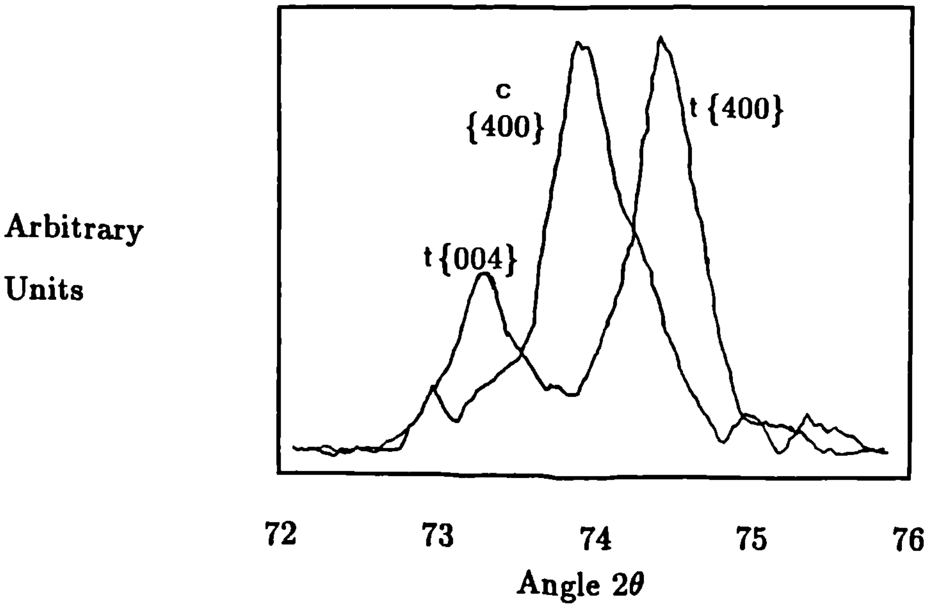

Figure 4.4: Tetragonal/Cubic ratios of zirconia

where M_c & M_t are the mole fractions of the cubic and tetragonal phase respectively, and the integrated intensities, I, are indicated with their appropriate Miller indices.

The X-ray diffractometer was generally operated at a rate of 2θ=1°/minute and with a chart paper rate of 1cm/minute. Average count sampling was conducted with a time constant of 1 second, having the effect of reducing the overall background noise level. When higher resolution was required, the angular rate was decreased and the chart recorder rate increased.

X-ray diffraction can give an insight into the overall orientation relationships of grains within the surface of a material. This powerful investigative tool was exploited when discussing the ferroelastic nature of tetragonal zirconia in chapter 7.

4.5 Scanning Electron Microscopy - (SEM)

The ability to resolve sub-micron dimensional features on the surface of a material and the added advantage of quantifying the elemental composition of these features is provided by the scanning electron microscope.[11] In this section, it is only necessary to detail sample preparation and particular modes of operation frequently used throughout the research.

The samples were sliced using a diamond annular saw[12] and polished in two stages; initially using SiC 'Wet or Dry' abrasive paper with water, and finally polished using diamond lapping paste. Alternatively, the sliced material was hot mounted in a 'bakelite' conductive plastic mould and ground and lapped on a cast iron lapping plate coated with successively finer grades of diamond slurry. A copper lapping plate was used in preference to cast iron at the finer grades to obtain an improved surface finish. Final polishing was attained using a cloth-backed aluminium lapping plate impregnated with $1/10\mu m$ alumina paste. The surface finish was continually assessed using a bench-top light microscope. The polished samples were washed in acetone and distilled water, dried and vacuum coated with a thin evaporated layer of carbon to eliminate surface charging of SEM samples. Some samples were thermally etched to delineate their sub-micron grain sizes ($< 1\mu m$)

---

[11] Cambridge 'Stereoscan' SEM S250 MKIII

[12] Capco diamond saw, England

when viewed in the SEM. In the case of TZP ceramics, the etching conditions were 1370°C for 10 minutes in air prior to carbon coating.

The detection of secondary electrons, generated within the top 50nm of the surface, yields topographical features of the surface of the sample. Features such as fracture surfaces were analysed using this imaging mode. Backscattered electrons originate from scattering events occurring within a larger interaction volume of the material than the volume associated with secondary electron generation. The number density of backscattered electrons emitted from the specimen for each incident electron is strongly dependent on the atomic number of the interaction volume, e.g. the detection of the backscattered electrons yields compositional information which is subsequently viewed as changes in image contrast on the SEM visual display monitor. The backscattered detector is a Si semiconductor device which is mounted beneath the objective polepiece.

When an electron beam interacts with a material X-rays are produced with a spatial extent depending on the original electron beam energy and the density of the material. Typically, this interaction volume for 10keV electrons is $1\mu m$ for a material of density $3gcm^{-3}$, which is larger than the interaction volume associated with the detection of backscattered electrons. The X-rays produced are of two types; characteristic X-rays whose energies depend on the nature of the atoms in the interaction volume and the Bremsstrahlung, or background, radiation. Detection of the characteristic X-rays permits qualitative analysis of the material's chemical composition. With appropriate computer analysis[13] and corrections based on atomic number Z, X-ray absorption A, and fluorescence F, (ZAF correction) quantitative analysis was achieved. To maintain the integrity of the vacuum, a thin beryllium window separates the specimen chamber from the X-ray detector. The absorption of X-rays, produced from electron interaction with elements of small atomic number, by the Be window limited the light element detection to atomic number $\geq$ 11. Therefore, the detection of elements with $Z<11$ neccessitates the opening of the Be window. This technique requires a much higher vacuum level within the chamber to avoid damaging the X-ray detector. ZAF computer correction analysis is not possible whilst the SEM is in this 'windowless' configuration.

4.6 Transmission Electron Microscopy (TEM)

Higher resolution imaging, including lattice imaging, and the additional benefit derived from electron diffraction studies were afforded by the TEM.

Samples were prepared in the following manner. Cross sections of material were sliced using a diamond annular 'Capco' blade and ground to approximately $100\mu m$. Discs, 3mm in diameter, were ultrasonically drilled from the material and mounted onto the base plate of an automatic dimpler/polisher. One side was polished, ul-

---

[13] The SEM is interfaced with a LINK EDS quantitative AN10000 analyser and LZ5 detector

timately using $1/4\mu m$ diamond paste, and the other dimpled and polished to the same finish. The final dimpled thickness was typically $20\mu m$. The discs were argon ion-beam milled and thinned to electron transparency, and finally lightly carbon coated as described in the preceding subsection. Transmission electron microscopy was conducted using a Jeol 2000FX, 200keV transmission electron microscope fitted with either a LaB_6 or W filament. The LaB_6 filament produced a higher intensity electron beam and additionally an increment in resolution due to the higher coherence of the beam. The majority of the research was completed using the (standard) Bright field imaging mode of the TEM.

Elemental compositional analysis was possible using the EDS system fitted to the TEM,[14] where regions $< 1\mu m$ could be analysed. A high angle detector avoided the problems associated with mechanically tilting the sample. Light element analysis was achieved using the windowless horizontal take-off detector.

Selected area electron diffraction (SAED) and microelectron diffraction techniques were used extensively to study the crystallinity and structure of the material. The resolution afforded by SAED is limited by the spherical aberration of the apertures used whilst the resolution attained through the use of microelectron diffraction is defined by the size of the beam and not the aperture, with the result that grains as small as 50nm across could be probed.

---

[14] LINK EDAX quantitative analyser

4.7 Fracture Toughness Evaluation

In K_c testing, critical fracture starts at an artificially generated flaw. There are various methods for determining the fracture toughness of a ceramic, but all methods rely on the generation of a sharp crack for a starting defect. The crack can be initiated by single indentation with a diamond or by machining a narrow notch into the surface of the ceramic.

Essentially there are three methods for determining the materials constant of fracture toughness. The first two use an indentation technique using a shaped diamond indentor [72,73,74]. The sample is either subsequently fractured in three point or four point bending or the indenting is repeated over much of the surface and the crack extension measured as a function of applied load. Three disadvantages using this method are; (1) the surface of the ceramic must be polished to to a finish less than the indent dimensions, (2) there is a practical problem of measuring the crack length accurately and (3) a dependence of K_{1c} on the crack length has been shown to exist (R-curve effect) for materials such as coarse-grained aluminas and zirconia or zirconia toughened ceramics [75,76,77].

Using notches as the starting defect (method 3) presents a different problem in the subsequent analysis of K_{1c} measurements. It has been shown that the depth of the notch exhibits little effect on the measurement whereas the width of the notch has considerable effect [75,78,79,77]. However, with notch widths below a certain limit ($<100\mu m$), both the dependence on depth and width of the starting defect is minimised [75,80]. The single edge notch beam (SENB) technique can be used in either the three-point or the four-point configuration. In this set of experiments the four-point bend configuration was adopted due to:

- the positioning of loading points is less critical in the four-point system

- there is less interaction between the stress produced from the loading points in 4-point bend with the root notch stresses [81]

The necessary apparatus was constructed and is shown in figure 4.5.

The critical stress intensity factor, K_c, is given by elastic analysis [81] in terms of the notch depth and critical applied load [80,82], equation 4.5.

$$K_{1c} = \left(\frac{3PL}{bw^2}\right) a^{1/2} \left(1.99 - 2.97(a/w) + 12.97(a/w)^2 - 23.17(a/w)^3 + 24.80(a/w)^4\right) \tag{4.5}$$

where

P=critical applied load

L=distance between inner and outer loading points

b=beam thickness

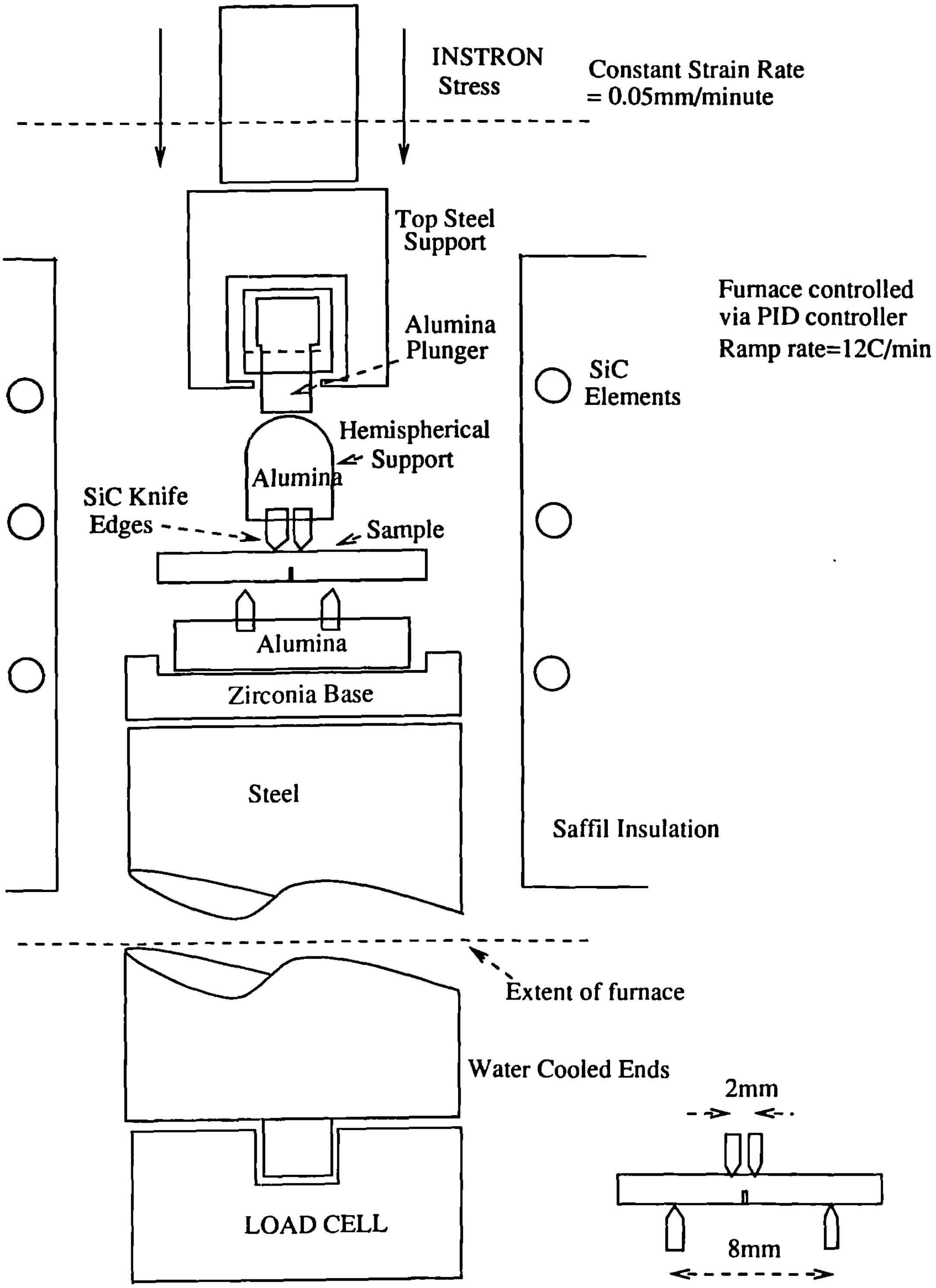

Figure 4.5: K_c Jig for room temperature and 800°C

w=beam height

a=depth of starting notch

An important feature used in the elastic analysis is the assumption that the crack has zero width. It has been found [80] that the narrowest possible notch width should be used in order to minimise the contribution to the final error from this assumption.

Samples were sliced into billets measuring approximately $3.5 \times 3.5 \times 5 \times 20$mm and lapped on all sides using a diamond lapping compound. A notch, measuring $\sim$ 0.1mm width, was cut into each billet to a depth of $\sim$ 0.6mm. The samples were thermally treated at $1050°C$ for 1hour in air to minimize transformation effects due to machining [77] and also to ensure that samples measured at room temperature and those measured at high temperature received a similar thermal annealing treatment allowing a direct comparison to be made. Following careful alignment within the jig, stress was applied at a rate of 0.05mm/minute using an Instron Universal Testing machine. The stress at the point of fracture was recordered and used to determine the fracture toughness.

The same jig was used to measure the fracture toughness at 800°C. The entire assembly, shown in figure 4.5, was loaded into the furnace which surrounded the Instron ram and support located on the load cell. A small applied load assured the stability of the jig prior to the furnace door being shut. The temperature was ramped at ~ 10°C/minute and an inevitable increase in the measured load, caused by the thermal expansion of parts within the furnace, was automatically adjusted via the Instron controller. Ten minutes after the preset temperature was established (to ensure thermal uniformity throughout the material) the load was allowed to increase as before, thereby fracturing the sample. For each composition, between 5 and 6 measurements of fracture toughness was made, thus yielding an average value with associated statistical error.

Chapter 5

Microstructure and Mechanical Properties of Hot Pressed Zirconia Toughened Silicon Nitride

5.1 Introduction

Presently, one of the main candidates for high temperature applications, is based on the silicon nitride range of alloys (Chapter 2). A feature common to most ceramic materials, however, is their low resistance to fracture. The fracture toughness of hot pressed silicon nitride is typically 3-5 $MPam^{1/2}$ but can be enhanced by additions of particulate zirconia, if the zirconia is retained either in the tetragonal or monoclinic structure [66-68]. The increased toughness can be linked to the martensitic tetragonal-monoclinic transformation or by the extension of pre-existing microcracks, respectively, in the vicinity of a propagating crack (chapter 3.3).

The addition of small amounts of zirconia, zircon or stabilised zirconia (such as zyttrite) promotes the densification of silicon nitride and forms more refractory grain boundary phases which can improve the strength and resistance to oxidation of the nitride [67,83-87]. The thermodynamic compatibility of the zirconia/βsilicon nitride (or substituted β'silicon nitride - SiAlON) couple has been studied extensively [84,85,88-98] and reactions such as $6ZrO_2 + 4Si_3N_4 \rightleftharpoons 6ZrN + 12SiO(g) + 5N_2 \uparrow$ have been shown to occur under reducing conditions or at temperatures in excess of 1600°C [89]. The ZrN or related ZrON products (e.g. via $xSi_3N_4 + ZrO_2 \rightleftharpoons ZrO_{2-3x/2}N_x + 3x/2Si_2N_2O$) can readily oxidise when heated at temperatures between 600 and 800°C, to form monoclinic zirconia, according to the reaction;

$$ZrO_{2-3x/2}N_x + 3x/2O_2 \rightleftharpoons mZrO_2 + x/2N_2 \qquad (5.1)$$

The transformation proceeds with an associated volume increase of ~ 4-5%, leading to a structural degradation of the ceramic. The formation of ZrN or Zr-oxynitride can be suppressed if the processing temperature is kept sufficiently low, the atmosphere carefully controlled and/or the zirconia is pre-reacted with a stabilising additive oxide such as yttria. If the above criteria are met then the retention of transformable tetragonal zirconia in a $Si_3N_4/SiAlON$ matrix may be accomplished.

This chapter deals with the microstructural evolution in $ZrO_2 - SiAlON$ composites with the zirconia partially stabilised with either Y_2O_3 or CeO_2. The retention of tetragonal zirconia in the yttrium and cerium - stabilised composites is investigated and later correlated with the observed mechanical properties. The mechanical properties and phase stability are compared in materials with differing volume fractions of zirconia and at different temperatures in order to identify the toughening mechanisms operating within these materials.

5.2 Composition Selection

As with all ceramic materials, full density is required so that the strength of the material is maximised and not unduly limited by the presence of large pores or voids. This fundamental requirement was considered to be of prime importance when considering the composition selection. The chosen powders had a proven high degree of sinterability, i.e. the powders were of a uniform, fine grain size and were of high purity. A second requirement when considering the phase evolution and subsequent retention of the metastable tetragonal zirconia in the presence of the nitride was the preclusion of the deleterious ZrN and ZrON phases. Previous work indicated that these phases could be precluded from the composite if the zirconia was pre-alloyed with sufficient stabiliser and also that the processing temperature was kept sufficiently low. The latter necessitated the powders to be hot pressed rather than pressureless sintered. The slightly reducing atmosphere experienced inside the hot press apparatus further suppresses any reaction of the oxide with the nitride.

The former stipulation - that is that the zirconia be pre-alloyed with the requisite amount of stabilising metal oxide - indicated that the use of 2 commercial TZP powders pre-alloyed with yttria and ceria would yield the most time effective results. The choice of yttria and ceria was based on mechanical property data available for TZP ceramics. The values of strength and fracture toughness for yttria- and ceria-doped TZP are higher than any other alloyed system. The requirement that the composite be hot pressed at the lowest possible temperature (to preclude unwanted phases) necessitated the use of liquid phase sintering aids such that full theoretical density could be attained. In a similar manner to the development of sialons, additions of alumina were predicted to react with the binary eutectic, created by a reaction of the oxide dopant (Y_2O_3 or CeO_2) and the surface silica layer always present on the silicon nitride powders, to form the familiar $Y_2O_3 - Al_2O_3 - SiO_2$ ternary eutectic glass, present in the form of a liquid at the sintering temperature. The generation of such a system was predicted to promote densification and ultimately produce a TZP - sialon matrix composite. Furthermore, the thermodynamic compatibility of the zirconia - sialon couple has been shown to be superior to that of the zirconia - silicon nitride couple (see section 5.1).

The research objective for this programme was to generate a silicon nitride ceramic with enhanced fracture toughness via incorporation of zirconia toughening agents. To meet this general objective, zirconia - sialon composites were fabricated with differing volume fractions of the second phase - zirconia. The subsequent variation in mechanical properties, phase evolution and microstructure of the range of composites investigated were later compared and discussed.

5.3 Experimental Techniques

$\alpha - Si_3N_4$[1], and either $3Y - TZP$[2] or $13Ce - TZP$[3] giving a final composition 10, 20 and 30vol.% zirconia, were dry mixed with 2wt.% $\alpha - Al_2O_3$[4] sintering aid, and attrition milled in distilled and deionised water using Tetragonal Zirconia Polycrystalline

---

[1] Ube Industries, Japan

[2] TS-3, TSK, Tokyo, Japan - prereacted with 3mol.% Yttria in solid solution

[3] UNITEC - prereacted with 12mol.% Ceria in solid solution

[4] Alcoa alumina, grade xx

(TZP) milling media. The suspension was spray dried to a fine powder which was subsequently hot pressed using a conventional graphite susceptor induction furnace and hydraulically operated ram. The hot pressing was carried out at a temperature of 1700°C $\pm 5°C$ at a pressure of 22±2MPa in a slightly reducing environment.

The hot pressed discs were cut, ground and polished for X-Ray Diffraction (XRD) analysis and Scanning Electron Microscopy (SEM) in the conventional manner (chapter 4.4 & 4.5). Thin discs were prepared in the manner described in chapter 4.6 for Transmission Electron Microscopy (TEM). The densities of all composites were measured using the standard Archimedes immersion method in deionised & distilled water. The fracture toughness was measured using a 4-point single edge notched beam (SENB) rig with SiC knife edges (chapter 4.7) at room temperature and also at 800°C, the temperature at which tetragonal zirconia becomes the thermodynamically stable polymorph and so will no longer transform to the monoclinic phase.

Vol%ZrO_2	ρ/ρ_{th} – %	Vol%ZrO_2	ρ/ρ_{th} – %
10%Y	99.1	10%Ce	99.9
20%Y	98.2	20%Ce	99.0
30%Y	96.0	30%Ce	97.8

Table 5.1: Hot pressed densities / theoretical density, all values ±1%

5.4 RESULTS

5.4.1 Composite processing and phase evolution

All the samples were hot pressed to >96% of their theoretical density, (table 5.1).

The rate of linear densification was plotted against time and temperature for each composition, calculated *using instrumentation fitted to the hot pressing apparatus* and associated computer analysis (see chapter 4). The graphs in figures 5.1 illustrate the marked differences in the temperatures at which the onset of linear shrinkage occurs. Further analysis indicates that three separate regions exist indicated on the sintering maps: an initial rapid rate of sintering occurring at temperatures which increase with a decreasing volume fraction of zirconia; a second peak in linear shrinkage which does not change significantly with composition; and a third plateau region occurring at the hold temperature of 1700°C.

The graphs depicted in figures 5.2 and 5.3 illustrate the differences observed in the hot pressing kinetics for both sets of composites.

The crystalline phase content of the Y-stabilised zirconia composites (named Y-

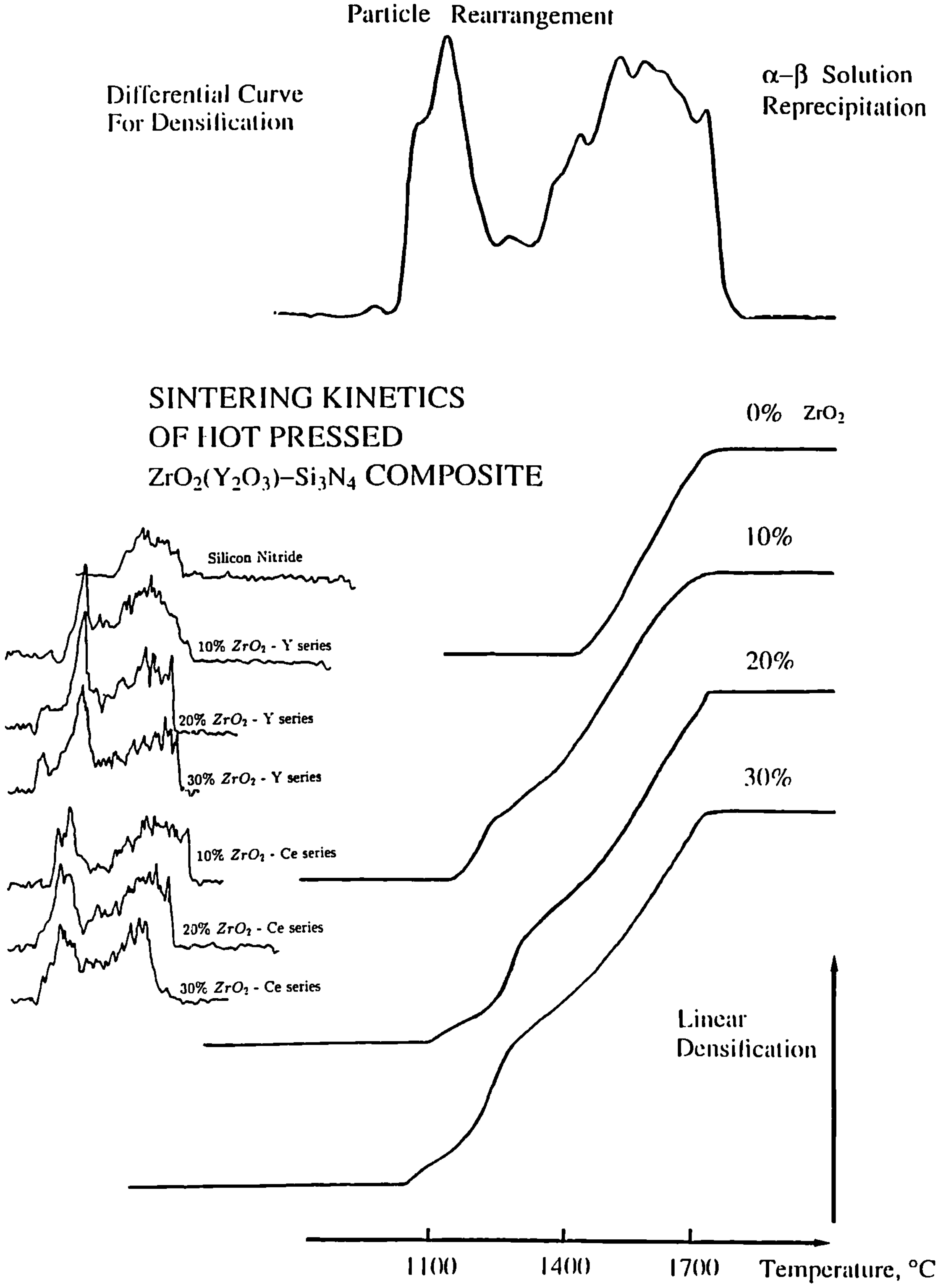

Figure 5.1: Hot Pressing Kinetics as a Function of Temperature and Time Illustrating Changes in the Onset of Sintering with Composition

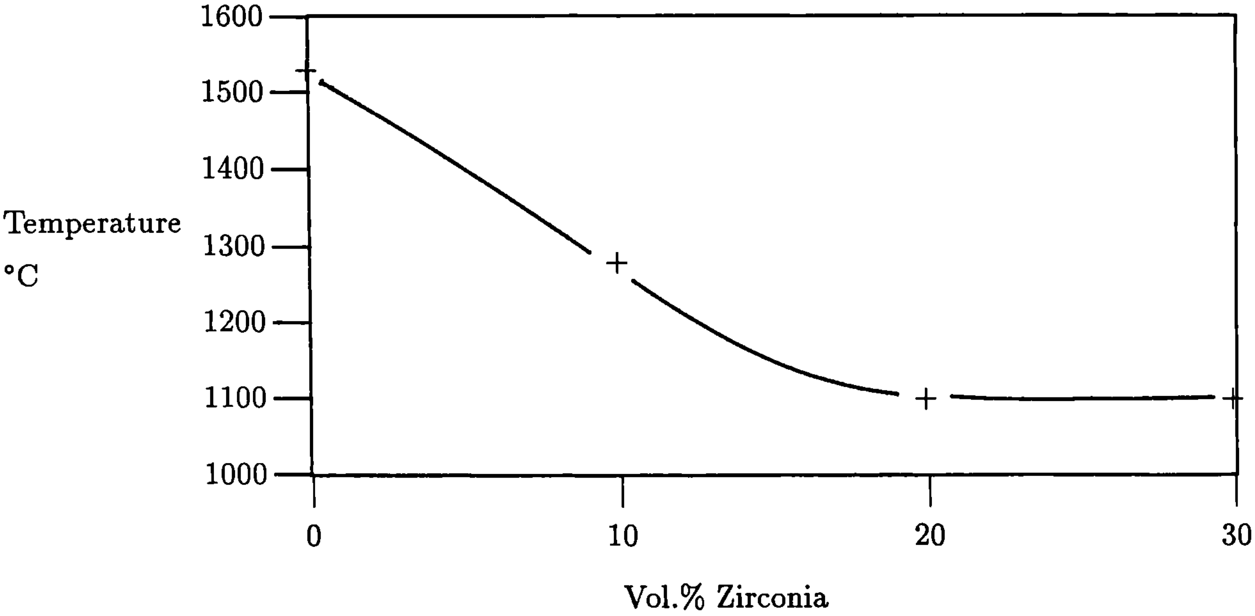

Figure 5.2: Initiation of Sintering Measured as a Function of Volume Fraction Zirconia Additive for Y Series

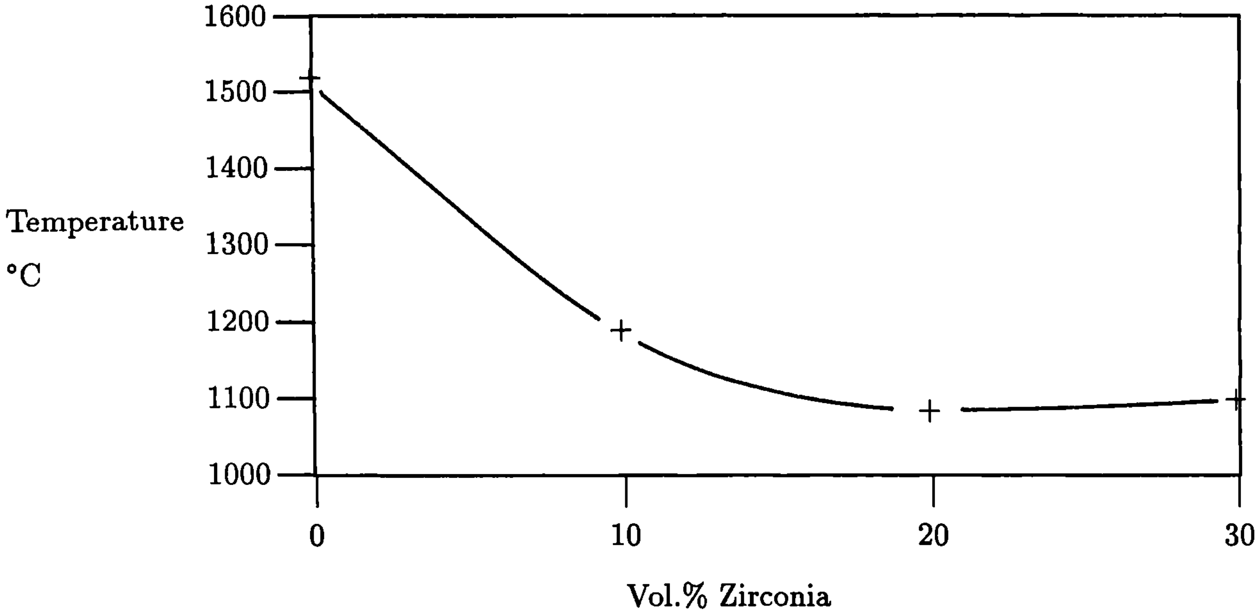

Figure 5.3: Initiation of Sintering Measured as a Function of Volume Fraction Zirconia Additive for Ce Series

series), figure 5.4, was typified by the presence of both the α and β polymorphs of silicon nitride and the tetragonal and cubic polymorphs of zirconia. The respective ratios for these phases and for the volume fraction of the tetragonal phase of zirconia are also indicated in figure 5.4.

The crystalline phase content of the Ce-stabilised zirconia composite series (Ce-series) is indicated in figure 5.5. The ratio of α/β silicon nitride and the composite volume fraction of monoclinic zirconia are plotted as a function of increasing zirconia level alongside the diffraction trace. The remaining zirconia phases in the Ce-series are the tetragonal and cubic polymorphs.

In the Y- and Ce-series the duration and the temperature of the hot pressing cycle were clearly insufficient for the complete transformation of the α to $\beta - Si_3N_4$. Furthermore, in both systems, the presence of silicon oxynitride (Si_2O_2N) was noted, whilst the deleterious ZrN/Zr-oxynitride phases were not detected in any of the compositions.

5.4.2 Microstructural Evolution and Microscopy

Features common to both systems (Y- and Ce-series) were the fine grain structure, no observable porosity and the homogeneous distribution of the zirconia phase indicated in the backscattered SEM micrographs of figure 5.6. The average particle size of the zirconia was $\sim 0.8\mu m$ for the Y-series and $\sim 1.0\mu m$ for the Ce-series, and that

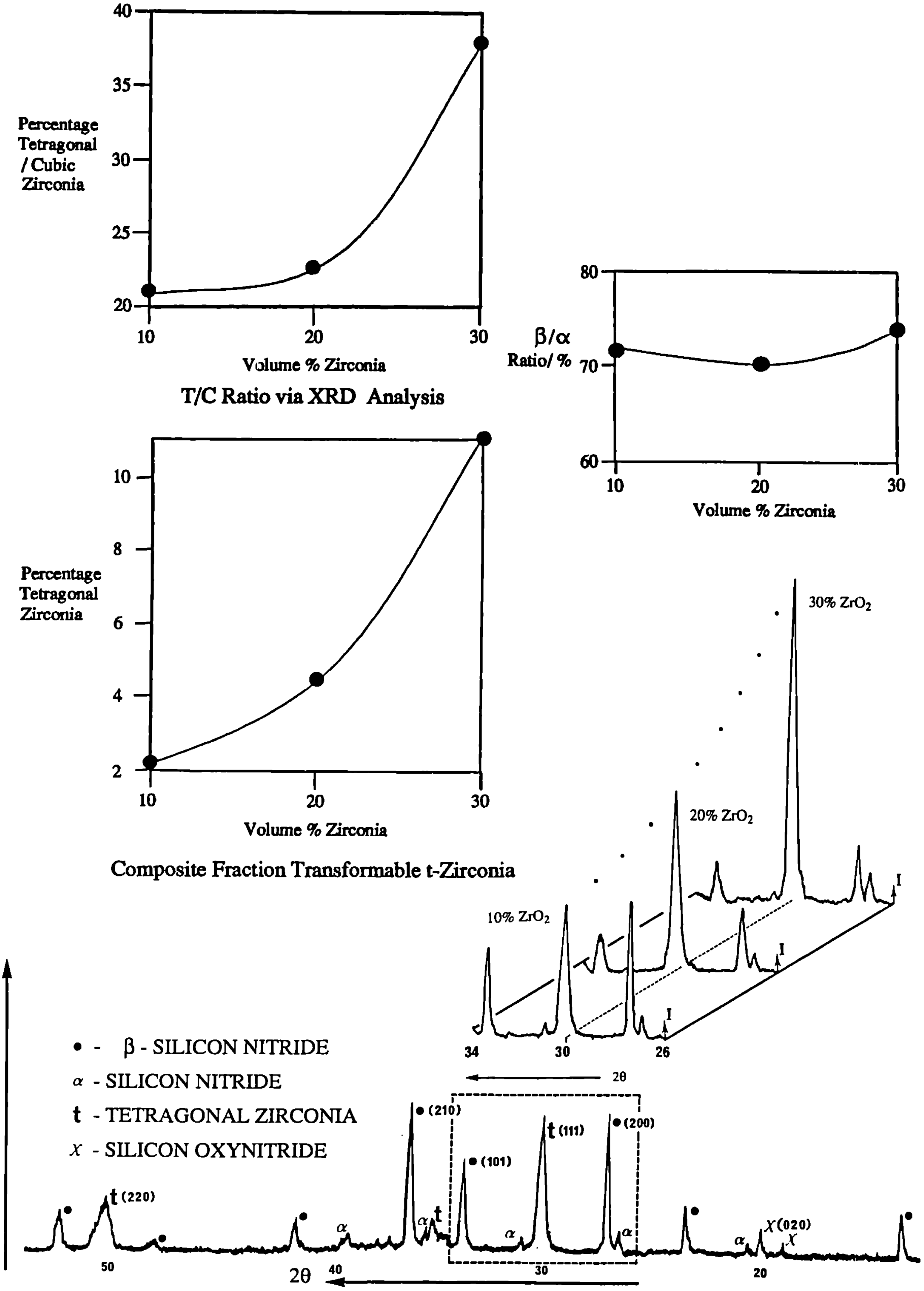
T/C Ratio via XRD Analysis

Composite Fraction Transformable t-Zirconia

Figure 5.4: XRD and phase content of Y-series - see text

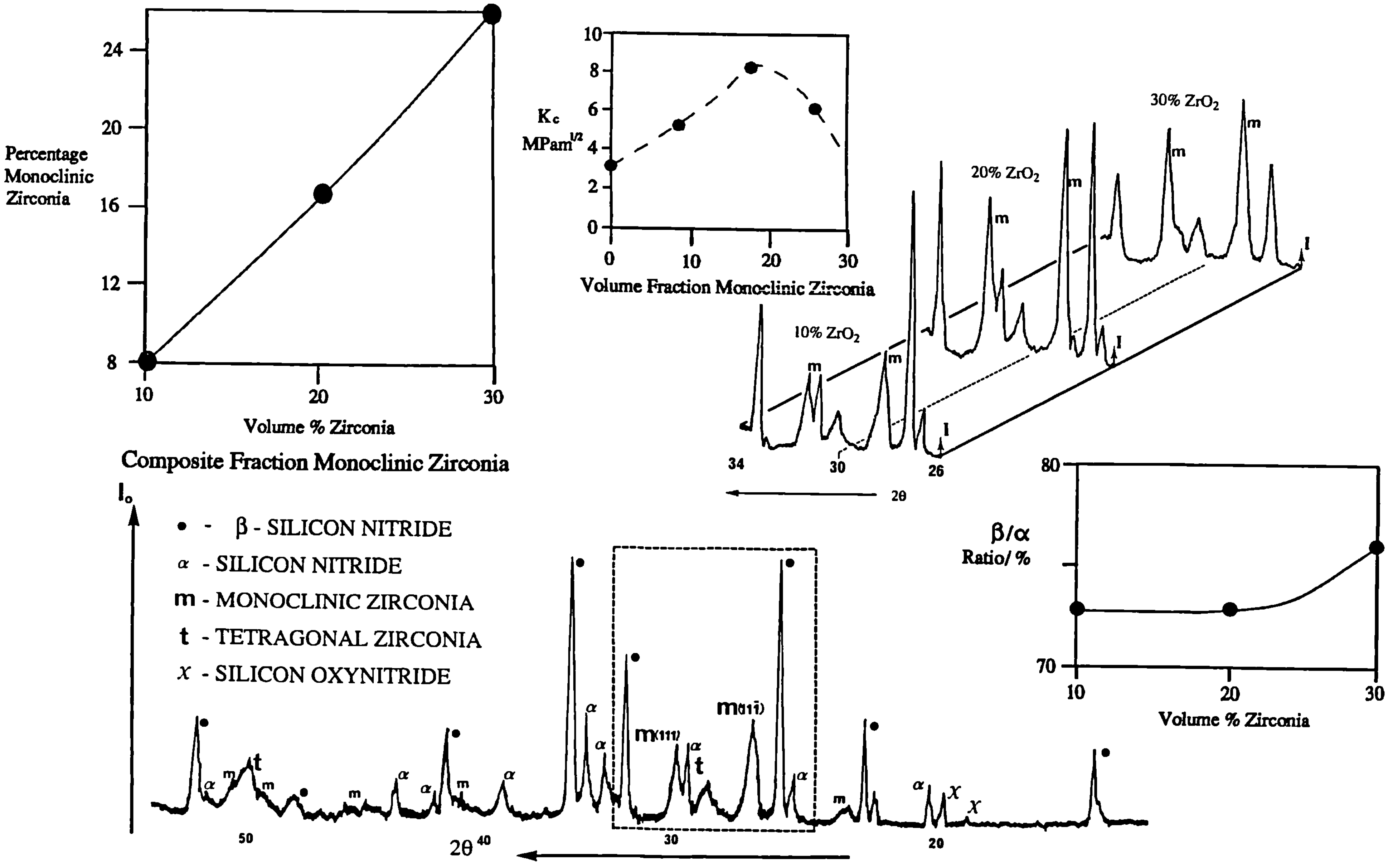

Figure 5.5: XRD and phase analysis of Ce-series - see text

for the silicon nitride $\sim 1 - 2\mu m$ with an aspect ratio ranging from 1:1 to 3:1. An additional feature for both the Y- and Ce- series was the observation of an intergranular phase surrounding the silicon nitride and zirconia grains, with a backscattered contrast midway between the zirconia and silicon nitride. This intergranular phase was especially pronounced for the Ce-series.

Yttria Series Composites - Microstructure

These features are further exemplified by the TEM images in figure 5.7. The Y-series consisted of uniformly sized tetragonal ZrO_2 grains of average composition indicated via the X-ray (EDS) spectra, figure 5.7b, and the substituted β' silicon nitride (SiAlON), often observed as lenticular, faceted, grains. The zirconia grains appear dark and, often, irregular in shape. The latter has previously been observed [99] with evidence suggesting that some zirconia grains participated in the formation of a liquid phase and thus partially acted as a sintering aid (this was first observed by Rice et al [83]). Several large grains identified via electron diffraction as cubic zirconia and lenticular Si_2N_2O grains were observed, the latter often characterised by the appearance of lattice defects such as stacking faults (figure 5.7c). A thin grain boundary phase was identified in these composites, predominant at multiple grain boundary junctions. It was not possible to quantify the composition of the minor intergranular phase using EDX analysis. The elemental components constituting

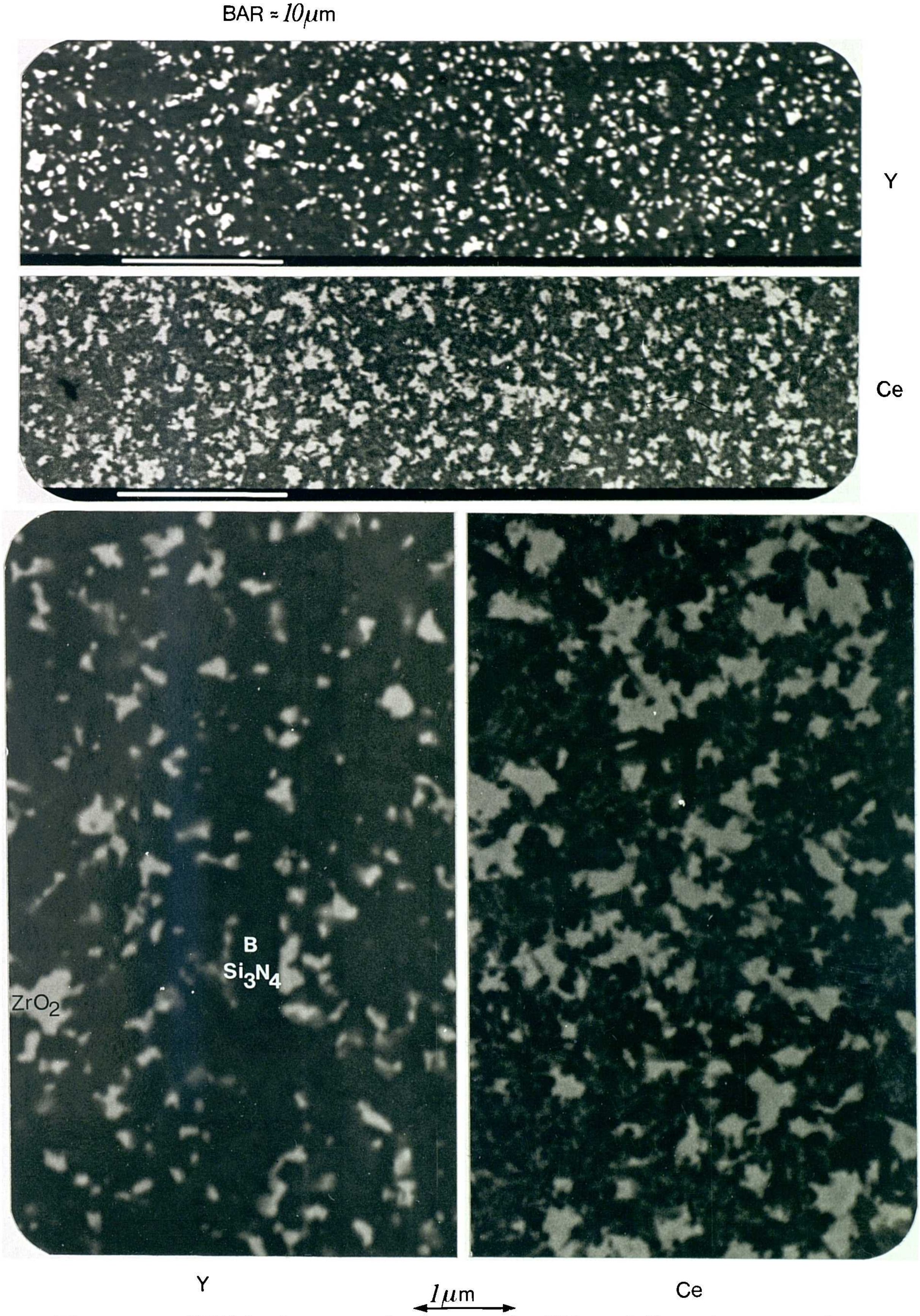

Figure 5.6: SEM backscattered micrograph of Y- and Ce-series composites.

the grain boundary phase were qualitatively determined using EDAX as Si, Al and Y, figure 5.7b.

Ceria Series Composites - Microstructure

The Ce-series showed marked differences in microstructural evolution to the Y-series of composites, exemplified in the TEM micrographs in figure 5.8 a,b,c.

The majority of the zirconia was in the unstabilised monoclinic structure, with an average grain size of $\sim 1\mu m$. Monoclinic zirconia is often characterised in the TEM by the observation of microtwinned lamellar crystals, a feature noted for all the Ce-series composites. A large amorphous grain boundary phase surrounded the silicon nitride and zirconia grains with an average composition (63%Ce-25%Si-7%Al-5%Zr, all ±5%). Furthermore, the majority of the zirconia grains contained less than 1wt.% Ce indicating that the majority of the ceria had diffused out from the precursor solid solution zirconia and dissolved in the surrounding sintering liquid. There are indications, however, that the Ce-stabilised zirconia actively took part in the formation of a liquid phase at the sintering temperature, creating a Zr & Ce-rich grain boundary silicate phase. During cooling the nucleation and growth of ZrO_2 occurring within the amorphous phase, figure 5.8c, would be accompanied by the simultaneous depletion of Zr present in the amorphous phase. The resulting zirconia polymorph would depend on stabiliser concentration and final particle size. Clearly

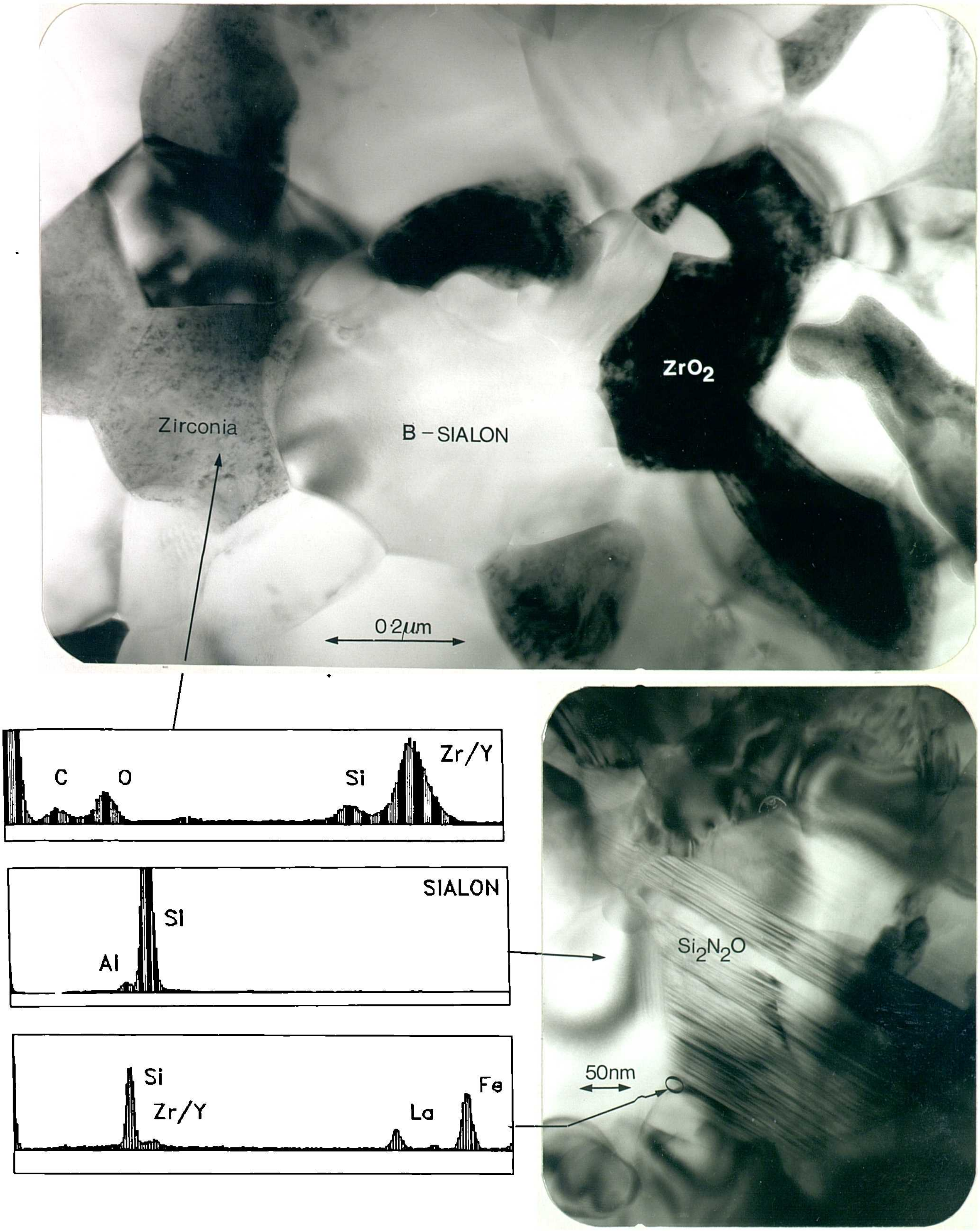

Figure 5.7: a) TEM micrographs of Y-series, b) EDX analysis and c)Presence of Si_2N_2O characterised by stacking faults.

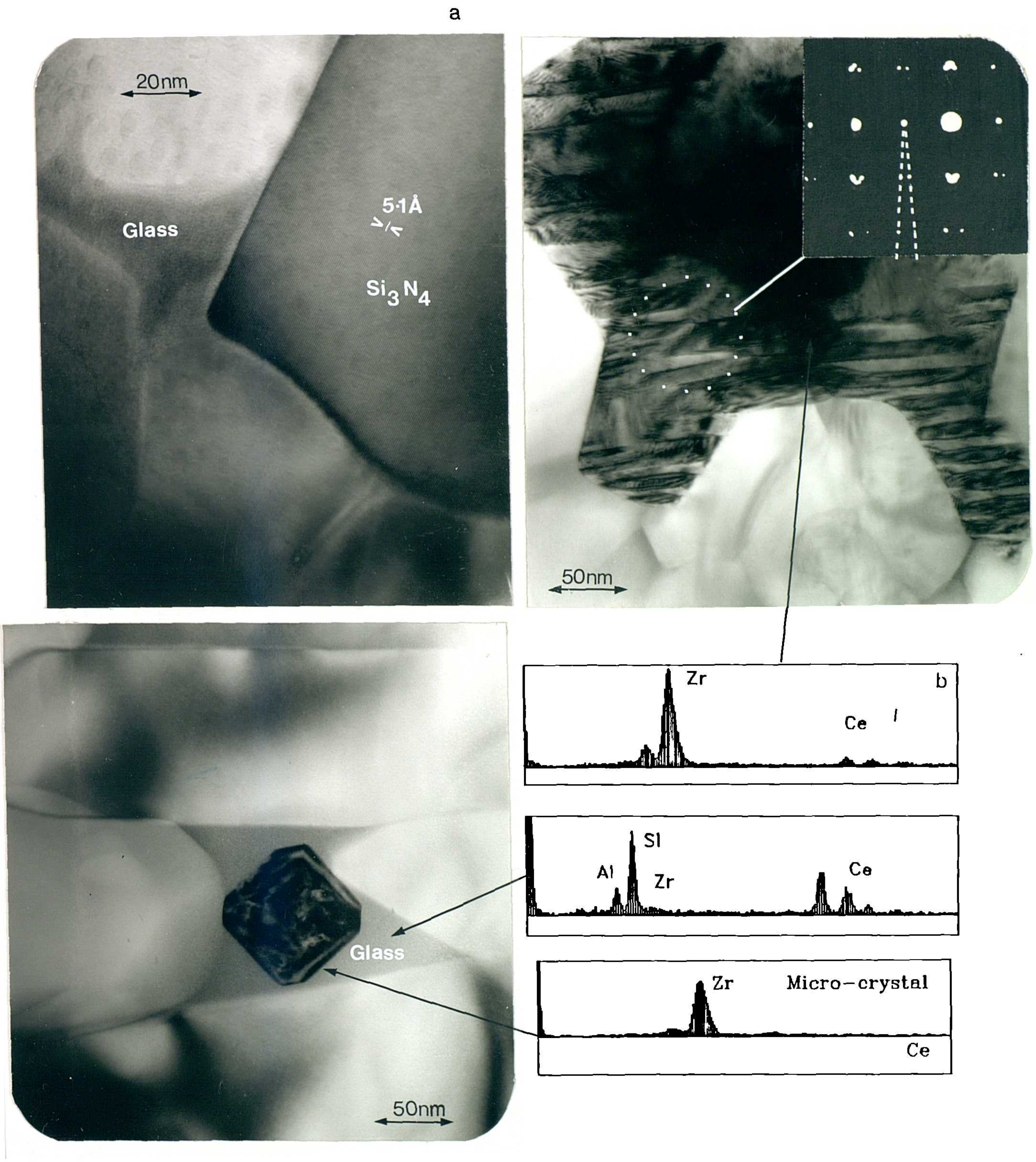

Figure 5.8: a)TEM micrograph of Ce-series with inset twinned monoclinic grain, b) EDX analysis and selected area electron diffraction (SAED) of twinned monoclinic grain and c) Grain boundary phase surrounding sub-micron zirconia grain.

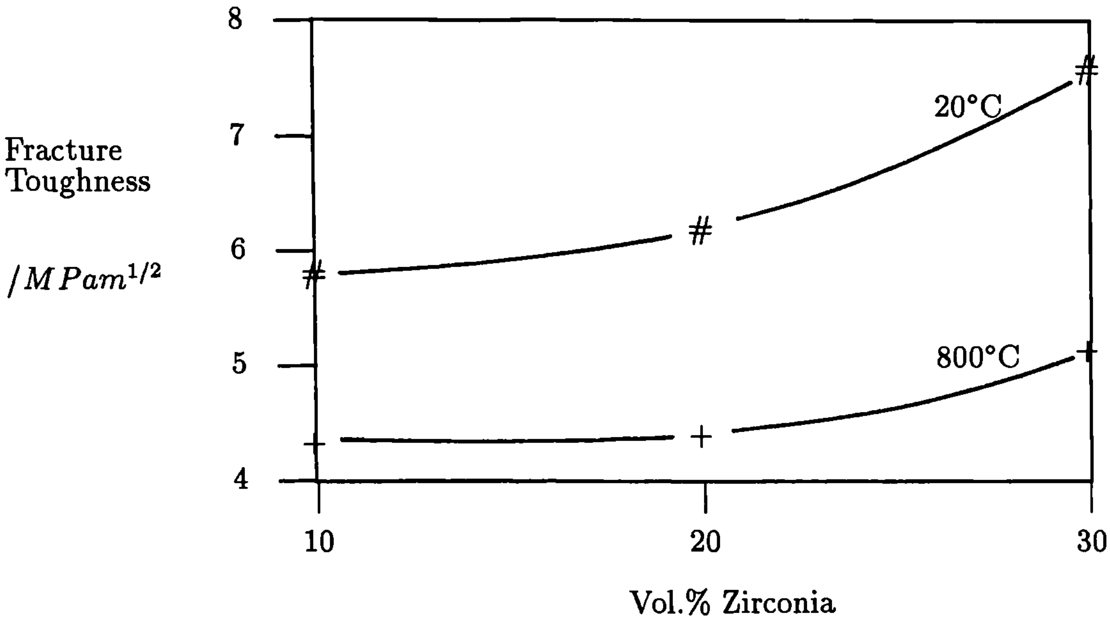

Figure 5.9: Fracture Toughness (Y-series) versus composition

the zirconia crystallite in figure 5.8c, indexed tetragonal by electron diffraction, was sufficiently small for the tetragonal structure to remain stable at room temperature even with such a low level of Ce in solid solution.

5.4.3 Fracture Toughness Evaluation - Y and Ce Series

The fracture toughness for both series of composites was measured at room temperature (25°C) and at 800°C, figure 5.9 & 5.10.

The fracture toughness of a hot pressed silicon nitride was also measured and found to be $3.1 \pm 0.1 MPam^{1/2}$ both at room temperature and at 800°C. The fracture toughness of a sialon material is normally higher than that for a hot pressed silicon nitride. This is normally attributed to toughening increments conferred by the

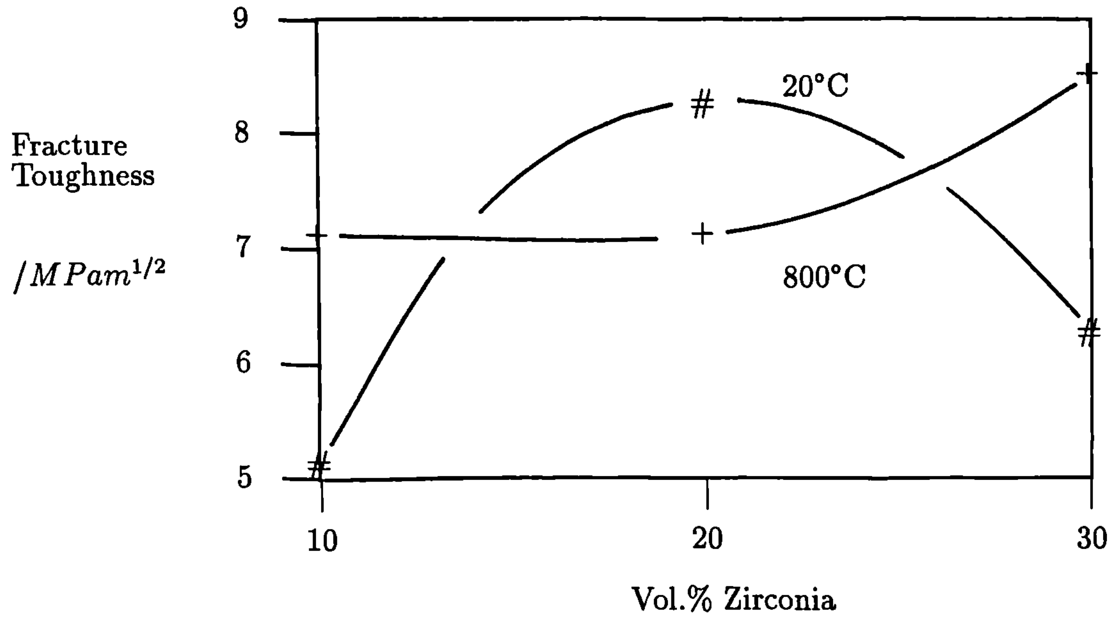

Figure 5.10: Fracture Toughness (Ce-series) versus composition

evolution of an anisotropic grain structure which is attained through the pressureless sintering process, and hence is not directly comparable with the values obtained for the composites.

The fracture toughness of the Y-series increased with added zirconia at both room temperature and 800°C, but at a lower level for the high temperature.

A peak in the room temperature fracture toughness was observed in the Ce-series composites at a value of 20vol.% added zirconia. The fracture toughness measured at 800°C did not exhibit this maximum, with the measured values for the 10% and 30vol.% composites being greater than the respective room temperature values whilst that measured for the 20vol.% sample was lower. The error associated with each value was considerable, leading to an overlapping of the error bars associated

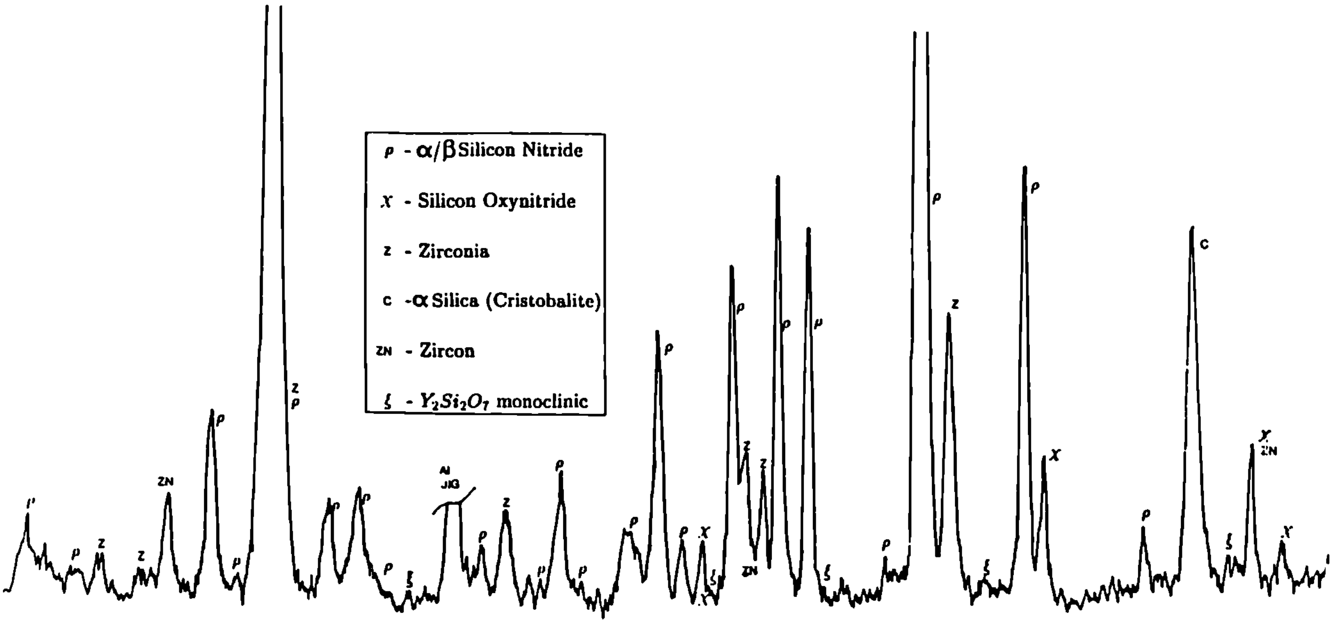

Figure 5.11: XRD Trace identifying oxidation products developed on the surfaces of Y-series composites heated to 1200°C for 10 hours.

with both temperatures for each composition.

5.4.4 High Temperature Stability in an Oxidising Environment

Analysis of the high temperature stability of the composites did not reveal the presence of the deleterious ZrN or Zr-oxynitride phases. Furthermore, no surface spalling, structural degradation or detectable weight gain was observed in any sample within the temperature range 800°C-1400°C for a 10hour exposure. Oxidation products consisted of varying amounts of cristobalite SiO_2, zircon and silicon-oxynitride as indicated in the X-ray diffraction trace, figure 5.11.

An additional minor phase was detected on the oxidised surfaces of the Y-series composites and identified as monoclinic $Y_2Si_2O_7$.

The oxide films developed during a 10 hour exposure in air at a temperature of

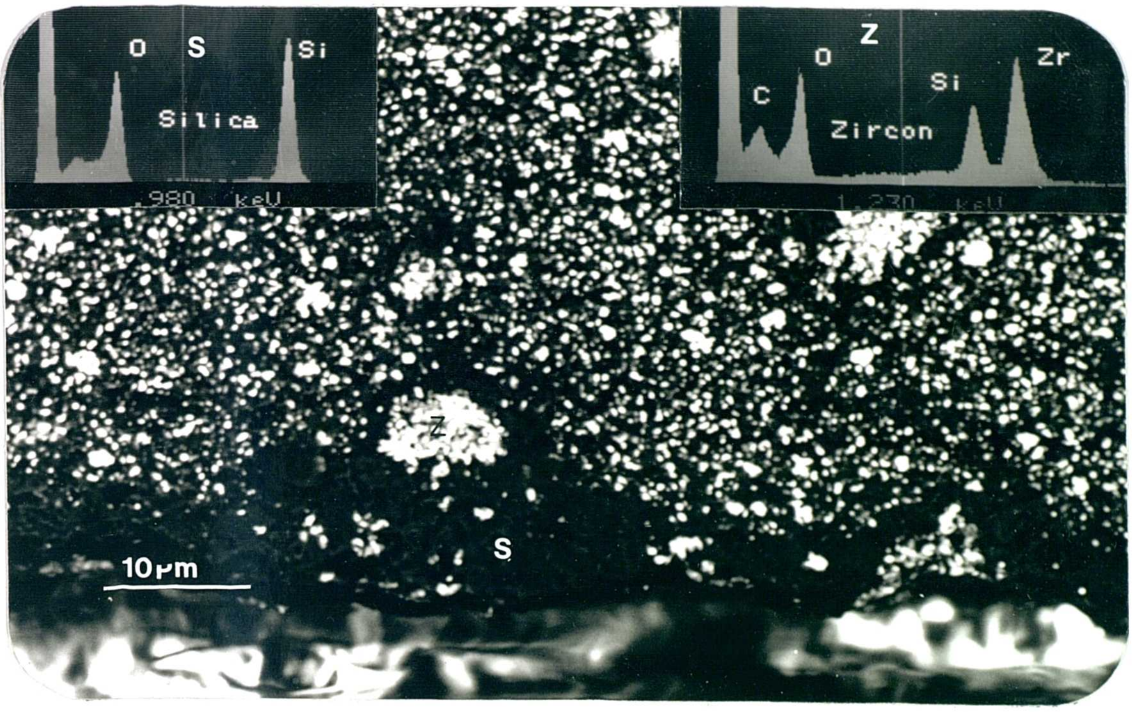

Figure 5.12: Scanning Electron Micrographs Depicting Features Common to the Y-Series Composites Following Oxidation at 1200°C for 10 Hours

1200°C are shown in the scanning electron micrographs, figures 5.12 & 5.13. The silica layer present on the surface of the yttria based composites has reacted with surrounding zirconia to form zirconium silicate (zircon via XRD). Further phases formed on the Y-series ceramics are identified via EDX analysis, figure 5.12. The presence of silica and zircon was also established on the oxidised surfaces of the Ce-series of composites. Both systems had developed oxide crusts of between 4-20μm at the exposure indicated in figures 5.12 & 5.13.

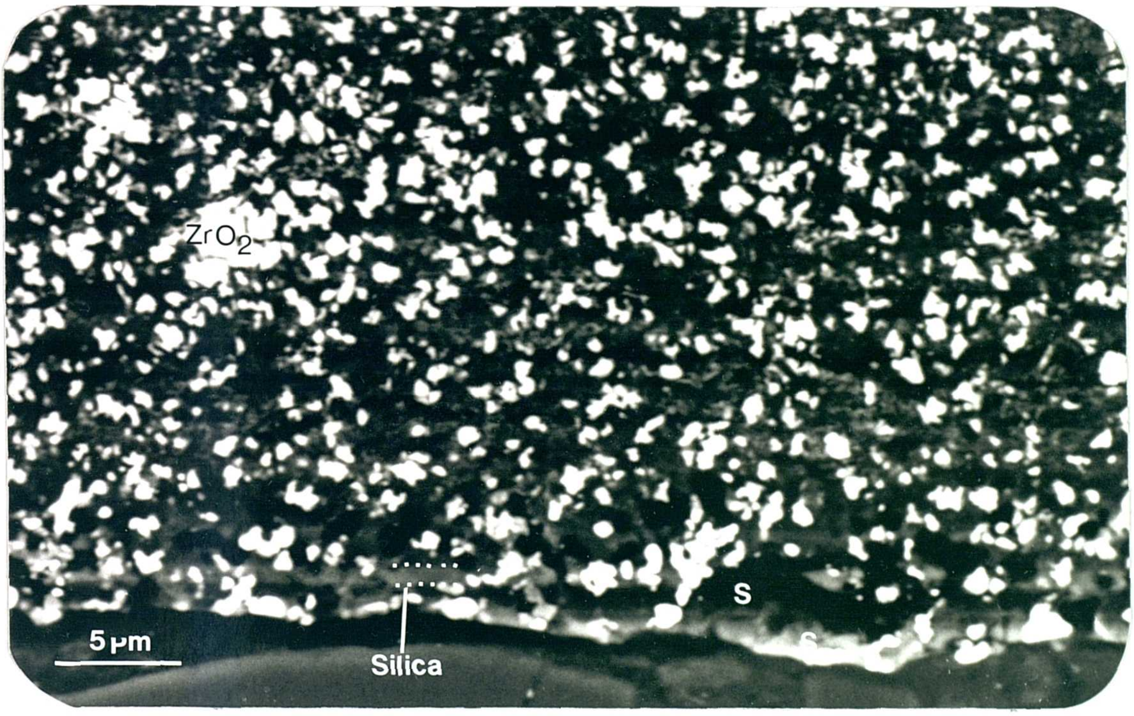

Figure 5.13: Scanning Electron Micrographs Depicting Features Common to the Ce-Series Composites Following Oxidation at 1200°C for 10 Hours

5.5 DISCUSSION

5.5.1 Densification and Microstructural Development

Studies concerned with the hot pressing kinetics of the composites identified three stages of shrinkage or densification;

1) initial particle rearrangement within a sintering liquid generated from a reaction between the added alumina, yttria/ceria and surface silica always present on the α grains and, at a higher temperature,

2) the simultaneous solution of the αSi_3N_4 and reprecipitation of the β silicon nitride grains within the interstitial liquid phase.

3) a final plateau densification rate synonymous with particle coalescence and possibly solid state sintering.

This process has been well studied and is, in some ways, similar to the Kingery model of liquid phase assisted sintering (but see chapter 2.1). In the systems studied, however, even more complex reactions occurred, due to the presence of aluminium as the oxide additive, which partitioned to generate the substituted form of βSi_3N_4 named β'Si-Al-O-N having general composition, $Si_{3-x}Al_xO_{4-x}N_x$ with 0-x-4.2. The β' form (structurally similar to β) has been shown to exhibit superior thermodynamic stability with zirconia [84].

Yttria-Series Composites

The microstructural evolution of the yttria doped series of composites can be understood from analysis of the densification kinetics and subsequent X-ray traces. The zirconia was observed to be present predominantly in the tetragonal form, although a minor amount was stabilised in the cubic polymorph and, some, unstabilised as the monoclinic variant. The silicon nitride was observed to be in the β form by XRD and later identified as a Sialon via EDAX analysis in the SEM. The sialon grains surrounded the zirconia grains often appeared as lenticular and faceted, whereas the zirconia often had a rounded morphology. A small grain boundary phase was identified via SEM and TEM and determined as amorphous in nature and located characteristically at multiple grain boundary junctions. The zirconia, additionally took on a mottled appearance, similar to that found in TZP ceramics. The pertinent results cited above are believed to account for the following description of phase evolution in the Y-doped series of composites.

The phase evolution can best be described with reference to the stages of densification described in sections 5.4.1 and 5.5.1, which are now listed:

- initial particle-particle sliding within the pressed powders to achieve enhanced packing densities. No significant densification occurs till the grain boundary liquid phase evolves - the temperature at which this occurs depended on the volume fraction zirconia.

- liquid phase assisted sintering acting in parallel to a partial solution of zirconia creating the observed rounded zirconia grain morphology.

- the third region of rapid densification occurring due to the simultaneous solution of αSi_3N_4 and reprecipitation of βSi_3N_4 in the presence of the liquid phase. The transformation would be time and temperature dependent. An incomplete transformation was observed in all composites indicating that the pressing temperature or the pressing time was either not high enough or not long enough respectively.

- a final plateau region already amply discussed in the preceding section.

Ceria-Series Composites

Similarly, the phase evolution corresponding to the Ce-series composites can best be described with reference to the stages of densification described in sections 5.4.1 and 5.5.1, listed below:

- the initial particle rearrangement, previously described above.
- the generation of a liquid phase at a temperature depending on the volume fraction of zirconia, with the simultaneous depletion of the dopant CeO_2 from solid solution with the zirconia. The grain boundary phase was considerably amplified due to the high dopant level necessary to stabilise the tetragonal form to room temperature. At this temperature, the zirconia was probably within the tetragonal phase field.
- the $\alpha - \beta$ solution - reprecipitation process occurring within the enhanced liquid phase has already been described above.
- the final densification process (vis a vis coalescence and solid state densification) has also been amply described.

- On cooling from the hot pressing temperature, the zirconia evidently absorbs little or no ceria from the surrounding amorphous phase and thus is left in an unstabilised form at room temperature and observed as the twinned monoclinic variant via XRD and TEM. At this stage there is no evidence to suggest whether the high temperature tetragonal zirconia transformed to its monoclinic variant either before or after the liquid phase solidified; this matter will be discussed in more detail in succeeding sections.
- The presence of small faceted tetragonal zirconia grains within regions of zirconia and ceria rich liquid was observed via transmission electron microscopy. Clearly, such supersaturated regions existed at the hot pressing temperatures indicating substantial solubility of the zirconia within the sintering liquid phase.

General Microstructural Observations

The ZrN or Zr-oxynitride phases are distinguished from cubic ZrO_2 by the detection of additional, very weak, reflections in the X-ray diffraction pattern. Positive identification of such phases was not possible, and indirect evidence for the existence of these deleterious phases was sought via high temperature stability analysis. The instability of the nitride and oxynitride phases of zirconium, at temperatures in excess of 800°C, leads to the oxidation to monoclinic ZrO_2 with an accompanying volume expansion. This, in turn, leads to a structural degradation of the composite observed either as surface spalling or a complete disintegration of the ceramic. Since this was not observed, it follows that the Zr-O-N phases were not present in the two series of composite.

5.5.2 Fracture Toughness at Room Temperature and 800°C

Y-Stabilised Composites

The increase in the retention of transformable tetragonal phase of zirconia, figure 5.4, measured as a function of overall crystalline phase composition in the Y-series, was paralleled by a corresponding increase in its fracture toughness. The enhanced values of fracture toughness are attributed to the martensitic tetragonal - monoclinic transformation of zirconia in the vicinity of the stress field of a propagating crack. The contribution to the fracture toughness arising from this phenomena is expected to decay as the temperature is increased to a value T_{ms}, the tetragonal-monoclinic martensitic start temperature (~800°C). At this temperature the driving force for transformation no longer exists and the tetragonal ZrO_2 becomes the thermodynamically stable polymorph (chapter 3). The fracture toughness, measured at 800°C, was consistently lower for each composition as expected from the above discussion, indicating that stress induced transformation toughening was the dominant toughening mechanism operating in these composites.

Ce-Stabilised Composites

The interpretation of the fracture toughness data of the Ce-system is more complex. A substantial partitioning of the cerium from zirconia solid solution to a grain boundary glassy phase left the majority of the zirconia in an unstabilised form. As the composite cooled the resulting matrix constraint imposed on the tetragonal zirconia further reduced the t-m transformation temperature. Two mechanistic models are proposed to explain the enhanced levels of fracture toughness observed in these composites. The first is based on the concept of microcrack toughening (see chapter 3.3.1).

MODEL1

It is assumed in the first model that the net tensile stresses associated with the t-m transition could not be *completely relieved* by viscous and plastic flow of the surrounding glass (T_g of the matrix glass is expected to be approximately 800-900°C). The volume expansion and shear strain associated with the onset of the t-m transformation would thus result in the generation of microcracks in the surrounding compressive matrix, with the resulting strain energy of transformation being minimised by the occurrence of a micro-twinned structure. Twinned monoclinic zirconia was a feature common to all the Ce-series composites. A similar scenario is observed in zirconia toughened aluminas (ZTA) [100,101] where the zirconia is present in the unstabilised monoclinic form dispersed in an alumina matrix. On cooling from the sintering temperature the t-m transformation occurs, accompanied by a volume expansion of 3-5%. The tensile stresses that develop in the material generates a high density of microcracks, which can act as an energy dissipation mechanism for propagating cracks.

The fracture toughness curves for the Ce-series exhibit a distinct maximum before dropping quickly with further increase in zirconia volume fraction. In this first model the increase is attributed to an increase in the density of microcracks and the decrease due to the interaction of microcracks between the zirconia particles. A further parallel can be made to the ZTA composites previously mentioned. The maximum in K_c for the ZTA composites was reported to occur at ~15vol.%ZrO_2(m) with an average zirconia grain size of ~1.5μm. If a graph of fracture toughness is plotted against total monoclinic content for the three compositions, figure 5.5, then a maximum in K_c is observed at ~18vol.%ZrO_2(m). The average grain size of the zirconia and silicon nitride are approximately equal to the corresponding grain sizes of the zirconia and alumina respectively in ZTA composites. It follows, by analogy, that the toughening mechanisms operating within the $Si_3N_4 - ZrO_2(Ce)$ composites are similar to those operating in the ZTA system, e.g. microcrack opening, subcritical crack propagation and crack branching in the vicinity of the stress field of a propagating crack front.

MODEL 2

The second model is, in many ways, similar to the first. The essential difference lies in the crack energy absorption mechanism attributed to the dispersion of monoclinic zirconia. It is assumed in this model that the tetragonal - monoclinic transformation occurred at a temperature above the glass transition temperature (T_g); e.g. where the grain boundary phase was still in a viscous, liquid state. The resultant shear strain and volume dilation associated with the transition could then be accommodated and absorbed by viscous and elastic grain boundary phase deformation. Upon further cooling, the grain boundary liquid phase solidifies to a glassy intergranular network, and, thus, can no longer absorb the strain associated with the difference in the linear thermal expansion coefficients of silicon nitride and zirconia. The resulting stress would be a net tensile component acting within the zirconia particles $(\alpha_{m-ZrO_2} \approx 7X10^{-6\circ}C, \alpha_{Si_3N_4} \approx 3X10^{-6\circ}C)$. The final situation, at room temperature, would then be a composite composed of a dispersion of monoclinic zirconia stressed in tension surrounded by a Sialon matrix. It is expected that the stresses generated within the zirconia would exceed the bonding strength between grains leading to grain boundary debonding and possibly the initiation of radial microcrack development within the matrix. The passage of a crack front throughout such a composite would be halted or at least hindered by such stress zones either through a crack bifurcation/blunting mechanism or via the energy absorbed during subsequent grain boundary debonding.

The high temperature fracture toughness of the Ce-series composites did not exhibit the peak observed at room temperature. If the dominant toughening agent operating in these composites is assumed to be based on a microcrack type mechanism, then it follows that, since monoclinic zirconia is the stable polymorph to a temperature of $\sim 1100°C$, the fracture toughness of the composites measured at $800°C$ is not expected to deviate significantly from the room temperature values. This, however, was not observed, with the fracture toughness of all three compositions (10%, 20%, 30% ZrO_2) being approximately equal and having a value of about the average of the room temperature values. Clearly the 'microcrack energy absorption mechanism' is not fully applicable at this temperature and other energy absorption mechanisms must be sought. Possible mechanisms based on crack healing via plastic flow and plastic deformation of the glassy intergranular phase may be operational at these elevated temperatures. For example, in fine grained aluminas an apparent increase in the fracture stress is observed at around $800°C$. This increase is associated with plastic effects due to the intergranular glassy phase, e.g. the viscosity of the glass (which increases with increasing temperature) permits a localised reduction of stress near the tips of critical cracks [102]. At even higher temperatures grain boundary sliding is initiated and becomes the dominant failure mechanism. A similar effect is observed in some silicon nitride ceramics where an initial increase in K_c is observed at elevated temperatures, typically over 900°C, followed by a decrease in K_c with increasing temperatures [6]. The mechanisms responsible for this transient increment are similar to those described above for the alumina ceramics. It is suggested that the increase in fracture toughness observed in the Ce-series range of composites is due to a similar pseudo-plastic stress relief mechanism. Additional evidence originates from the slight increase in K_c as the volume fraction of zirconia (and hence glassy phase) increases.

A similar explanation can be sought if the toughening mechanism is assumed to be based on the second model, i.e. the difference in thermal expansion coefficients producing regions of tensile stresses and/or grain boundary microcracking. As the temperature approaches T_g relaxation of the tensile stresses set up in the zirconia particles (due to the thermal expansion coefficient mismatch) occurs and so negates the effect of crack debond toughening. Further increments in temperature ultimately place the zirconia in a state of compression. This state of stress, however, would be relieved by the softening of the grain boundary phase as the temperature approached T_g. Clearly, both models can account for the observed values of fracture toughness measured at room temperature and at intermediate temperature.

The high temperature thermal stability of the hot pressed composites was typified by a gradual increase in surface SiO_2 (cristobalite) as a function of temperature. Other phases such as zircon and silicon oxynitride were observed on oxidised surfaces of all composites as expected from previous work [eg.88,89]. ZrN or Zr-O-N phases were not observed as an oxidation product on any surface indicating that the $ZrO_2 - \beta'$ Si-Al-O-N couple is stable with respect to the formation of the deleterious Zr nitride/oxynitride phases. This can be attributed to either the observed Al^{3+} content in the β' solid solution [89] or the Y^{3+} content in solid solution with the zirconia [99] which have been shown to suppress the reactions necessary for the production of such phases. The low level of porosity detected in all the composites would also suppress the formation of these nitride phases [96]. It is also expected that the silicate-cerium rich grain boundary phase present in the Ce series of composites would partially isolate the zirconia grains, thereby minimising detrimental reactions with the surrounding Si_3N_4 grains, and hence the generation of ZrN or Zr-O-N.

5.6 CONCLUSIONS

The generation of a fine grained, dense ZrO_2 toughened β' silicon nitride ceramic composite is possible via conventional hot pressing techniques. The microstructure and mechanical properties are dependent on the initial chemistry and especially on the type of stabilising additive pre-reacted with the zirconia. If 3 mol.% yttria is prereacted to form a solid solution with the zirconia then the tetragonal polymorph can be retained within the composite. The fracture toughness of these composites is enhanced and is proportional to the vol.% of retained tetragonal phase. The mechanism responsible for the increments in K_c is believed to be the stress-induced martensitic tetragonal-monoclinic transformation of zirconia in the stress field of a propagating crack. The high temperature fracture toughness measurements further augment this conclusion.

If the zirconia is prereacted with 13 mol.% ceria, however, the resulting microstructure and mechanical properties are markedly different from the Y-series. The salient microstructural features are a large grain boundary amorphous phase (5%) with the majority of the zirconia present in the unstabilised twinned monoclinic variant. The room temperature fracture toughness exhibits a maximum at a monoclinic fraction of 18vol.%, analogous to the fracture toughness observation in ZTA composites. Two mechanisms were suggested to account for the properties observed, 1) a microcrack toughening mechanism and 2) a mechanism reliant on the generation of tensile stress zones resulting from the thermal expansion coefficient mismatch between silicon nitride and monoclinic zirconia. The high temperature fracture toughness did not exhibit a maximum but remained at a relatively high level indicative of crack healing or localised stress relief at crack tips due to the presence of the amorphous grain boundary phase.

The detrimental Zr nitrides or oxynitrides were not observed either within the hot pressed samples or on oxidised surfaces indicating the thermodynamic stability of the $\beta' Si_3N_4 - ZrO_2(Y, Ce)$ couple.

Chapter 6

Evidence For Additional Toughening Mechanisms in TZP and Silicon Nitride - Zirconia Composites

6.1 Introduction

The relatively high values of fracture toughness and strength exhibited by many zirconia based ceramics are well documented. The mechanisms thought to be responsible for these impressive mechanical properties have already been discussed in some detail (see chapter 3) and arise from the dilatational (martensitic) transformation of metastable tetragonal zirconia to the thermodynamically stable monoclinic polymorph within the stress field of a propagating crack. Other toughening mechanisms such as microcrack toughening and surface compressive layers have also been shown to operate in many zirconia based ceramics.

The contribution to the fracture toughness from transformation toughening, however, decreases with increasing temperature up to a temperature of about 800°C, (T_{t-m}), when the tetragonal zirconia becomes the stable polymorph and so will no longer transform in the stress field of a propagating crack. A survey of the literature though identifies many instances where higher than expected values of fracture toughness have been observed at temperatures in excess of T_{t-m}. Furthermore, in many cases,[1] the high values of fracture toughness could not be correlated with the low levels of monoclinic zirconia analysed on the surfaces of fractured billets.

For example, the fracture toughness and flexural strength of single crystals of tetragonal zirconia (Y-PSZ) measured at temperatures in excess of 1100°C, remained approximately twice that of cubic stabilised zirconia [103]. Since the tetragonal - monoclinic transformation occurs at ~1000°C the observed increment was attributed to a crack-precipitate interaction[2] mechanism and was not considered a result of the

---

[1] Specific examples will be cited within the next few paragraphs

[2] A toughening effect resulting from the lattice, elastic and thermal expansion mismatch between the cubic matrix and tetragonal precipitates [103,104]

stress induced transformation toughening mechanism. The fracture toughness of yttria doped single crystals [105] of tetragonal zirconia was reported to be ~3X that of cubic zirconia and, again, was not considered to be a result of transformation toughening. Fractographic studies indicated that the toughening was induced by microcrack crack deflection along the {001} domain planes. The greater fracture toughness was attributed to the rough fracture mode (faceted on {001}) on PSZ as against smooth cleavage on {111} for FSZ [106].

Lankford demonstrated that YSZ single crystals exhibited two modes of toughening, depending on temperature. At low temperature, crack growth resistance was governed by crack-precipitate interactions as outlined before, and, at higher temperatures, deformation via plastic flow would dominate the mechanical properties producing an increment in the measured fracture toughness. The tetragonal - monoclinic transformation was not observed during compressive loading in any of the single crystals measured. Additional work on fine grained Y TZP [107] concluded that the high values of fracture toughness were not consistent with the low levels of monoclinic phase detected on fractured surfaces.

Recently, an additional toughening mechanism has been proposed by Virkar [33,108] and is based on a ferroelastic transition of the tetragonal zirconia in the presence of an applied external stress field. It was proposed that the ferroelastic properties of tetragonal zirconia would provide the required mechanism for absorption of mechanical energy [33]. X-ray diffraction analysis of polished, ground and fractured surfaces of Ce-TZP ceramics were cited as evidence for the existence of ferroelasticity in TZP [33] . Similar work relating to Y-TZP further substantiates the proposed hypothesis, and forms a section of this chapter. Additional evidence was afforded by Virkar in the form of stress-strain plots of Ce-TZP under compressive loading. A hysteresis was observed in the σ/ϵ plot with the occurrence of a residual strain when the material was unloaded, indicative of a ferroelastic material (see below).

6.2 Ferroic Transitions

A crystal is ferroelastic if it has two or more stable orientation states in the absence of mechanical stress and can be reproducibly transformed from one state to another by the application of mechanical stress [109]. By analogy to ferromagnetic and ferroelectric crystals a ferroelastic material is characterised by the existence of a permanent strain (ϵ_s) following compressive loading and a hysteresis between the applied stress and resulting strain, figure 6.1.

The area enclosed by the loop represents mechanical energy dissipated in a single compressive/tensile cycle. This energy absorption mechanism is thought to contribute to the materials fracture toughness.

In the case of tetragonal zirconia the two stable orientation states that are thought to be linked to the ferroelastic transition are sketched in figure 6.2. Appli-

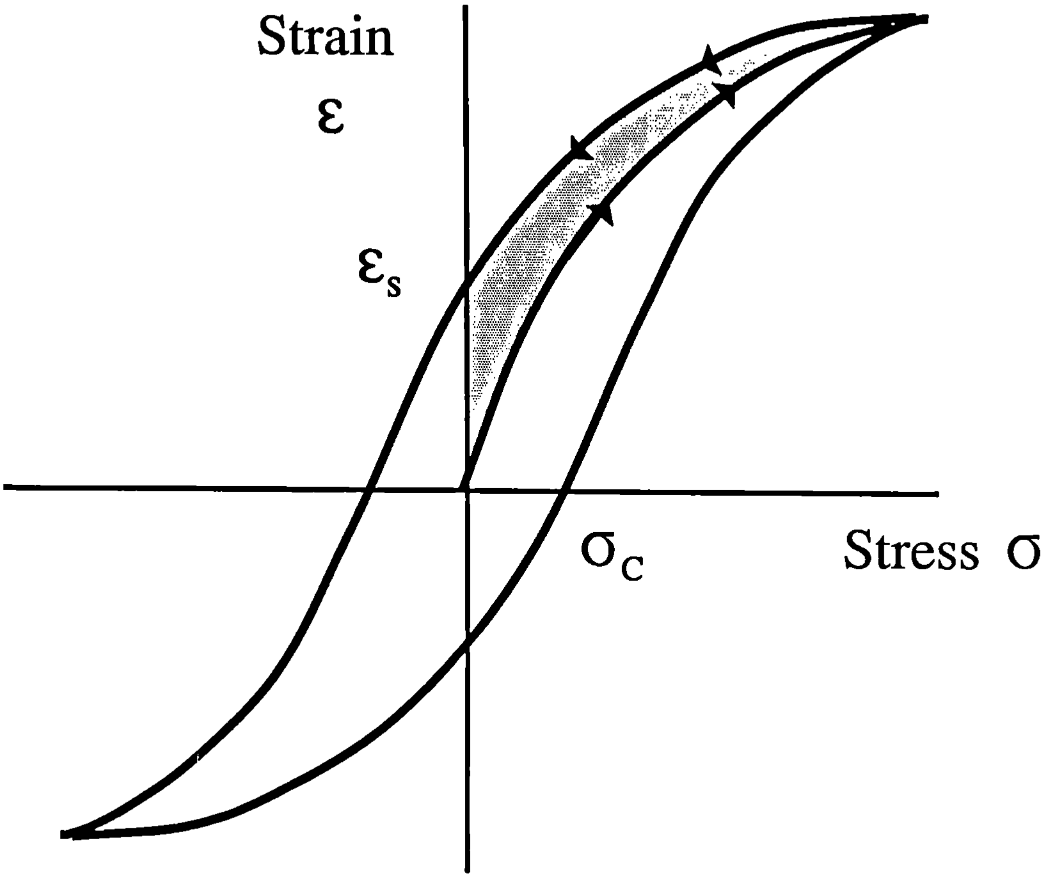

Figure 6.1: Hysteresis loop generated for one complete cycle in a ferroelastic material. σ_c is the critical stress required to initiate the transition.

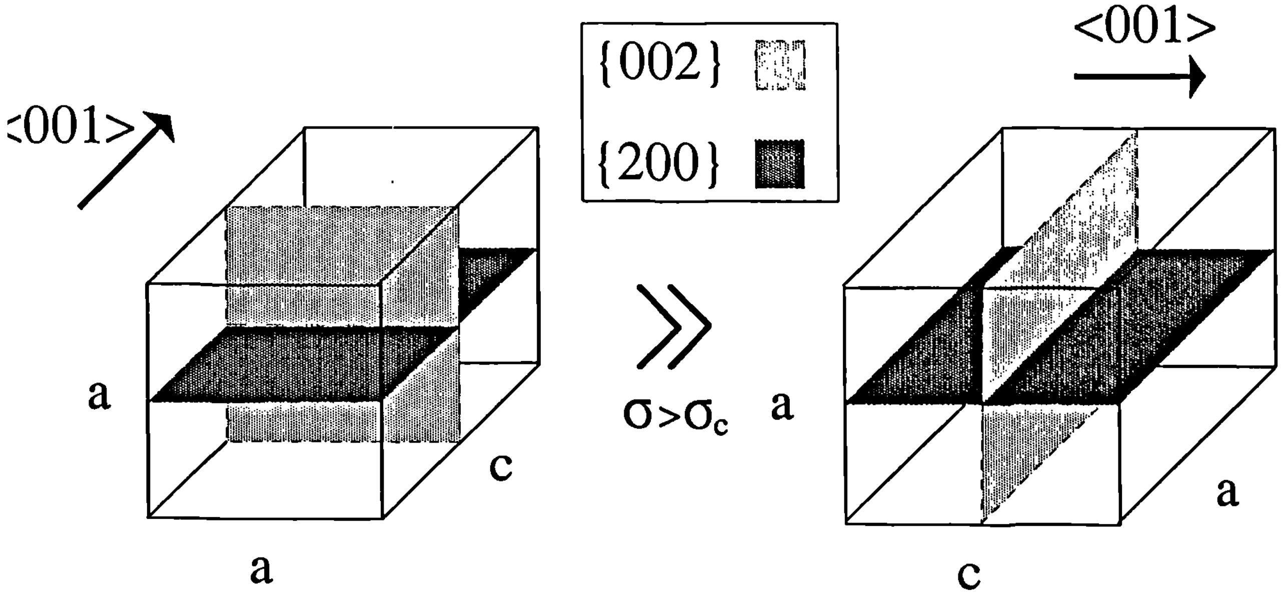

Figure 6.2: Crystallography of the ferroelastic transition. The [001] direction is essentially switched through 90°.

cation of a compressive stress in excess of the coercive stress σ_c (the stress required for ferroelastic transition to occur) along the c-axis of the tetragonal unit cell will transform it into an a-axis and conversely the a-axis into a c-axis. This effectively results in a rotation of the [001] direction through 90°.

A direct indication of this ferroelastic transition can be accomplished by analysing the relative intensities of the x-ray diffraction peaks of the (002)/(200) doublet and the (113)/(131) doublet [33] of TZP ceramic. The relative intensities of the (200) and the (002) planes can be determined from considering the relevant multiplicity factors and the corresponding structure factors. The structure factors, F, are approximately the same but the multiplicity of the 00l Laue group [001] is 2 whereas the h00 Laue group [200] is 4. The intensity of a given reflection is given by equation 6.1:[108]

$$I = p|F|^2 \left(\frac{1 + cos^2(2\theta)}{sin^2(\theta)cos(\theta)} \right) \tag{6.1}$$

where

F = structure factor

p = multiplicity

θ = diffracted angle.

Since θ values do not differ substantially for (200) and (002) peaks then it follows that $I_{002}/I_{200} \sim 0.5$, assuming random crystallite orientation. In a similar manner the ratios of the (113) and (131) peaks is ~0.5.

Subsequent to a ferroelastic type transition, in which the [001] direction is switched through 90° a form of preferential alignment can occur in which the diffracted intensity from the (200) set of planes is decreased while that from the (002) set is equally increased. Figure 6.3 illustrates this 'alignment' process when a polished TZP surface is subjected to severe mechanical stress (eg via grinding) initiating either the martensitic dilatational transformation and/or the ferroelastic transition.

The resulting anisotropy has been observed in Ce stabilised TZP ceramics [33] both on ground and fractured surfaces.

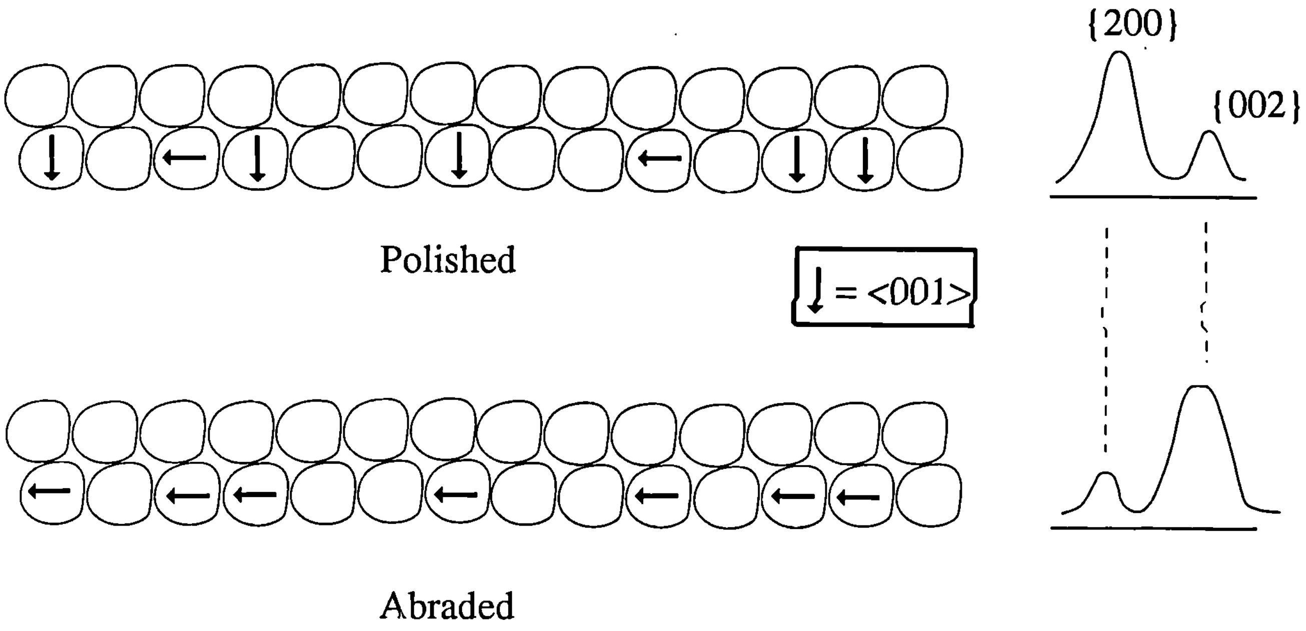

Figure 6.3: Alignment model describes why the ferroelastic transition could be observed in a diffraction experiment.

The texture of the tetragonal and monoclinic phases were determined for fractured, ground and polished surfaces of Y-TZP [110] and partially correlate with the results obtained by Virkar [33], except for the fractured surface where the t002/200 phase orientation was opposite to that found on ground surfaces, and was found to be dependent on the residual monoclinic content. Furthermore, at temperatures in excess of 1000°C, fracture surfaces did not exhibit the t002/200 anisotropy indicative of ferroelastic transition and hence it was postulated that the ferroelastic transition was not operating during fracture of 4.5wt% Y-TZP.

Recent research, obtained from XRD and electron diffraction, [111] indicated that tetragonal zirconia polydomain single crystals are ferroelastic and, as such, can act as an energy absorption mechanism and thus contribute to toughness increments. Negita [32] has proposed that the cubic - tetragonal transformation in Y stabilised zirconia proceeds via the condensation of a particular unstable phonon mode located at the edge of the cubic Brillioun zone boundary which, subsequently, becomes the centre of the tetragonal Brillioun zone. The transition is accompanied by the spontaneous generation of elastic strains associated with the tetragonal phase, indicating that the tetragonal D_{4h}^{15} phase of zirconia is improper ferroelastic. Furthermore, Negita proposed that a similar phonon mode instability could also be responsible for the tetragonal-monoclinic transformation indicating that monoclinic zirconia could also be ferroelastic.

This chapter reports some experimental observations on yttria stabilised TZP, using x ray diffraction similar to related work on ceria stabilised TZP's [33] and transitions occurring within the *bulk* of the material were observed using ultrasound non-destructive testing measured as a function of applied uniaxial stress. Any transitions that occur within the bulk would be indicated by discontinuous changes in the ultrasound velocity.

6.3 Experimental Details

X ray diffraction studies were conducted using a Philips type 1130/00 powder diffractometer (λ =1.5405 Å) which was operated at 2θ = 1°/minute.

A 3mol%Y-TZP ceramic was ground flat to dimensions of 10 × 4 × 5mm. The stress was applied in compression[3]using an Instron universal testing machine with a constant imposed strain rate. A small Lead Zirconate (PLZT) ultrasound transducer was attached to the sample using vacuum grease. An ultrasonic signal of 15MHz was generated and transmitted through the sample, reflecting off the opposite wall and was received by the same transducer, figure 6.4.

In this way the time of flight between transmission and reception could be used to determine the ultrasonic velocity. Longitudinal waves were analysed and effects

---

[3] To generate the high levels of stress associated with the stress fields of crack fronts within the bulk, it was necessary to harness the much higher compressive strength of the ceramic compared to its tensile strength. Fracture would certainly have occurred in the latter case.

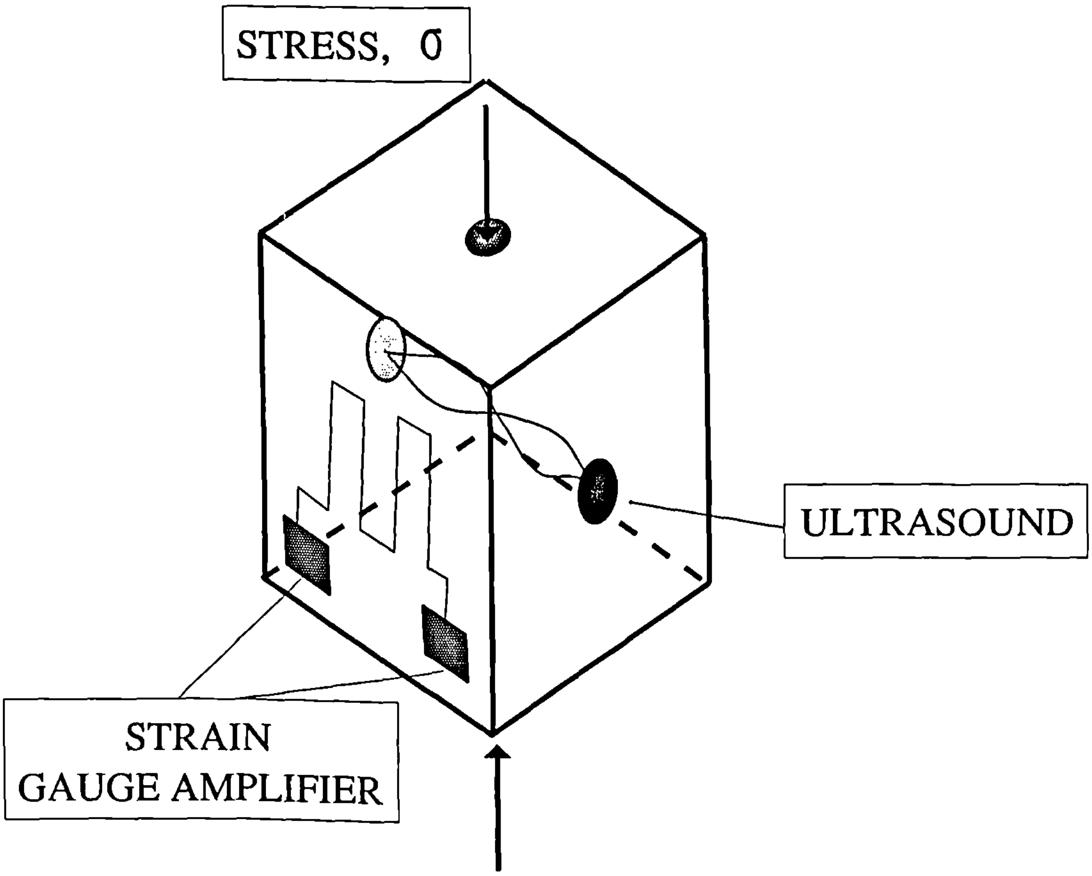

Figure 6.4: Schematic showing sample orientation, direction of pressure and ultrasound arrangement

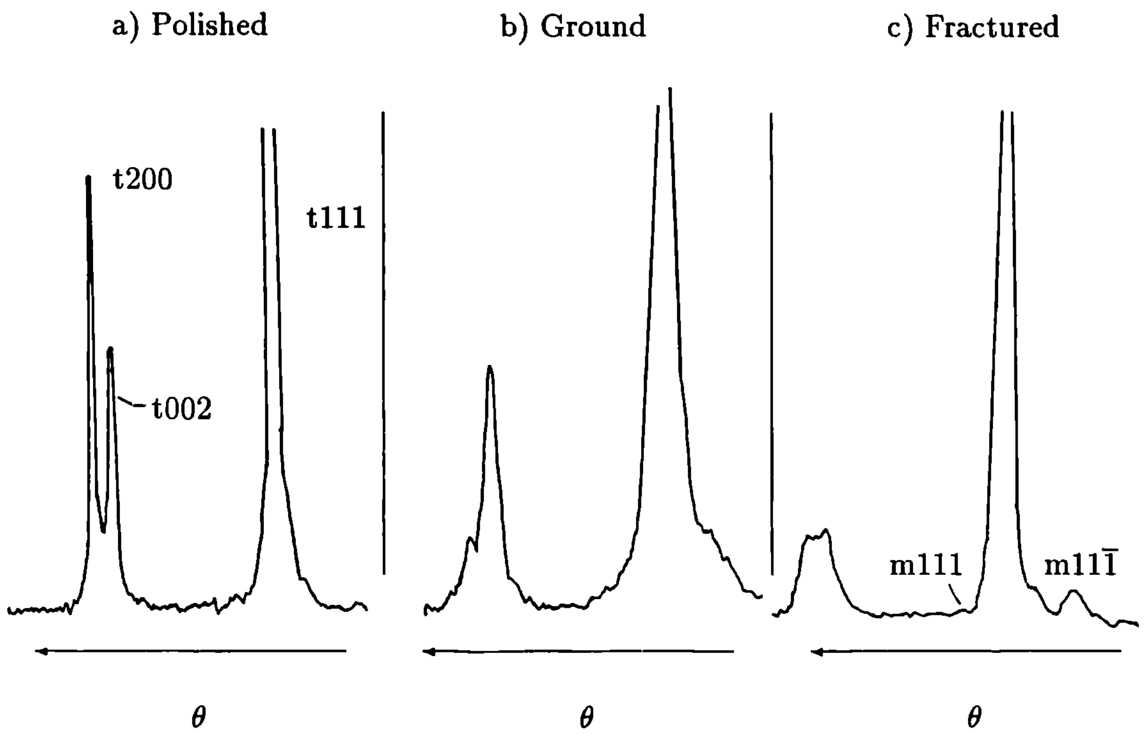

Figure 6.5: X-ray traces identifying the change in crystallite orientation.

such as side wall reflection were assumed to be negligible. The ultrasound results were recorded every few seconds and later correlated with the stress.

6.4 Results

The surface crystallography of a mirror finish polished 3Y-TZP ceramic was compared to that of a coarsely ground surface using x ray diffraction, figure 6.5 a,b. No monoclinic content was detected on the polished surface and a barely detectable level on the ground surface indicated that a negligible tetragonal to monoclinic martensitic transformation had occurred.

As expected the ratio of the (200)/(002) doublet for the polished surface was very

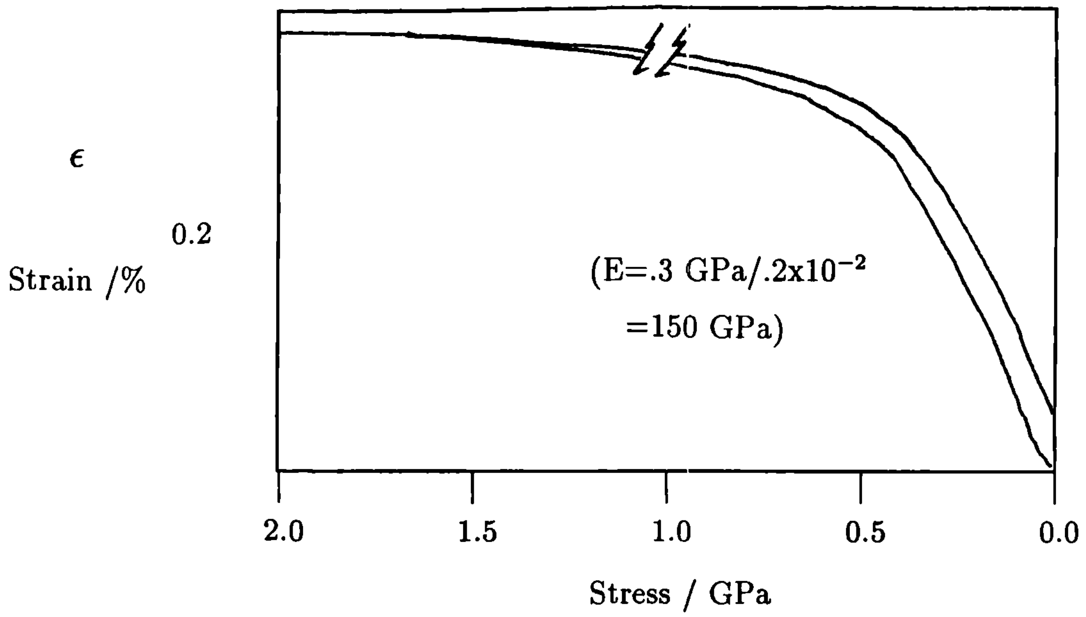

Figure 6.6: Hysteresis between stress and strain indicates an energy dissipation mechanism is operating in this stress strain map.

nearly 2. The same ratio for the ground surface, however, was reduced to a value of ~ 0.3, indicative of an anisotropic surface reorientation of the tetragonal crystallites. The x ray diffraction pattern of a fracture surface of the same material, figure 6.5c, reveals similar features to that of the ground surface, i.e. a reduction in the (200)/(002) ratio to a value of ~ 1.0. Interestingly, there is also a small monoclinic content which indicates that some stress induced martensitic transformation had occurred. The (113)/(131) ratios further augment these observations.

The stress-strain map for one set of experiments is reproduced in figure 6.6. Clearly a hysteresis between stress and strain is visible with a permanent residual strain of approximately 0.003.

It is very difficult to separate true sample hysteresis from the possible hysteresis of the measuring equipment or the Instron. Furthermore, the form of the hysteresis loop is not the same as that reported by Virkar. The reason for this is believed to be due to the difference in stress application equipment. Here a constant strain rate cross-head was used to apply the stress. If any transformation occurred, such as the dilatational tetragonal to monoclinic transition, then any resulting tensile strain would be suppressed by the motion of the cross-head thereby yielding discontinuities in the measured stress. This was observed where such a transition in stress occurred at a stress level, σ_{c1} of ~400MPa. A further significant change in the stress/strain slope occurred at a stress level, σ_{c2} of ~1.7GPa.

The ultrasound results are shown in figure 6.7. Here, the square of the ultrasonic velocity is plotted against applied uniaxial stress (the elastic moduli is very nearly proportional to the square of the velocity). Any significant change in the velocity may indicate a structural change within the bulk of the ceramic.

Two such transitions occur at stress levels, σ_{c1} = 400MPa$\pm 50MPa$ and σ_{c2} =1.6GPa$\pm 0.2GPa$. A hysteresis between ultrasound velocity and stress was observed in the ultrasound/stress map, both after $\sigma = \sigma_{c1}$ and after $\sigma = \sigma_{c2}$. Further analysis of figure 6.7 indicates that the second transition, σ_{c2}, is more pronounced than the first and, additionally, exhibits a smaller separation between the loading line and unloading line than does the first transition. The larger separation between

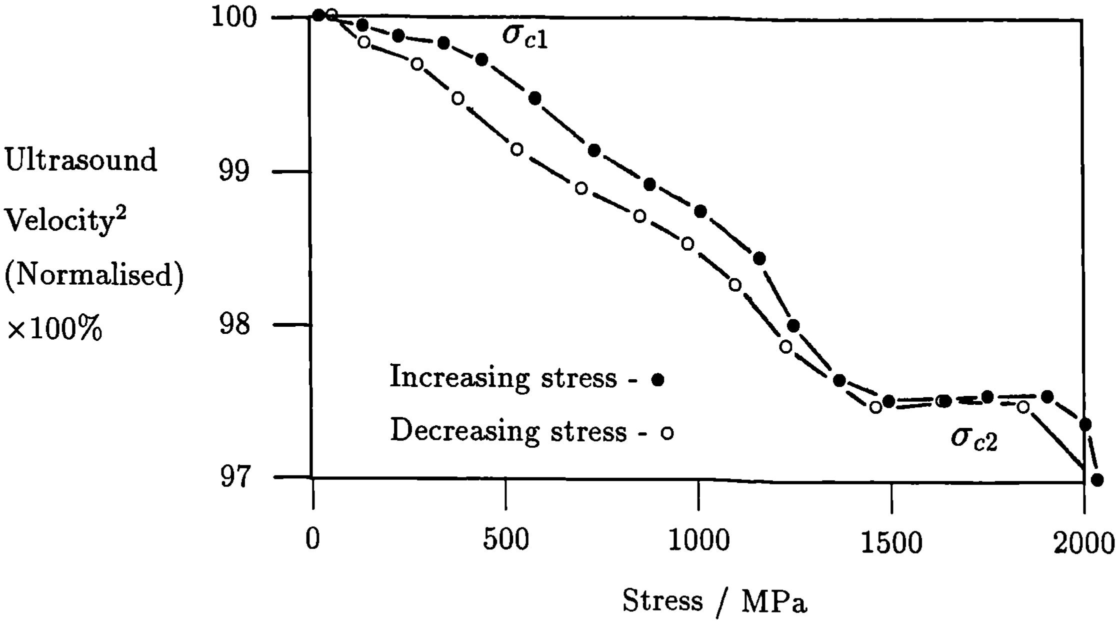

Figure 6.7: Ultrasound velocity squared plotted against stress indicating the two transitions σ_{c1} and σ_{c2}.

the loading and unloading characteristics associated with the first transition (σ_{c1}) is indicative of the irreversibility of this particular transition.

The resulting structure of a surface that was positioned normal to the application of stress was measured using x ray diffraction, figure 6.8. A small amount of monoclinic zirconia was observed on the surface ($< 5\%$) and an alteration in the (200)/(002) peak ratio implies some surface reorientation had occurred.

6.5 Discussion and Conclusions

The data obtained from x ray analysis of polished and ground Y stabilised TZP is similar to related work by Virkar on Ce stabilised TZP [33]. Furthermore, analysis of

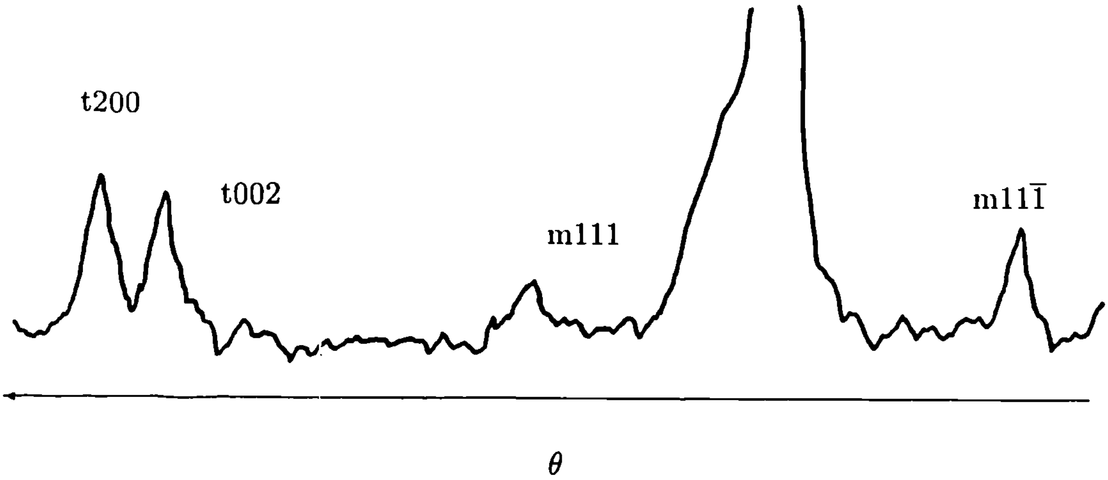

Figure 6.8: X-ray trace for the resulting stressed material identifying the crystalline changes.

the fracture surfaces of Y-TZP reveals similar characteristics to that of the ground surface. It is apparent that significant reorientation of the tetragonal crystallites had occurred on the surface of the ceramic such that the grains with a favourable orientation had their [001] directions switched through an angle of 90°.

It is probable that the data obtained during the ultrasound measurements is not a surface effect and the observed transitions do not result from alternative stress induced phenomena such as shear cracking. This is indicated by the high degree of reversibility in the ultrasound response at σ_{c2} when the zirconia was repeatedly loaded and unloaded.

The ultrasound velocity decreased with increasing applied load as expected from the Poissons ratio of the material. From considerations of the strain energy, it is clear that, if any reorientation of the tetragonal grains were to occur, then their c-axes would align in a direction that was perpendicular to the applied stress. Since the ultrasound was measured in a direction perpendicular to the applied stress, then the *relative increase* in the ultrasound velocity at $\sigma = \sigma_{c2}$ indicates that the ultrasound time of flight along the c-axis of tetragonal zirconia is longer than that along the a-axis. This implies a difference in elastic modulus along the two orthogonal axes.

It is generally accepted that the tetragonal phase in TZP is stablised with respect to the tetragonal to monoclinic martensitic transformation by virtue of the surrounding matrix constraint. The martensitic transformation may be initiated when sufficient constraint is removed and additional strain energy is available as found, for example, in the vicinity of a propagating crack or at a fractured or ground surface. It is clear that, as external stress is applied, the probability of such a transformation is more likely to occur on the surface of the ceramic rather than within the bulk. Since the transformation would be limited to the first few tens of microns (several layers of grains) at the surface then the change in ultrasound time of flight as a function of applied stress would not be particularly pronounced, as observed. This assumes, of course, that the sample dimensions were an order of magnitude larger than this surface depth. Furthermore, it is probable that the martensitically transformed crystallites would be stable against retransformation when the material was unloaded. This would show up as a non-reversibility in the loading/unloading ultrasound characteristic, as observed. The second transition is more pronounced than the first and is largely reversible, indicative of a bulk ferroelastic transition with matrix constraint.

Now, the contribution to the fracture toughness from transformation toughening alone can be determined from the amount of residual monoclinic phase present on the surfaces of fractured samples. Using the model proposed by Lange ^{43ptIII} the fracture toughness K_{1c} of a transformation toughened ceramic can be determined using equation 6.2:

$$K_{1c} = \left(K_0^2 + \frac{2RE_cV_i(|\Delta G^c| - \Delta U_{sef})}{(1-\nu_c^2)}\right)^{1/2} \tag{6.2}$$

where

K_0 = Critical stress intensity without transformation toughening.

$(|\Delta G^c|$-$U_{sef})$ = Work done/unit volume by stress field to induce transformation.

E_c = Youngs Modulus, ν_c = Poissons ratio,

V_ii = Volume fraction of retained tetragonal phase,

R = transformed zone (approx. inclusion size)

Now, assuming a fully dense ceramic and using standard values for the constants and analysis of the m/t ratios by Gaussian peak fitting we obtain a value for the fracture toughness of $5.3MPam^{1/2}$ assuming transformation toughening is the sole toughening mechanism. This value of course depends on a whole variety of constants and assumptions but when compared to the measured value of $10MPam^{1/2}$ the discrepancy between the two figures far outweighs any inaccuracies made above. Clearly another toughening mechanism, acting in parallel with transformation toughening, must be responsible for the observed fracture toughness.

If we can assume that the area enclosed by the stress/strain map is indicative of the energy absorbed by the ferroelastic transition then the contribution from ferroelastic domain switching to the fracture toughness can be calculated using the following equation [33]:

$$K_c = K_0 \left(1 + 2h \frac{E}{(1-\nu^2)K_0^2} \int_{area}^{Shaded} \sigma d\epsilon \right)^{1/2} \tag{6.3}$$

where K_0 is the toughness in the absence of switching and all others have their usual meaning.

Taking $K_0 = 5.3MPam^{1/2}$ yields a fracture toughness of $9MPam^{1/2}$ which is in reasonable agreement [4] with the experimentally determined value of $10MPam^{1/2}$.

This work indicates that Y stabilised TZP is ferroelastic, the transition may occur in the bulk as well as on fracture surfaces where it may contribute significantly to toughness increments. Confirmation of the bulk transition has been sought from direct neutron diffraction measurements in stressed material at the ILL neutron

---

[4] The residual strain used was that obtained using Ce-TZP data obtained by Virkar. The residual strain determined in these sets of experiments could not be used due to the nature of the apparatus which essentially dictated the strain imposed upon the sample.

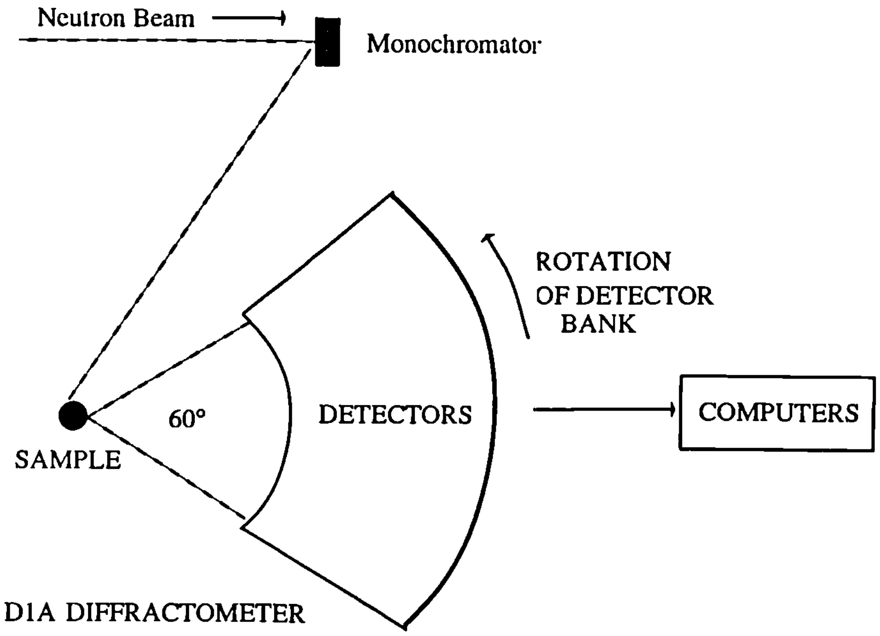

Figure 6.9: Neutron Diffraction Experiment set up showing configuration of sample, neutron beam and detectors.

scattering facility at Grenoble, France. Preliminary results are shown in the graph affixed at the end of this chapter (figure6.10). The experiment was conducted using the ILL's 'D1A' powder diffraction apparatus in the configuration shown in figure 6.9. A set of 10 detector banks recorded the diffracted beam intensity collecting a total of 8000 counts per each 0.05° step. The intensity of the neutrons diffracting from the 002/200 set of planes was, unfortunately, insufficient to afford reliable peak area data analysis and so the 113/131 set was chosen which yielded an increased total scattering intensity over the former doublet. Pressure was applied uniaxially in discrete steps up to approximately 2GPa. The pressure rig was calibrated using a strain gauge affixed to one of the steel supporting legs. In this way the applied load was converted into a true stress. The diffraction spectrum from nineteen levels of applied stress were analysed, 15 with increasing pressure and 4 with decreasing pressure.

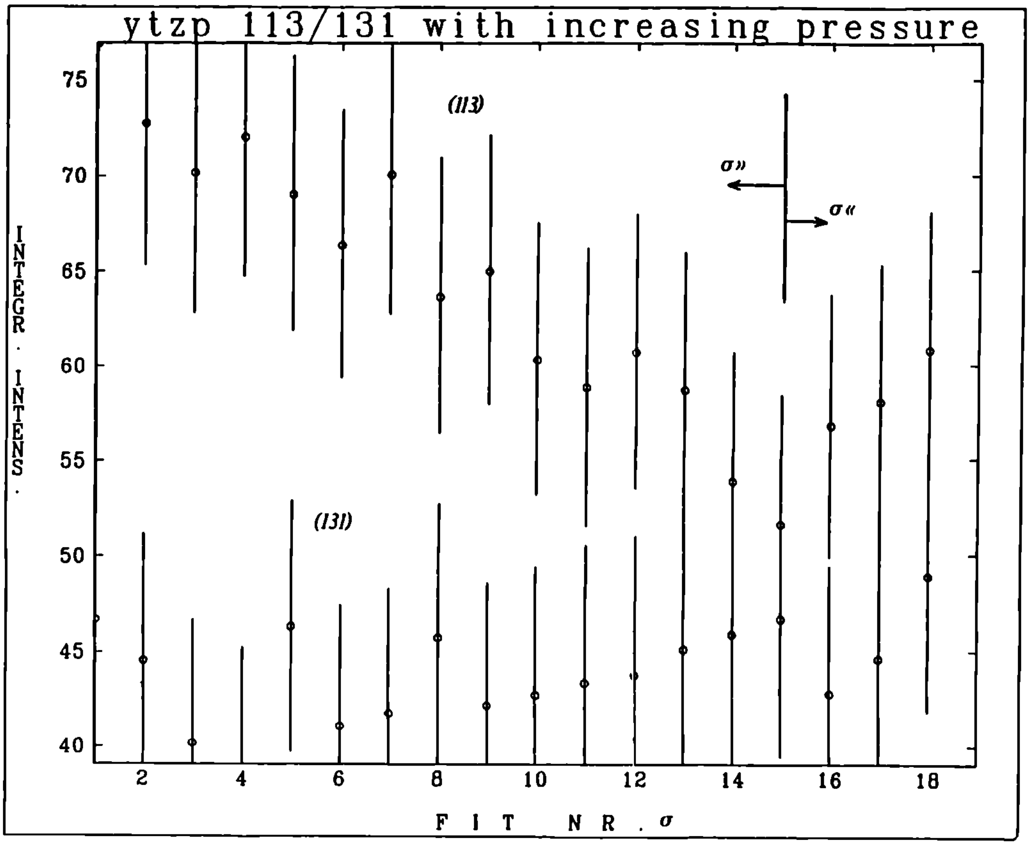

Figure 6.10: Neutron Diffracted intensity plotted for both the 131 and 113 set of planes as a function of applied uniaxial load, see text.

The experiment took place after the completion of this thesis, but, due to the relevance to this chapter, *some* of the results will be discussed here.

The main feature of the graph depicted in figure 6.10 is the relative decrease in the 113 peak area intensity as a function of applied uniaxial stress and a corresponding increase in the 131 peak area intensity. This fact suggests a change in crystallographic orientation had occurred or perhaps a change in crystallographic type had occurred. A high pressure orthorhombic phase of zirconia has been reported to exist (see ref. 26) but only at pressures in excess of 4GPa. Furthermore the occurrence of such a phase would, quite probably, be accompanied by additional diffraction anomalies such as a further splitting of the 113/131 or 002/200 tetragonal peaks which occurs in the cubic - tetragonal transition. Such features were not observed at any of the applied pressures. Furthermore the substantial change in the 113/131 peak area ratio from zero applied pressure to the maximum applied pressure cannot be readily explained in terms of a tetragonal - orthorhombic (t-o) transition, even though a change in peak heights might well be expected to occur during such a t-o transition. Further analysis of figure 6.10 indicates that the transition appears to be reversible, i.e. the 113 peak area intensity starts to increase whilst the 131 peak area intensity starts to decrease as the pressure is released back to zero applied load.

The data strongly suggests that Y-TZP exhibits a reversible stress induced phase change which can be explained in terms of a tetragonal - tetragonal ferroelastic transition, described earlier in this chapter. Further work will be carried out at the Rutherford Appleton Laboratory, December 1990, where a similar experiment will be conducted but with improved statistics for both the 113/131 and 002/200 set of peaks.

Chapter 7

Grain Boundary Modifications to Y-TZP Ceramics

7.1 Introduction and Research Objectives

The superior mechanical properties of zirconia based ceramics have been widely recognised and discussed in detail in chapter 3. Although it is clear that TZP ceramics exhibit excellent mechanical properties at ambient to medium temperatures, there is a degradation in the fracture toughness and creep resistance at temperatures in excess of the martensitic start temperature of $\sim$ 800C. The loss in strength can be attributed to the following:

1) As the operating temperature, T, approaches the martensitic start temperature (T_{ms}), the tetragonal phase becomes increasingly stable, becoming fully stable at T=T_{ms}. Since, from thermodynamic reasoning, the fracture toughness is inversely proportional to the difference between operating temperature and T_{ms} then, as the temperature is increased, a gradual decrease in the fracture toughness will be observed (see chapter 3). Strategies for incrementing the martensitic start temperature, i.e. resulting in high temperature fracture toughness increments, are limited.

(2) The sintering temperature of a TZP ceramic is set by the solute oxide content and the need to sinter within the single phase tetragonal phase field. At the low sintering temperatures encountered, complete densification cannot be obtained via the thermally activated solid state diffusion process but, rather, is accomplished via a liquid phase sintering mechanism. The transient liquid acts as a high diffusivity medium for cation transport - primarily Zr - thus enabling rapid densification to occur. The liquid phase, which surrounds the zirconia grains at the sintering temperature, is thought to be a low viscosity liquid in the $M - Al_2O_3 - SiO_2$ ternary system, where M is the solute stabiliser additive and Al_2O_3 and SiO_2 are impurities present in the starting powders (chapter 3). In the Y-TZP system, the sintering liquid phase solidifies as a grain boundary glass having the composition based on the $Y_2O_3 - Al_2O_3 - SiO_2$ eutectic. Supporting evidence stems from Transmission Electron Microscopy (TEM) microanalysis of the grain boundary film present in

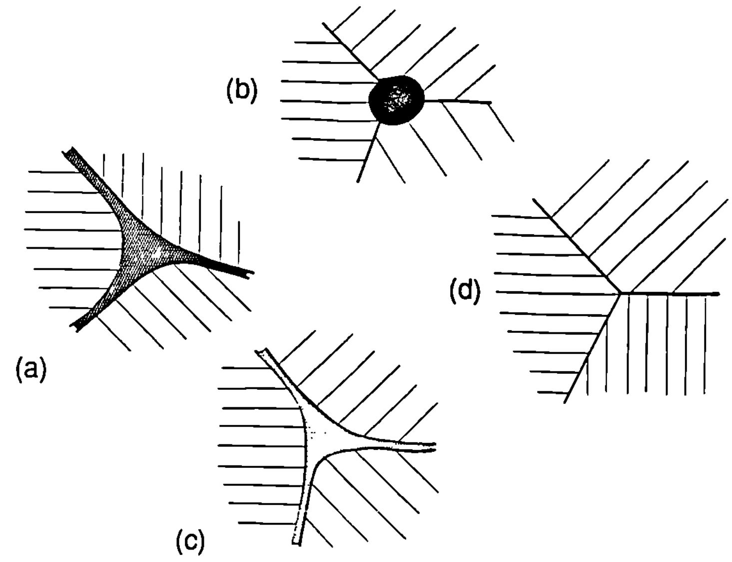

Figure 7.1: Grain boundary modifications applicable to TZP ceramics:(a) amorphous phase wetting the grain boundaries; (b) non-wetting grain boundary; (c) crystallised grain boundary and (d) clean grain boundary

TZP and the attainment of full theoretical density at 1400°C, the ternary eutectic temperature. The small grain size of the TZP and softening of the intergranular sintering residue at high temperatures severely impairs the creep resistance of the ceramic. The specific creep mechanism will depend on glass composition and the applied stress [ref21,22-1styrrep], but it is generally applicable that grain boundary sliding and viscous crack nucleation and growth, (e.g. particle rearrangement initiating crack development due to the softening of the glassy grain boundary phase), represent the main contributions to the deformation process.

Several strategies for the improvement of the high temperature properties, via modifications to the grain boundary phase, are outlined below and in figure 7.1.

The total elimination of the glassy intergranular phase would prove to be difficult and expensive (figure 7.1(d)) but could be accomplished by Hot-isostatic pressing ultra pure TZP powders. An alternative possibility for retarding creep is to reduce the wetting of the grain boundaries by appropriate compositional changes, figure 7.1(b). The final strategy for grain boundary refinement is sketched in figure 7.1(c). In this case, modifications to the glass composition, followed by controlled annealing procedures, results in a completely crystalline grain boundary phase or, at least, an increase in the original grain boundary glass viscosity. This approach has been successfully applied to the silicon nitride range of alloys where grain boundary modifications have incremented the useful operating temperature to about 1300°C. It is this final strategy that is the subject of this chapter.

The silicon nitride, or the substituted M-Sialon/Syalon, ceramics are pressureless liquid phase sintered and are distinguished by the use of a low melting temperature eutectic sintering liquid based on the $Y_2O_3 - Al_2O_3 - SiO_2$ system, analogous to the TZP ceramic. Subject to the sintering conditions, this liquid cools to a glassy state as a semi-continuous matrix for the silicon nitride β' grains (see chapter 2 for more details). As previously described, this phase severely impairs the high temperature creep behaviour and mechanical properties. In β' ceramics the glass composition is controlled via additions of AlN which effectively enhances the N/O ratio within the glass forming network thereby increasing its viscosity and making it susceptible to total crystallisation as the mixed oxide Yttrogarnet (YAG). Commercial ceramics based on this bi-phase system are currently available.

The analogy between the Y-TZP and SYALON ceramics now becomes clear and efforts to chemically alter and thus to realise a more refractory grain boundary phase in Y-TZP's form the fundamental objectives of this chapter/paper.

7.2 Experimental Objectives

In Y-TZP ceramics the yttrium exists in solid solution with the zirconia and, as a result of the Y^{3+}/Zr^{4+} ionic size ratio, the tetragonal polymorph is stabilised to temperatures below the tetragonal-monoclinic transformation temperature of pure zirconia. During sintering, a fraction of the added yttria partitions to generate the eutectic liquid which assists the densification of the ceramic.

In an effort to chemically alter the grain boundary phase, via substitution of N for O within the oxide glass, it was considered necessary to enhance the grain boundary residue already present in TZP to a value of ~10 volume %. This would generate a ceramic system with a well defined, controlled, chemistry and to permit the identification of any subsequent interactions with the matrix phase. In this way the partitioning effect of yttria between the formation of an enhanced solid solution with the zirconia to that of grain boundary segregation could be attained.

Two methods for incrementing grain boundary levels were adopted and compared.

(1) The individual oxide powders of Al, Y and Si were mixed in their appropriate

proportions and attrition milled in water with 3Y-TZP powder for 20 minutes.

(2) The $Al_2O_3 - Y_2O_3 - SiO_2$ glass eutectic was premelted, crushed and attrition milled in water with the 3Y-TZP powder for 20 minutes.

Phase partitioning, dopant ion segregation and phase homogeneity were studied as a function of method and processing temperature and time.

Finally, single additions of AlN (added as a polytypoid for increased stability) were milled with 3Y-TZP powder to determine the limit of dissolution of N within the grain boundary glassy phase.

7.3 Experimental Details

The oxide powders of Al, Si and Y were mixed in proportions corresponding to the ternary eutectic composition indicated by a '#' on the ternary eutectic phase diagram of figure 2. The final mixed composition is also indicated in figure 7.2.

The glass powders were milled in a rotary attrition mill and either further milled with 3Y-TZP powders or prereacted at 1450°C for 1 hour in air, crushed, milled and finally milled with 3Y-TZP powders. The subsequent TZP powders contained 10vol.% glass additive. The milled powders were spray dried, uniaxially die pressed at 0.5ton/sq.inch and cold isostatically pressed in sealed polythene bags in oil at

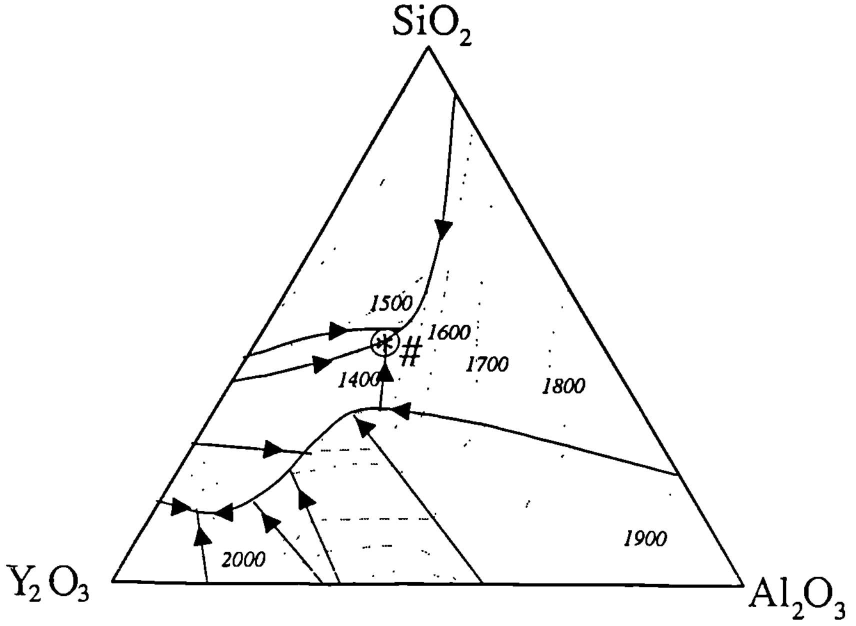

Figure 7.2: $Al_2O_3 - SiO_2 - Y_2O_3$ ternary phase diagram with '#' indicating the chosen ternary eutectic point

170MPa.

Billets were sintered in air within a protective TZP powder bed at temperatures of 1400 and 1500°C for 1 hour and at 1450, 1500, 1550, 1600 and 1650° for 4 hours duration. Fired densities were measured using conventional water immersion techniques and crystalline phase content analysed using X-ray diffraction (see chapter 4). High angle X-ray diffraction ($2\theta = 72 - 76°$) differentiated cubic zirconia from the tetragonal polymorph identified by the splitting of the cubic {400} peak into the tetragonal {400}/{004} peaks. The cubic/tetragonal ratio was determined using equation 4.4 (see chapter 4).

Microstructural phase analysis was determined by Scanning Electron Microscopy (SEM) studies of polished and thermally etched surfaces. Further analysis was conducted on argon ion-beam thinned samples in the Transmission Electron Microscope (TEM). Phase compositional analysis was determined using semi-quantitative X-ray microanalysis.

A final series of experiments were conducted to determine the likelyhood of N incorporation within the grain boundary glass of a standard 3T-TZP. Additions of 1/2, 1 2 and 5 wt% AlN (added as the 21R polytypoid due to its increased stability) to 3Y-TZP were prepared as above and sintered in a Nitrogen gas environment using the sintering schedule described above. Phase evolution, via XRD and SEM, and elemental characterisation via X-ray microanalysis in the SEM was determined for all compositions.

7.4 Experimental Results

7.4.1 Premixed Unreacted Oxides

The densities of material produced by this method exhibited little variation either as a function of time or temperature, with an average value of $5.6gcm^{-3}$ or about 92% theoretical tetragonal zirconia density. The cubic/tetragonal (c/t) ratio, determined from XRD analysis, is shown in figure 7.3.

The c/t ratio increased with increasing temperature and time as expected from analysis of the $ZrO_2 - Y_2O_3$ phase diagram. Scanning electron microscopy identified all major phases, figure 7.4. Clearly, the milling process has resulted in the inhomogeneous isolation of the precursor powders thus minimising any subsequent

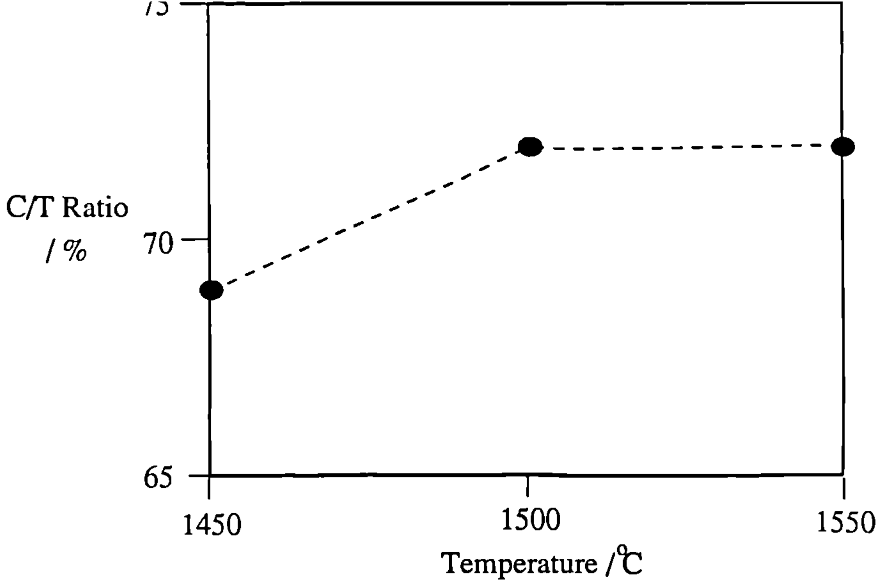

Figure 7.3: Cubic/tetragonal ratio for material produced via the first method of manufacture, shown as a function of temperature and time

reactions necessary for liquid generation. Separate pockets of Al_2O_3 and SiO_2 were observed (XRD, SEM and TEM) together with large grains of zirconia, in addition to the smaller tetragonal zirconia grains. The level of yttrium, within successively larger grains of zirconia, was observed to increase as shown in the EDS analysis of figure 7.4.

XRD studies identified the larger grains as cubic zirconia and the smaller grains as the tetragonal polymorph. Limited reaction between the zirconia and additive silica resulted in the formation of zircon ($ZrSiO_4$), (XRD and SEM). The grain boundary composition was determined from X-ray microanalysis using the TEM, figure 7.5. The composition, labelled in figure 7.5, is an average value obtained from many amorphous areas and, as such, has a ±10% associated error.

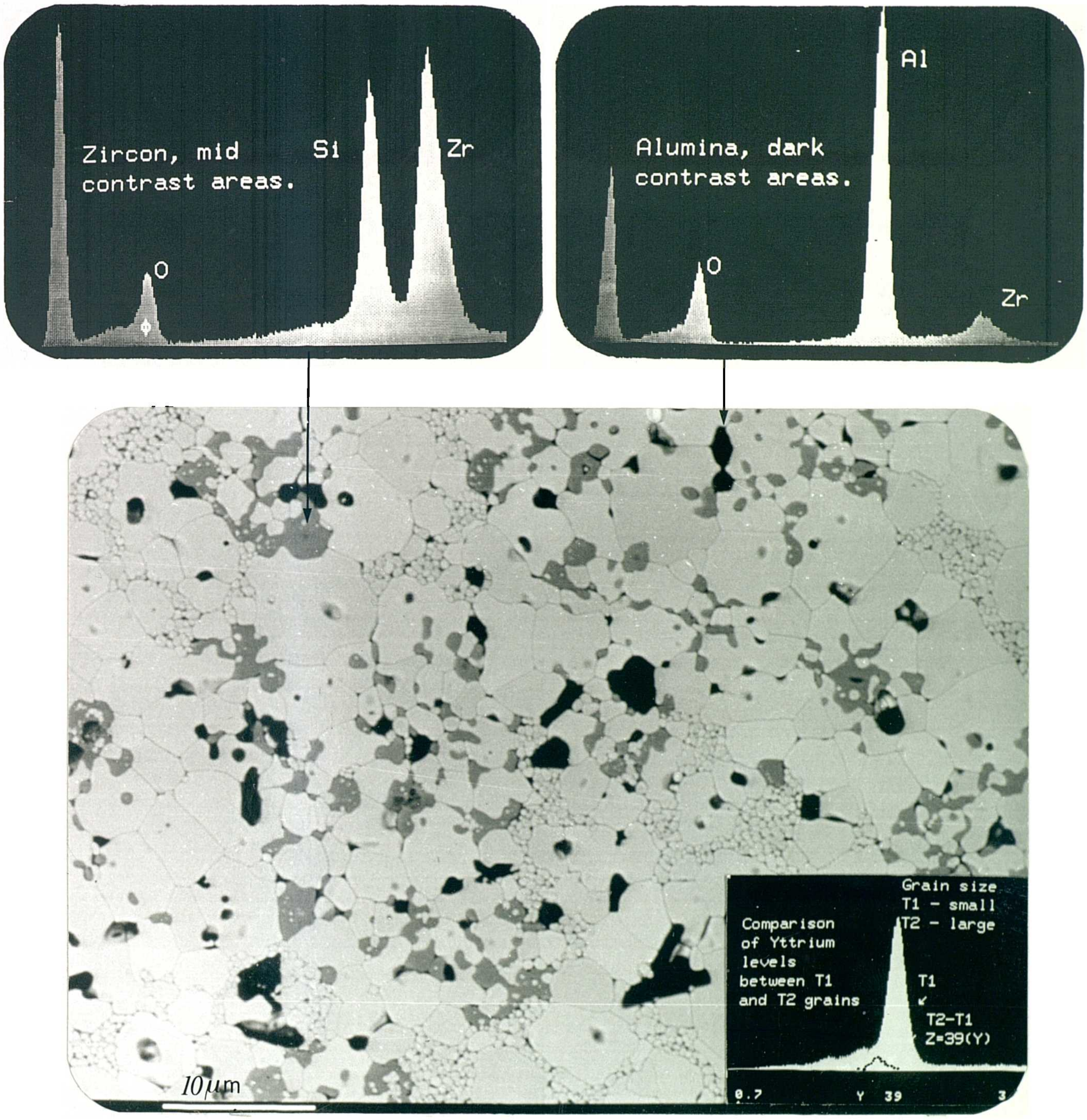

Figure 7.4: Scanning Electron Microscope image of TZP sintered with premilled additives at 1450°C for 4 hours and associated EDS analysis.

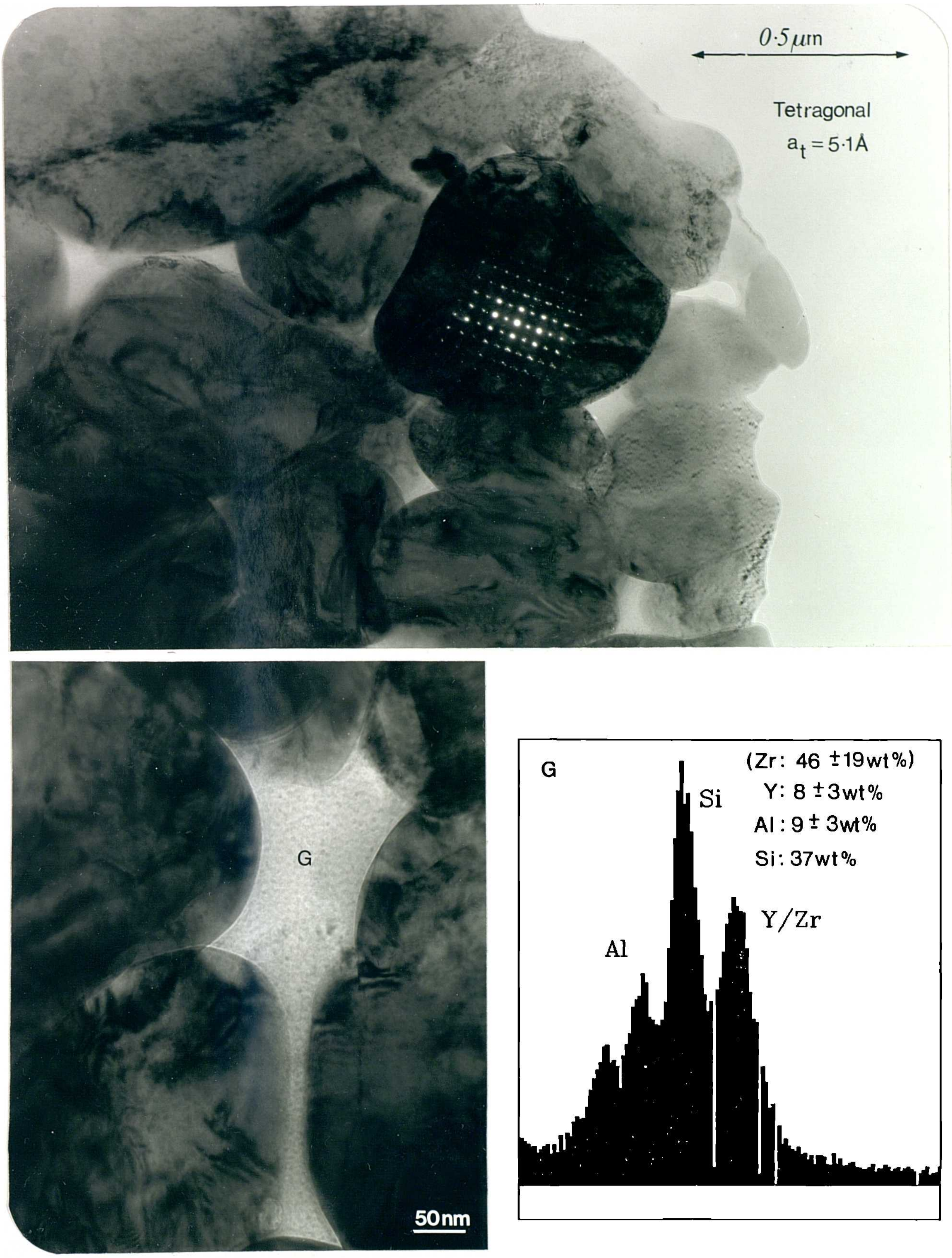

Figure 7.5: Transmission electron micrograph image of sample sintered at 1500°C for 4 hours identifing grain structure, amorphous grain boundary phase and associated X-ray microanalysis.

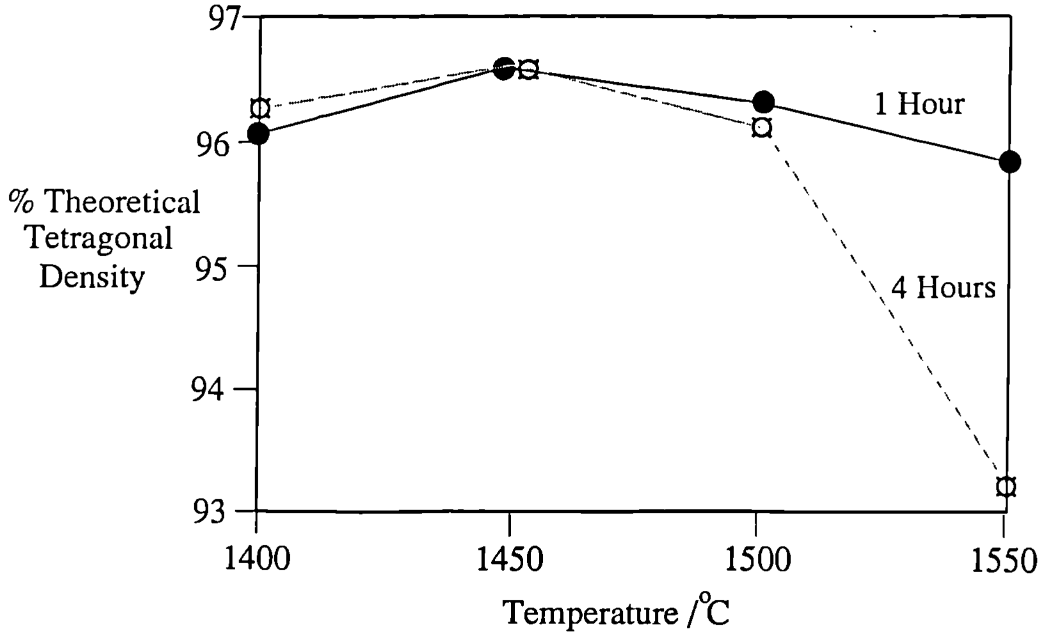

Figure 7.6: Percentage of theoretical tetragonal densities of fired samples corresponding to the second method of manufacture.

7.4.2 Premelted Glass Additive

The crystalline content of the premelted glass was analysed using XRD, and was shown to be completely amorphous. The milled samples were sintered at 1400-1550°C at 50°C intervals as before for 1 hour and additionally for 4 hours duration. Their fired bulk densities were measured and are compared in figure 7.6.

The measured densities exhibited little variation with temperature or time except for the highest sintered temperature, where a noticeable difference was observed between the 1 hour and 4 hour sintered samples. The cubic - tetragonal zirconia ratio was determined from XRD anaysis, where a significant time dependence was noted, figure 7.7.

At temperatures in excess of 1450°C the samples sintered for 4 hours exhibited little variation in their c/t ratio whilst those sintered for only 1 hour showed a

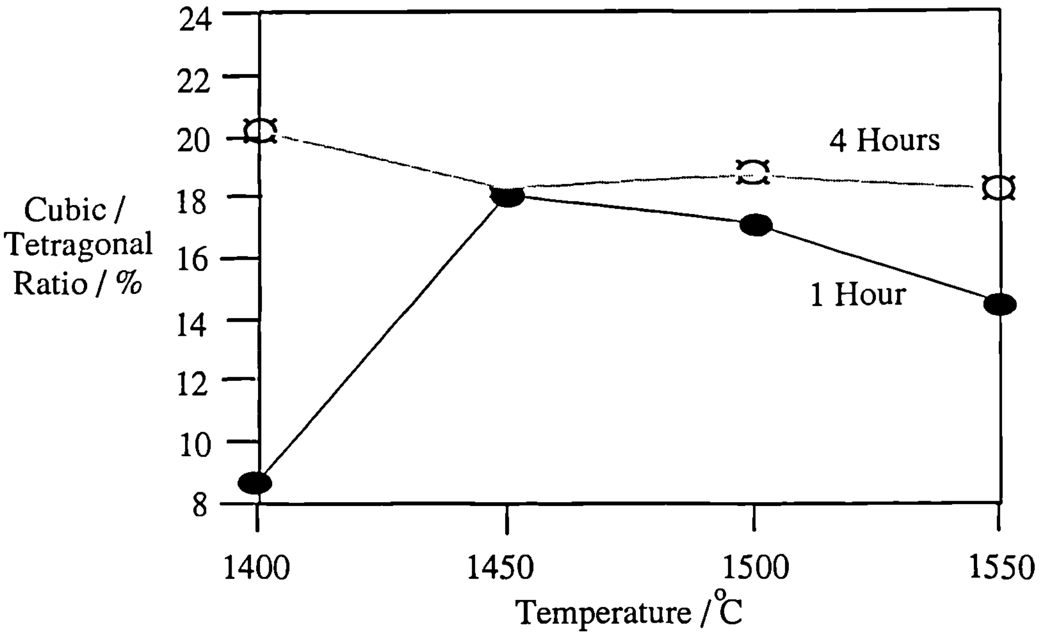

Figure 7.7: XRD c/t polymorph ratio for premelted glass additions. The c/t ratio dependence on time is especially noted.

gradual decrement in their corresponding c/t ratios. The sample sintered at 1400°C for 4 hours exhibited an increase in its c/t ratio compared to that sintered for just 1 hour by a factor of ~2.4. Microstructural analysis further clarifies these observations, figure 7.8, where, it was noted that the average pore size increased with increasing temperature and increasing time.

The partitioning effects of the Y^{3+} is now evident by the observation of cubic zirconia grains (distinguished by their size and solute composition) and an amorphous phase 'wetting' the grain boundaries. No appreciable grain boundary phase was observed, however, for samples sintered at 1400 or 1450°C. At increasingly higher temperatures an enhanced level of grain boundary phase, emanating from the centres of clusters of the original milled additives was observed. The closed cell porosity was observed to increase with increasing temperature.

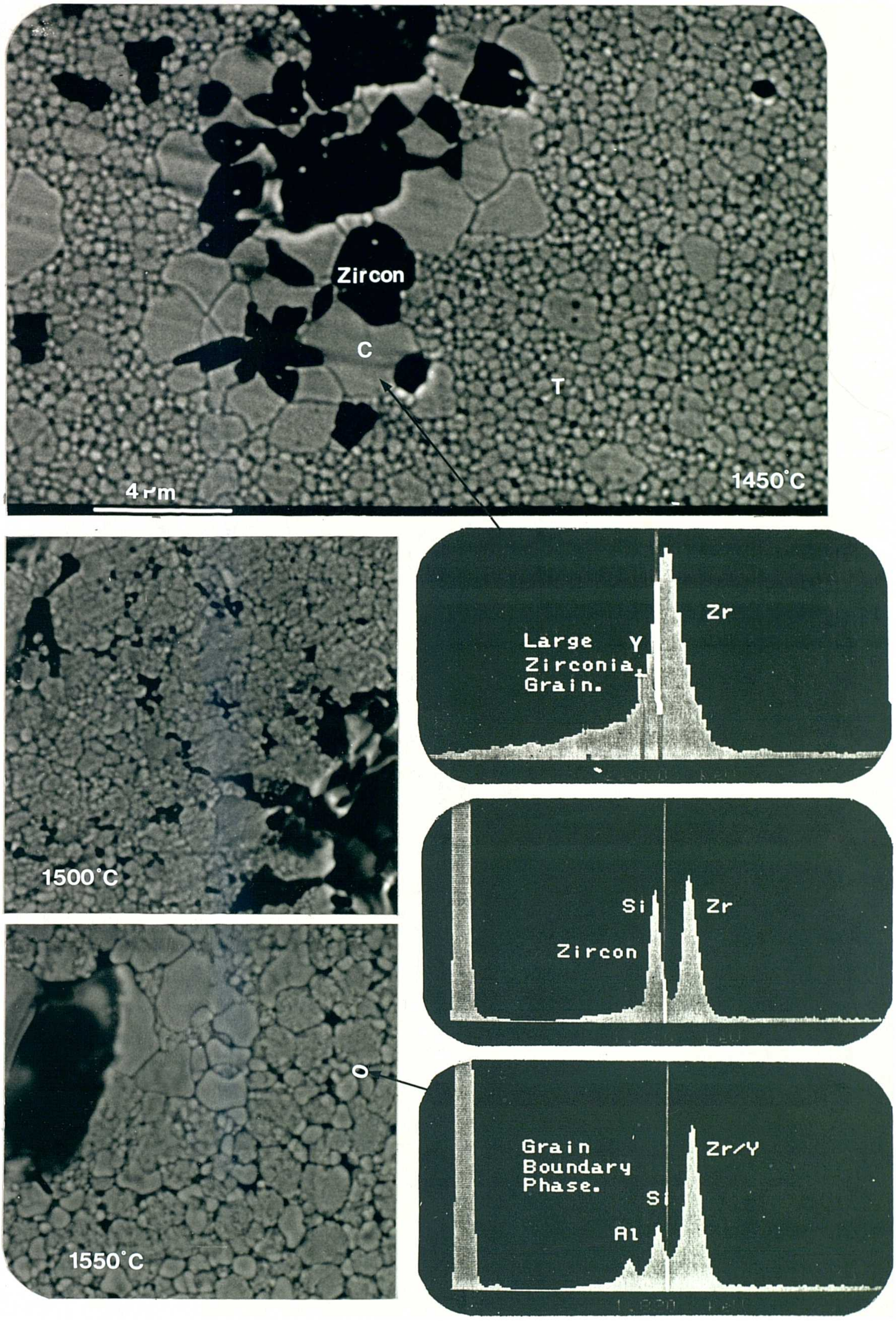

Figure 7.8: Scanning elctron micrographs depicting the evolution of grain structure and phase composition for the samples sintered with the premelted glass additives.

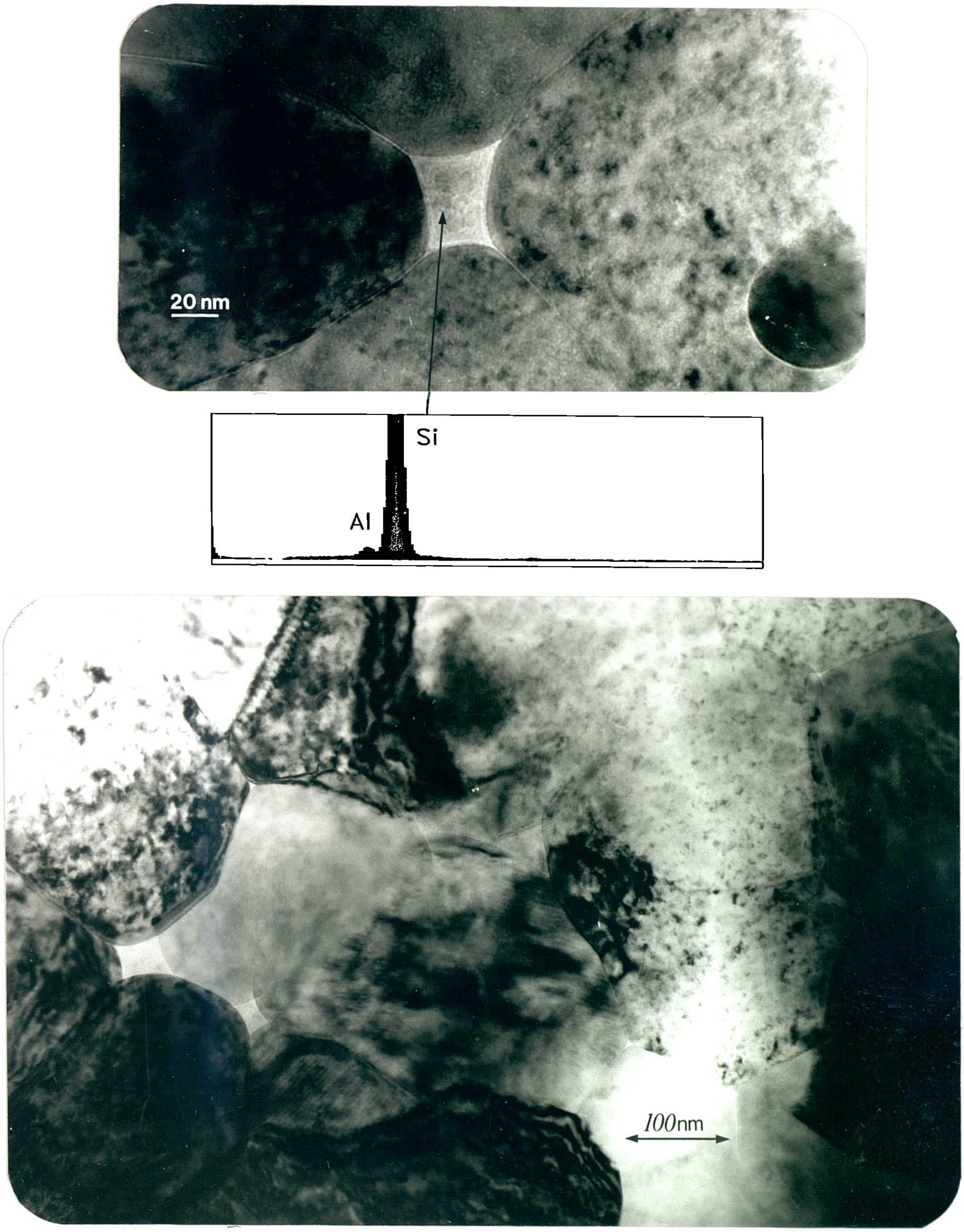

Figure 7.9: Transmission electron micrograph of sample sintered with premelted glass additive. The amorphous grain boundary phase wets all grains and has a composition indicated by X-ray microanalysis.

Further compositional analysis was obtained using transmission electron microscopy and X-ray microanalysis, figure 7.9.

The composition of the grain boundary phase is in close agreement with that obtained using the SEM.

7.4.3 The dissolution of N in the grain boundary phase in TZP

Sole additions of AlN in 3Y-TZP ceramics resulted in widespread porosity, even at additive levels of 1/2% AlN. Additional phases such as αAl_2O_3, monoclinic zirconia and cubic zirconia were identified using XRD and SEM. The grain boundary phase was analysed and its composition is indicated in figure 7.10.

No dissolution of N was observed in the grain boundaries of any composition.

7.5 Discussion

The samples that were milled with the unreacted oxide powders exhibited islands of unreacted Si- and Al-oxide phases due to non-homogeneous mixing of the precursor powders. It was inferred from this and the noticeable lack of the yttria phase, that the yttrium partitioned from the additive oxide to overstabilise the tetragonal zirconia thus generating the cubic polymorph. It appears that secluded $Y_2O_3 - ZrO_2$

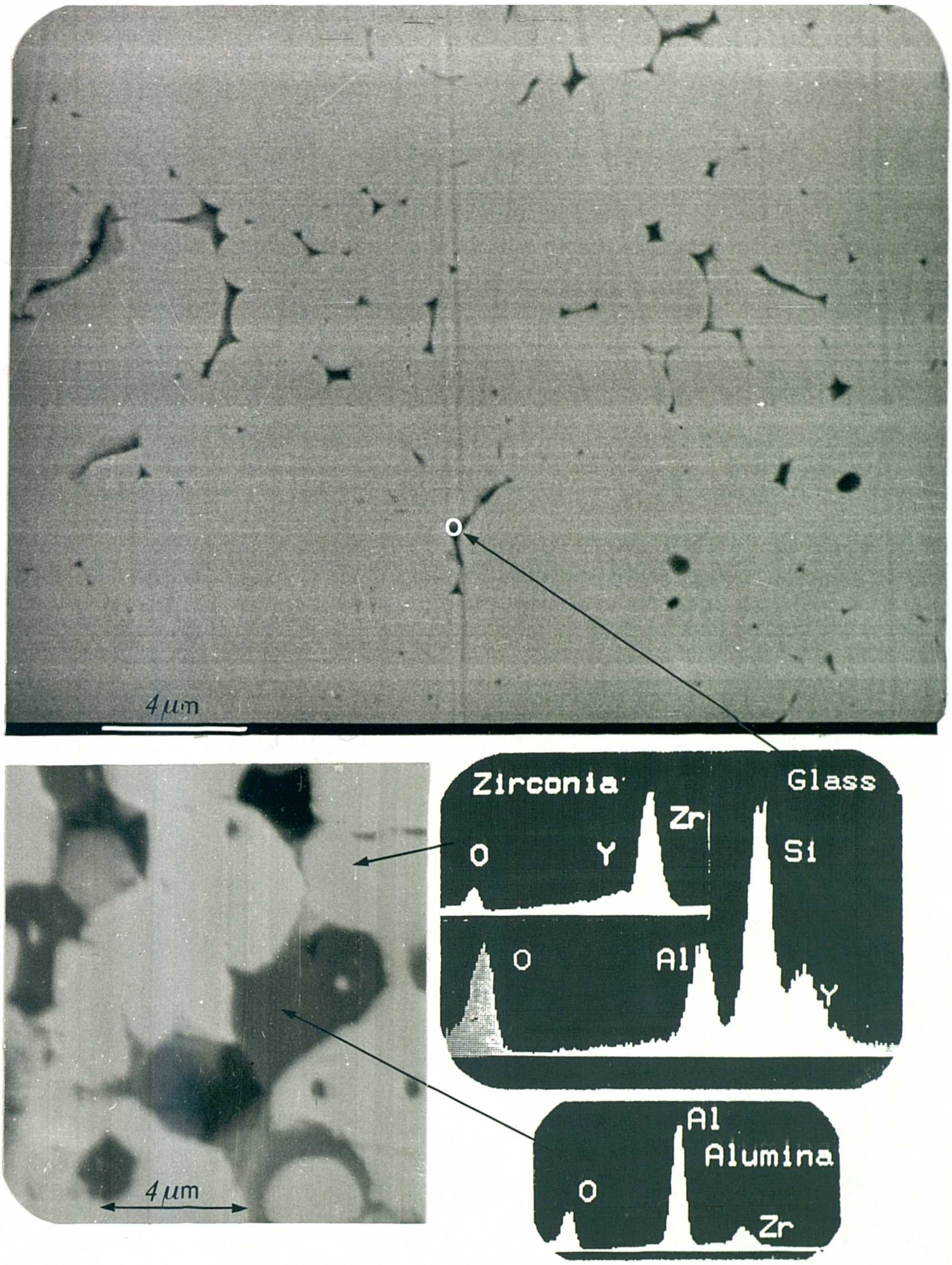

Figure 7.10: Phase analysis of 5wt% AlN composition. Note the ceramic was not thermally etched and so only some grain structure is visible.

reactions occurred, removing Y_2O_3 from the glass forming system. With the more rapid solid-state diffusion of Y_2O_3 competing with liquid phase generation (and hence densification) islands of unreacted Al_2O_3 and SiO_2 were left dispersed throughout the material.

The samples sintered with prereacted glass additions exhibited similar sintering behaviour to that described above, except that sintered densities were on average higher and liquid penetration occurred at temperatures in excess of 1450°C. The Y^{3+} diffusivity at 1400°C is clearly very small with the result that little, if any, cubic stabilisation occurs as a direct result of the glass additions. This is not the case, however, for those sintered at the same temperature for longer times, when a 2.4 times increment in c/t ratio was observed. As expected, liquid penetration was not observed until the materials were sintered at a temperature of at least 1450°C. The partitioning of the yttria from the prereacted melt to a solid solution with the zirconia is clearly in competition with the generation of the liquid phase, liquid penetration and subsequent densification of the material. It appears that, at the higher sintering temperatures, the partitioning of the yttria from the amorphous grain boundary liquid reached a plateau value, corresponding to an overall stabilisation of 18vol.% of the bulk to the cubic polymorph. Evidently, the rate of diffusion of yttria through the additive glass and into the zirconia grains was surpassed by the rate of flow of liquid between the grains of the zirconia, at the liquid forming temperature (~1430°C). At increasingly higher temperatures, the observation of enhanced grain boundary phases, which seemed to emanate from the centres of clusters of the original milled additives, indicate changes in the viscosity of the glass, and hence diffusivity, with temperature. This process of liquid generation and subsequent grain boundary diffusion is sufficiently rapid at higher temperatures that the out-diffusion of Y^{3+} ions from the glass into the zirconia grains becomes less significant. The closed cell porosity, increasingly observed at higher temperatures, results from the liquid phase generation and liquid flow away from the glass clusters leaving a void surrounded by, predominantly, cubic stabilised zirconia. For these pores to close, *either a solution/reprecipitation process must occur or* pressure applied during sintering.

It is probable that longer sintering times would be synonymous with an increase in the distribution of the grain boundary phase throughout the material, although the generation of pores at the centres of the original clusters would inhibit the attainment of full density. A finer dispersion of the added glass would possibly prevent the occurrence of such defects.

The sole additions of AlN resulted in samples having a low fired density, due to the evolution of nitrogen bubbles within the material caused by reaction of the AlN and ZrO_2 producing Al_2O_3, ZrN and $N \uparrow$. The ZrN was not detected in the final sintered material but probably oxidised to monoclinic zirconia which was detected.

No dissolution of N in the grain boundary phase was observed, indicating that this approach is not suitable for grain boundary refinement within TZP ceramics.

7.6 Conclusions

Grain boundary phases in TZP ceramics are of the composition indicated on the ternary phase diagram, figure 7.2. The volume of grain boundary residues can be increased in TZP by the addition of a prereacted glass with a similar composition only. In the systems analysed, the initial particle size of pre-reacted glass additive was clearly too large for homogeneous distribution of the grain boundary phase, leading to a subsequent overstabilisation of the zirconia surrounding the glass additive. The level of porosity was observed to increase with an increase in pressing temperature and time and was linked to the gradual depletion of the glass phase into the surrounding zirconia matrix, either into solid solution with the zirconia or into the grain boundaries, both resulting in the formation of pores emanating from the centres of the original glass particles.

Additions of the component oxides leads to the removal of the yttria from the ternary glass forming system with the result of overstabilisation of tetragonal zirconia and the isolation of unreacted silica and alumina. A plateau level for the partitioning of yttria from the grain boundary phase into solid solution with zirconia is observed at $\sim$18vol.% c/t ratio and occurs for samples sintered at temperatures in excess of 1450°C.

The substitution of N for O within the grain boundary phase of a 3Y-TZP ceramic via additions of AlN 21R Polytypoid is not observed within materials sintered within the temperature range investigated.

Further investigations are required to determine the effects that a finer dispersion of additive glass would have on the density and liquid homogeneity of the material and, finally, the additions of a nitrogen containing glass on the resulting microstructure, phase stability and, of course, on the possibility of grain boundary crystallisation.

Chapter 8

Thesis Summary and Future Work

The thesis initially concerned itself with the current and future trends in ceramic materials science (chapter 1) with special emphasis on the silicon nitride and zirconia family of materials. Chapters 2 and 3 further developed the pertinent history for the two classes of ceramics concentrating particularly on the physics and chemistry of the materials. The main aims of the research were introduced at the end of chapter 3.

The following few paragraphs will outline the main features discussed at the ends of chapters 5, 6 and 7. Additionally, some more general comments are included discussing the philosophical content contained within this thesis.

This thesis was concerned with the development of tough, high temperature ceramics, utilising the toughening modes inherent to zirconia ceramics. To this aim, the fundamental objectives have been realised with the successful generation of a tough, stable zirconia/Sialon composite ceramic. The increased toughness over silicon nitride materials alone was attributed to the toughening agents inherent to zirconia which existed either in the form of the tetragonal polymorph or the monoclinic variant. By judicious control of particle size, processing route and chemistry relatively dense composites were fabricated. The toughening modes were dependent on initial chemistry of the composite system. When the zirconia was prestabilised with yttria the tetragonal polymorph was retained within the composite. The enhanced toughness was attributed to a transformation toughening mechanism. However, when the zirconia was prestabilised with ceria the depletion of Ce from solid solution with the zirconia during processing resulted in the formation of the unstabilised monoclinic variant. The enhanced toughness was attributed, in this case, to a microcrack type energy absorption mechanism, similar to several ZTA composite ceramics. Further work is clearly required to determine whether the microcracks developed as a result of the martensitic tetragonal - monoclinic transformation, via the differential thermal expansion coefficient between zirconia and silicon nitride, via the action of a passing crack on the stressed zirconia particles (eg. either stress-induced microcracking or microcracking via stress induced transformations -see chapter 3) or, indeed, a combination of these mechanisms acting in parallel with each other.

The relatively large values of fracture toughness determined for yttria stabilised TZP (3Y-TZP) and, furthermore, the crystallographic anomalies observed on fracture surfaces of TZP and the composites, provided the research impetus eventually culminating in the observations set out in chapter 6 and also in the publication affixed at the rear of this thesis. The general conclusions following the novel but essentially simple set of experiments were that TZP is ferroelastic and, as such, can provide a significant contribution to enhanced levels of fracture toughness in these materials or composites containing the same. Further work has been conducted to actually observe, as a function of applied uniaxial stress, the crystallographic changes occurring within the *bulk* of a 3Y-TZP ceramic via neutron elastic scattering at the ILL, Grenoble, France. This experiment has provided clear direct proof of the ferroelastic nature of tetragonal zirconia. A similar experiment will be carried out at the Rutherford Appleton Laboratory neutron scattering facility, Oxford, England, though with significantly improved statistics.

The final chapter, chapter 7, indicated that the chemical alteration of the grain boundary phase in TZP ceramics is hindered by the solute additive partitioning from the generation of an enhanced grain boundary phase to overstabilisation of the zirconia resulting in the formation of cubic stabilised zirconia. Furthermore, the incorporation of nitrogen within the grain boundary phase, via sintering TZP with sole additions of AlN, resulted in the attainment of poor fired densities and hence was not considered a suitable method for grain boundary modification. Further research could include a similar programme as the above but with a finer dispersion of the additive glass resulting in an increased homogeneity of milled additives. The partitioning effect of the added yttria would still, however, play a major role in phase evolution. The addition of a finely milled nitrogen containing glass to TZP powders should produce interesting results, especially with respect to the effect nitrogen has on solute partitioning.

The original concept of toughening a nitride ceramic matrix with a dispersion of zirconia has been proven. The extent to which the zirconia additions affect the inherent high temperature properties of the nitride have yet to be evaluated although, of course, preliminary work suggests that the ZrO_2/Sialon couple is stable to 1400°C. The advantages of a material with a toughness approaching that of the best ceramic (TZP) but with a potential high temperature operating ceiling similar to that of a nitride are manyfold, the most important being that of increasing the viability of the use of ceramics for commercial/industrial application. The determination of any particular use for such a material will ultimately depend on a catalogue of properties and design requirements and will be as much a job for the engineers and designers as for the materials scientists and physicists.

It is easy to imagine further interesting experiments to conduct concerning the development of the zirconia toughened nitride composites concept. For example, the effect different stabilising dopants have on the properties and microstructure, how the grain boundary composition and structure changes with dopant and thermal heat treatments (i.e. grain boundary crystallisation). In this context, it would be of interest to ascertain the creep mechanisms operating within these materials, e.g. whether the creep properties are simply a summation or average of the individual phases or depend on a more complex interactive effect.

In a similar vein, and perhaps more relevant to this thesis, there seems much work that can be conducted to elucidate and to differentiate between the different toughening mechanisms already discussed in chapters 5 and 6. The contribution to fracture toughness from transformation toughening and, potentially, from ferroelastic toughening of TZP alone has not been fully evaluated. It is of technological importance to realise that the contribution from each will be a function of alloy dopant, microstructure and temperature. As the operating temperature approaches the martensitic monoclinic-tetragonal temperature (T_{ms}) then the contribution to the fracture toughness from transformation toughening will slowly disappear, whereas that arising from the tetragonal-tetragonal ferroelastic transition will still be operational up to the tetragonal-cubic transformation temperature. It is possible to imagine that, with a carefully tailored microstructure and chemistry, the contribution from any one of these toughening mechanisms (and indeed other mechanisms such as microcrack toughening) can be maximised. Detailed X-ray diffraction studies from fracture surfaces would yield information regarding the relative contribution from these different mechanisms.

Similarly, the exact contribution to fracture toughness arising from transformation toughening, microcrack toughening and ferroelastic toughening for the zirconia toughened nitride composites must also be researched and determined. The first two mechanisms, that is transformation toughening and microcrack toughening are both temperature dependent, the former especially so, and hence a series of high temperature mechanical property measurements should provide information on the mechanisms still operational at these temperatures (if any). Further X-ray diffraction studies on the fracture surfaces would indicate the existence of the ferroelastic transition, an energy absorbing mechanism which may be operational at high temperatures, when the martensitic tetragonal-monoclinic transformation is not.

The generation and refinement of a 'micromechanistic' model describing the ferroelastic transition should prove very interesting. Such work will be carried out once data from the neutron diffraction experiments at RAL and the ILL have been fully analysed. It is clear that the energetics of the t-t ferroelastic transition would depend very strongly on the tetragonal c/a unit cell ratio (the tetragonality), since the ferroelastic distortion is along these two orthogonal directions. An optimum in crystallographic tetragonality can be envisioned where the t-t ferroelastic transition occurs at a predetermined anisotropic stress level. The tetragonality can be varied through the chemistry and dopant level. The constraint imposed from the surrounding matrix would also alter the energetics of the transition. In this context, any differential thermal expansion mismatch between matrix and the TZP would affect the high temperature energetics of the transition.

Some general comments regarding the chemical alteration of the grain boundary phase in Y-TZP have already been made (chapter7) but, for consistency, will be reinforced here. The fundamental objectives in this programme were to chemically redesign the grain boundary sintering phase to achieve a more refractory grain boundary bonding phase. The objectives were not realised due to a number of problems, the most significant being that of dopant stabiliser partitioning from the enhanced grain boundary volume to overstabilisation of the zirconia. Several suggestions were made in the discussions in chapter 7 for improving the high temperature properties of TZP, others may include grain boundary pinning by hard, large obstacles (see chapter 3 - Duplex toughening [7]), or the incorporation of fibres in a TZP matrix. (The former has one benefit; that is, it does not pose serious health risks.)

It is important to compare all forms of toughening applicable to ceramic materials when discussing the merits of one particular toughened composite. Fibre, whisker and platelet toughened matrices are actively being researched. The main objection to this form of toughening is, of course, the serious threat to health when preparing the material. Platelets are less of a threat but are expensive and commercially available in only a few materials. Modest increments in fracture toughness, however, have been widely reported [115]. An additional hindrance to the use of fibres is the directional nature the use of them imposes on the mechanical properties, though this can be put to an advantage.

For further general discussions on the many toughened materials currently being researched and developed the reader is referred to the plethora of review articles appearing almost monthly published in the journals cited in the references at the end of this thesis [115].

References

1. Lewis M H 'Nitride Ceramics for Gas Turbine Applications', in First Parsons International Turbine Conference, Parsons Press, Trinity College Dublin, Institution of Mechanical Engineers London, 181-189 (1984).
2. Kamo R, 'Ceramics For Advanced Heat Engines', Int. J. High Tech. Cer., p 2473 (1987).
3. Fisher G, Bull. Am. Cer. Soc., 68, [2], 249-252 (1984).
4. Mecholsky J J, Bull. Am. Cer. Soc., 68, [2], 367 (1989).
5. Mecholsky J J, ibid, p.367-368.
6. Lewis M H, 'Ceramics, Applications and Limitations', in Materials at their Limits, Proc. Inst. Metals, Inst. Metals, 1-20 (1986).
7. Stevens R, 'An Introduction to Zirconia', Written for Magnesium Elektron Publication No.113.
8. Garvie R C, Nature, 258, 703 (1975).
9. Jack K, J. Mat. Sci., 11, 1135 (1976).

10. Lewis M H, 'Plasticity and Fracture Mechanisms in Ceramic Alloys Based on $\beta - Si_3N_4$', in Micromechanisms of Plasticity and Fracture, ed. Lewis M H & Taplin D M R, S M Publications, University of Waterloo Press, 183 (1983).

11. Kingery W D, J. Am. Cer. Soc., 46, [8], 391 (1963).

12. Jasper C, PhD Thesis, University of Warwick, Coventry (1990).

13. Lewis M H & Lumby R J, Powder Metall., 26, [2], 73 (1983).

14. Richerson D W, Cer. Bull., 52, 560 (1973).

15. Jack K H, Nature, 238, 28 (1972).

16. Oyama, J. Appl. Phys. Jpn., 10, 1637 (1971).

17. Gazza, J. Am. Cer. Soc., Diss. & Notes, 56, 662 (1973).

18. Lewis M H, 'Microstructural Engineering of Ceramics for High Temperature Application', Centre for Advanced Materials Technology, University of Warwick, Coventry (1985).

19. Lewis M H, J. Mat. Sci., 15, 103 (1980).

20. Evans A G & Rana A, Acta. Metallurgica 28,129 (1980).

21. Lewis M H, 'Plasticity and Fracture Mechanisms in Ceramic Alloys Based on $\beta - Si_3N_4$', in Micromechanisms of Plasticity and Fracture, ed. Lewis M H & Taplin D M R, S M Publicatins, University of Waterloo Press, 198 (1983).

22. Evans A G, in Progress in Materials Science, ed. Chalmers, Christian & Massalski, Pergamon Press, 21, 314 (1976).

23. Lewis M H, in Deformation of Ceramics II, ed Tressler, Plenum Press, 605 (1984).

24. Fisher G, Bull. Am. Cer. Soc. 65, [10], 1355 (1986).

25. Garvie R C, 'ZrO_2 and Some of its Binary Systems', in High Temperature Oxides II, ed. Alper A M, Academic Press, (1970).

26. Heuer A H et. al., J. American Cer. Soc., 65, [12], 642 (1982).

27. Miller A R et. al., 'Phase Stability in Plasma Sprayed PSZ-Yttria', in Science and Technology of Zirconia - Advances in Ceramics 3, 241 (1981).

28. Andersson C A & Gupta T K, 'Phase Stability and Transformation Toughening in Zirconia', in Advances in Ceramics 3, 184 (1981).

29. Ce-Wen N, Mat. Sci. & Engineering, B3, [L1-L3] (1989).

30. Morinaga M et. al., J. Phys. Chem. Solids, 44, [4], 301 (1983).

31. Pauling L, 'The Nature of the Chemical Bond', Cornell University Press (1960).

32. Negita K, Acta. Metallurgica, 37, [1], 313 (1989).

33. Virkar A V, J. Am. Cer. Soc., 69, [10], C224 (1986).

34. Toledano J C, J. Solid State Chemistry, 27, 41 (1979).

35. Heuer A H et. al., Acta. Metallurgica, 35, [3], 661 (1987).

36. Andersson C A et. al., 'Diffusionless Transformations in Zirconia Alloys', in Advances in Ceramics 12, 78 (1984).

37. Subbarao E C et. al., Phys. Stat. Solidi (a), 21, 9 (1974).

38. Wolton G M, J. Am. Cer. Soc., 46, 418 (1963).

39. Bain, Trans. AIME, 70, 25 (1925).

40. Ruhle M & Heuer A H, 'Phase Transformations in ZrO_2 - Containing Ceramics: II, The Martensitic Reaction in t-ZrO_2', in Advances in Ceramics, 12, 14-32 (1984).

41. Grain & Garvie, US Bur. *Mines Rep. Invest. No.6619, 19 (1965).*

42. Bansal G K & Heuer A H, Acta. Metallurgica, 20, 1281 (1972).

43. Lange F F, J. Mat. Sci., 17, 225-262 (1982).

44. Olson & Cohen, Met. Trans. AIME A, 7, I-III (1976).

45. Bergman B, J. Mat. Sci. Lett., 4, 1143-1146 (1985).

46. NILCRA-PSZ, Technical Data, Nilcra Ceramics Pty. Ltd., Northcote, Victoria, Australia.

47. Faber K T, 'Microcracking Contributions to the toughness of ZrO_2 - Based Ceramics', in Advances in Ceramics, 12, 293-305 (1984).

48. Claussen N & Ruhle M, 'Design of Transformation-Toughened Ceramics', in Advances in Ceramics, 3, 137-163 (1981).

49. Claussen N, J. Am. Cer. Soc., 59, [1-2], 49-51 (1976).

50. Claussen N, J. Am. Cer. Soc., 65, [11], C190-C91 (1982).

51. McMeeking R M & Evans A G, J. Am. Cer. Soc., 65, [5], 242-246 (1982).

52. Evans A G & Heuer A H, J. Am. Cer. Soc., 63, [5-6], 241-248 (1980).

53. Green et. al. 'Residual Surface Stresses in $Al_2O_3 - ZrO_2$ Composites', in Advances in Ceramics, 12, 240 (1984).

54. Swain M V & Hanninck R H J, in Advances in Fracture Research, 4, ed. D Francis, Pergamon Press, 1559 (1981).

55. Claussen N, 'Microstructural Design of Zirconia - Toughened Ceramics (ZTC)', in Advances in Ceramics, 12, 325-351 (1984).

56. Stevens R & Evans P A, Br. Cer. Trans. & J., 83, 28-31 (1984).

57. Tsukuma K & Shimada M, J. Mat. Sci.., 20, 1178-1184 (1985).

58. Brook R J, 'Preparation & Electrical Behaviour of Zirconia Ceramics', in Advances in Ceramics, 3, 272-285 (1981).

59. Wakai F, Government Industrial Research Institute, Nagoya, Japan.

60. Ruhle M et. al., 'Microstructural studies of Y_2O_3-containing TZP', in Advances in Ceramics, 12, 352-370 (1984).

61. Claussen N, Mat. Sci. & Eng., 71, 23-38 (1985).

62. Dunlop G L, 'Grain Boundaries in High Temperature Deformation', in Micromechanisms of Plasticity and Fracture, ed. M H Lewis & D Taplin.

63. Nakajima et. al., 'Phase Stability of Y-PSZ in Aqueous Solutions', in Advances in Ceramics, 12, 399 (1984).

64. Schubert H et. al., Proc. Br. Cer. Soc., 34, 157 (1984).

65. Sato T & Shimada M, J. Am. Cer. Soc., [10], C212 (1984).

66. Lange F F et. al., 'Structural Ceramic Composites based on $Si_3N_4 - ZrO_2(+Y_2O_3)$ Compositions', J. Mat. Res., 2, [1], 66-76 (1987).

67. Dutta S & Buzek B, J. Am. Cer. Soc., 67, [2], 89-92 (1984).

68. Claussen N, J. Am. Cer. Soc., 59, [1-2], 49-51 (1976).

69. Gazzazara C P & Messier D R, J. Am. Cer. Bull., 56, [9], 777-780 (1977).

70. Evans A G et. al., Br. Cer. Trans. & J., 83, 39-43 (1984).

71. Porter D L & Heuer A H, J. Am. Cer. Soc., 62, 298 (1979).

72. Binner J G P & Stevens R, 'The Measurement of Fracture Toughness by Indentation', Br. Cer. Trans. & J., 83, [6], 168-172 (1984).

73. Lawn B R & Marshall D B, J. Am. Cer. Soc., 62, [7-8], 347 (1979).

74. Evans A G & Charles E A, J. Am. Cer. Soc. Diss. & Notes, 59, [7-8], 371-372 (1976).

75. Wieninger H et. al., J. Mat. Sci., 21, 411-418 (1986).

76. Rose L R F, J. Mat. Sci. Lett., 5, 455-456 (1986).

77. Paterson A W & Stevens R, Int. J. High Tech. Cer., 2 (1986).

78. Bretfeld H et. al., 'Ermittlung des Bruchwiderstandes an Oxidkeramik und Hartmetallen mit verschiedenen Methoden', Z. Werkstofftech., 12, 167-174 (1981).

79. Popp G, PhD Thesis, Stuttgart University, FRG (1982).

80. Simpson J A, J. Am. Cer. Soc., 57, [4], 151-54 (1974).

81. Timoshenko S, in 'Strength of Materials', Von Nostrand Reinhold, New York, PtII, 57 (1958).

82. Brown Jr. W F & Srawley J E, 'Plane Strain Crack Toughness Testing of High-Strength Metallic Materials', Am. Soc. Test. Mater., Spec. Tech. Publ., No.410 (1966).

83. Rice R W & McDonough W J, J. Am. Cer. Soc. Diss. & Notes 58, [5-6], 264 (1975).

84. Claussen N & Jahn J, J. Am. Cer. Soc. Diss. & Notes, 61, [1-2], 94 (1978).

85. Lange F F, J. Am. Cer. Soc., 63, [1-2], 38-40 (1980).

86. Rundgren K & Pompe R, J. de Physique C1, 2, [47], 515-519 (1986).

87. Sanders W A & Mieskowski D M, Adv. Cer. Mat., 1, [2], 166-173 (1986).

88. Weiss J, J. Am. Cer. Soc. Diss. & Notes, 62, [11-12], 632 (1979).

89. Weiss J, J. Mat. Sci., 16, 2997-3005 (1981).

90. Tjernlund A K et. al., 'Sintering & Phase Studies in the System $Si_3N_4 - ZrO_2 - Al_2O_3$', in Advances in Ceramics 24B, 1015-1022 (1988).

91. Tjernlund A K et. al., Brit. Cer. Proc., 37, 29-34 (1986).

92. Gilles J-C, Bull. Chim. Broc. Fr., 2118-2122 (1962).

93. Trigg M B & McCartney E R, J. Am. Cer. Soc., [11], C151 (1981).

94. Deeley G G et. al., Powder Metall., 8, 145 (1961).

95. Claussen N & Jahn J, J. Am. Cer. Soc. Diss. & Notes, 61, [1-2], 95 (1978).

96. Gauckler L J et. al., 'Stability of Si_3N_4 and SiC Based Materials Containing ZrO_2', in Energy and Ceramics, ed. P Vincenzini, Elsevier, Netherlands, 671-679 (1980).

97. Babini G N et. al., Science of Ceramics 12, Ceramurgica, Sri, Faenza, Italy, ed. P Vincenzini, 471-479 (1984).

98. Vincenzini P et. al., Cer. International, 12, 133-145 (1986).

99. Falk L K L et. al., J. Mat. Sci. Lett., 8, 1032-1034 (1989).

100. Claussen N, J. Am. Cer. Soc., 59, [1-2], p.51 (1976).

101. Witek S R & Butler E P, J. Am. Cer. Soc., 69, [7], 523-529 (1986).

102. Lewis M H, 'Plasticity and Fracture Mechanisms in Ceramic Alloys Based on $\beta - Si_3N_4$', in Micromechanisms of Plasticity and Fracture, ed. Lewis M H & Taplin D M R, S M Publicatins, University of Waterloo Press, 218 (1983).

103. Ingel R P et. al., J. Am. Cer. Soc., [10], C150-152 (1982).

104. Rice R W, Cer. Eng. & Sci. Proc., 2, [7-8], 661-701 (1981).

105. Michel D et. al., 'Polydomain Crystals of Single-Phase Tetragonal ZrO_2 : Structure, Microstructure and Fracture Toughness', in Advances in Ceramics, 12, 131-138 (1984).

106. Lankford J, J. Mat. Sci., 21, 1981-1989 (1986).

107. Tsukuma K et. al., 'Thermal & Mechanical Properties of Y_2O_3-Stabilised TZP', in Advances in Ceramics 12, 382-390 (1984).

108. Virkar A V & Matsumoto R L K, 'Toughening Mechanisms in TZP Ceramics', in Advances in Ceramics, 24B, 653-622 (1988).

109. Aizu K, J. Phys. Soc. of Japan, 27, 2 (1969).

110. Reidinger F & Whalen P J, 'Texture on Ground. Fractured and Aged Y-TZP Surfaces', in Advanced Structural Ceramics, ed. Becher, Swain & Somiya, MRS, 78 (1987).

111. Srinivasan G et. al., J. Am. Cer. Soc., 75, [1], 2098-2103 (1989).

112. Smith D K & Newkirk H W, Acta. Cryst., 18, 983-991 (1965).

113. Teufer G, Acta. Cryst., 15, 1187 (1962).

114. Smith D K, J. Am. Cer. Soc., 45, 5 (1962).

115. Evans A G, J. Am. Cer. Soc., 73, [2], 187-206 (1990).

APPENDICES

1. BBC Basic Program for Hot Pressing Data Analysis
2. BBC Basic Program for α/β XRD Ratio Analysis

```
  5ONERROR PROCsetup
 10CLS:MODE128:*SHADOW 1
 15VDU19,0,4,0,0,0
 20DIM dax%(1000),day%(1000),diff(1000)
 30PROCsetup
 40END
 50REM ##################################
100DEFPROCsetup
110REM SET UP MAIN MENU AND SCREEN
120VDU28,50,10,79,0
130*KEY1 PROCdigitise |M
140*KEY2 PROCgetdata |M
150*KEY3 PROCview |M
160*KEY4 PROCviewdump |M
170*KEY5 PROCtodisc |M
175*KEY6 PROCsmoothdiff |M
180PROCscroll
190PRINT"DIGITISER PROGRAM = M G CAIN"
200PRINT"MENU"
210PRINT"New Digitising - F1"
220PRINT"Previous Data - F2"
230PRINT"View - F3"
240PRINT"Screen Dump - F4"
250PRINT"Output Save To Disc - F5"
255PRINT"Smooth Differential - F6"
260PRINT"PLEASE CHOOSE"
280ENDPROC
290REM ####################################
400DEFPROCscroll
410FOR D%=1 TO 30
420VDU23 7 0 0 0 0 0 0 0 0
430NEXT D%
440ENDPROC
450REM #####################################
500DEFPROCdigitise
510PROCscroll
520REM Set up new screen
530PRINT"DIGITISER PROGRAM"
```

```
540PRINT"Press S to start"
560A$=GET$:IF A$<>"S" THEN GOTO 560
570REM START INPUTTING DATA
580X%=ADVAL(2)
590C%=0
600REPEAT
610day%(C%)=ADVAL(1)
620dax%(C%)=ADVAL(2)
630IF dax%(C%)<=X% THEN GOTO 610
640X%=dax%(C%)
650C%=C%+1
660UNTIL C%>1000
661VDU7:PRINT"Working out the differential"
662C%=1
663REPEAT
664diff(C%)=(day%(C%+1)-day%(C%-1))/(dax%(C%+1)-dax%(C%-1))
665C%=C%+1
666UNTIL C%>999
675PROCsetup
680ENDPROC
700REM ######################################
800DEFPROCgetdata
810REM Set up directory and titles
815CLEAR:DIM dax%(1000),day%(1000),diff(1000)
820*DIR
830PROCscroll
840PRINT"DATA RETRIEVAL"
850INPUT"Input title of data ";title$
860title1$=title$+"diff"
870A%=OPENIN title$
880B%=OPENIN title1$
890C%=0
900REPEAT
910INPUT#A%,dax%(C%),day%(C%)
920INPUT#B%,diff(C%)
930C%=C%+1
940UNTIL C%>1000
950CLOSE#A%:CLOSE#B%
```

```
 955PROCsetup
 960ENDPROC
 970REM #######################################
1000DEFPROCview
1010PROCscroll
1020REM Want new menu list
1025CLG
1090REM Set up graphics window
1100VDU24,0;0;1280;768;
1110REM CURRENT DATA
1115MOVE0,0
1120PROCscroll
1125PRINT"VIEW PROGRAM"
1130PRINT"Raw R, Differentiated D or Both B ?"
1140A$=GET$:IF A$="R" THEN GOTO 1240
1145IF A$="B" THEN GOTO 1300
1150REM This is differentiated data
1155MOVE0,0
1160C%=1:REPEAT
1170PLOT5,(dax%(C%-1)+((dax%(C%+1)-dax%(C%-1))/2)-dax%(0))/35,(diff(C%)*100)
1180C%=C%+1
1190UNTIL C%>999
1200REM HOLD GRAPHICS
1210VDU158
1220REM End of this bit - pass control back to main menu
1225PROCsetup
1230ENDPROC
1240REM This is Raw data
1250C%=0:REPEAT:PLOT5,(dax%(C%)-dax%(0))/35,(day%(C%)-day%(0))/40
1260C%=C%+1:UNTIL C%>1000
1270REM HOLD GRAPHICS
1280VDU158
1285PROCsetup
1290ENDPROC
1300REM Draw both
1310C%=0:REPEAT:PLOT5,(dax%(C%)-dax%(0))/35,(day%(C%)-day%(0))/80
1320C%=C%+1:UNTIL C%>1000
1325MOVE0,339
```

```
1330VDU29,0;339;
1340C%=1:REPEAT
1350PLOT5,(dax%(C%-1)+((dax%(C%+1)-dax%(C%-1))/2)-dax%(0))/35,(diff(C%)*50)
1360C%=C%+1
1370UNTIL C%>999
1380REM HOLD GRAPHICS
1390VDU158
1394VDU29,0;0;
1395PROCsetup
1396ENDPROC
1397REM #######################################
1400DEFPROCviewdump
1410PROCscroll
1420INPUT"Input title ";title$
1430REM set up plotter
1440REM Default, black pen, clear interface, vertical speed slow
1450GOSUB 8100
1460N=1:GOSUB 7800
1470GOSUB 9600
1480GOSUB 7100
1481X=25:Y=25:GOSUB8700
1482N=45:GOSUB 7500
1484N=0:GOSUB7400
1485X=100:Y=100:GOSUB 8400
1486 X$=title$:GOSUB 9500
1488GOSUB9800
1489X=0:Y=0:GOSUB 8400
1490C%=0:xchange=2670/1279:ychange=1920/768
1500PRINT"VIEW DUMP TO PLOTTER"
1510PRINT"Raw data R, Differentiated data D or Both B ?"
1520A$=GET$:IF A$="D" THEN GOSUB 1650
1530IF A$="B" THEN GOSUB 1750
1540IF A$<>"R" THEN PROCsetup:ENDPROC
1550REM Thus plot the raw data
1560REPEAT
1570X=(dax%(C%)-dax%(0))/35:Y=(day%(C%)-day%(0))/40
1580X=X*xchange:Y=Y*ychange
1590GOSUB 8000
```

```
1600C%=C%+1
1610UNTIL C%>1000
1620REM Move to rest
1630GOSUB 9700
1635PROCsetup
1640ENDPROC
1650REM PLOT THE DIFFERENTIAL
1660C%=1
1670REPEAT
1680X=(dax%(C%-1)+((dax%(C%+1)-dax%(C%-1))/2)-dax%(0))/35:Y=diff(C%)*100
1690X=X*xchange:Y=Y*ychange
1700GOSUB 8000
1710C%=C%+1
1720UNTIL C%>999
1730GOSUB 9700
1740RETURN
1750REM PLOT BOTH
1760REM 1st plot the raw to half y scale then plot diff half way up
1765C%=0
1770REPEAT
1780X=(dax%(C%)-dax%(0))/35:Y=(day%(C%)-day%(0))/80
1790X=X*xchange:Y=Y*ychange
1800GOSUB 8000
1810C%=C%+1
1820UNTIL C%>1000
1830REM Now move back to zero but half up the Y axis
1840X=0:Y=960:GOSUB 8400:GOSUB8200
1850REM Now plot the diff/2
1860C%=1
1870REPEAT
1880X=(dax%(C%-1)+((dax%(C%+1)-dax%(C%-1))/2)-dax%(0))/35:Y=diff(C%)*50
1890X=X*xchange:Y=Y*ychange
1900GOSUB 8000
1910C%=C%+1
1920UNTIL C%>999
1930GOSUB 8100
1935GOSUB 9700
1940RETURN
```

```
1950REM ########################################
2000DEFPROCtodisc
2010REM SAVE TITLE AND/OR DIFF TO DISC
2020REM MUST KNOW WHAT TO SAVE
2030PROCscroll
2050PRINT"SAVE TO DISC"
2090PRINTTAB(7);"Both data sets"
2095INPUT"Input title ";title$
2096*DIR
2310REM Both
2320title1$=title$+"diff"
2330A%=OPENOUT title$
2340B%=OPENOUT title1$
2350C%=0
2360REPEAT
2370PRINT#A%,dax%(C%),day%(C%)
2380PRINT#B%,diff(C%)
2390C%=C%+1
2400UNTIL C%>1000
2410CLOSE#A%:CLOSE#B%
2420PROCsetup:ENDPROC
2430REM ########################################
3000DEFPROCsmoothdiff
3002PROCscroll
3004PRINT"Smooth Routine"
3007INPUT"Input smoothing level 1-9 ";A%
3009D%=0:PRINT"Please wait a moment"
3010REPEAT
3018C%=1
3020REPEAT
3030diff(C%+1)=(diff(C%)+diff(C%+1)+diff(C%+2))/3
3040diff(C%)=diff(C%+1)
3050C%=C%+2
3060UNTIL C%>998
3063D%=D%+1
3065UNTIL D%>A%
3070REM FINISHED
3080PRINT"Smoothing completed"
```

```
 3090PROCsetup
 3100ENDPROC
 7100 X8$="VS"+STR$(INT(N)):GOTO9900
 7200 X8$="RM"+STR$(INT(N)):GOTO9900
 7300 X8$="EM"+STR$(INT(N)):GOTO9900
 7400 X8$="DI"+STR$(INT(N)):GOTO9900
 7500 X8$="SL"+STR$(INT(N)):GOTO9900
 7600 X8$="VO"+STR$(INT(N)):GOTO9900
 7700 X8$="AM"+STR$(INT(N)):GOTO9900
 7800 X8$="SP"+STR$(INT(N)):GOTO9900
 7900 X8$="LT"+STR$(INT(N)):GOTO9900
 8000 X8$="DA":GOTO9200
 8100 X8$="DF":GOTO9900
 8200 X8$="OR":GOTO9900
 8300 X8$="IF":GOTO9200
 8400 X8$="MA":GOTO9200
 8500 X8$="CA":GOTO9400
 8600 X8$="CR":GOTO9100
 8700 X8$="SI":GOTO9200
 8800 X8$="DR":GOTO9200
 8900 X8$="TL":GOTO9200
 9000 X8$="MR":GOTO9200
 9100 X8$=X8$+STR$(INT(X))+","+STR$(INT(Y))+","+STR$(INT(Z)):GOTO9900
 9200 X8$=X8$+STR$(INT(X))+","+STR$(INT(Y)):GOTO9900
 9300
X8$=X8$+STR$(INT(A))+","+STR$(INT(B))+","+STR$(INT(C))+","+STR$(INT(X()+","+STR$(
 9400
X8$=X8$+STR$(INT(A))+","+STR$(INT(B))+","+STR$(INT(X))+","+STR$(INT(Y))+","+STR$(
 9500 X8$="LA"+X$:GOTO9900
 9600 X8$="CI":GOSUB9900
 9700 X8$="HO":GOTO9900
 9800 X8$="RC":GOTO9900
 9900 VDU2,21:PRINTX8$:VDU6,3
 9910 RETURN
```

```
 5MODE3
 10 CLS
100 ATOT=0:BTOT=0:STOT=0
110 DATA 101,110,200,201,102,210,301
120 DATA 110,200,101,210,111,220
130 DATA 7.5,3.58,2.44,7.44,6.66,6.79,3.13,4.21,10.53,10.9,11.21,26.69,17.56

140 DIM P(13),L(13),H(13),A(13)
150 FOR I=1 TO 13:READ P(I):NEXT I
160 FOR I=1 TO 13:READ L(I):NEXT I
170 PRINT"ENTER ALPHA PEAK HEIGHTS"
180 FORI=1TO7:PRINTP(I);"  ";:INPUTH(I):NEXTI
190 PRINT"ENTER BETA PEAK HEIGHTS"
200 FORI=8TO11:PRINTP(I);"  ";:INPUTH(I):NEXT I
210 PRINT"ENTER SILICON PEAK HEIGHTS"
220 PRINTP(12);"  ";:INPUT H(12)

230 PRINTP(13);"  ";:INPUT H(13)

240 FOR I=1 TO 13
250 A(I)=H(I)/L(I)
260 NEXT I
270 FOR I=1 TO 7
280 ATOT=ATOT+A(I)
290 NEXT I
300 FOR I=8 TO 11
310 BTOT=BTOT+A(I)
320 NEXT I
330 STOT=A(12)+A(13)
340 AAV=ATOT/7
350 BAV=BTOT/4
360 SAV=STOT/2
370 IA1=L(4)*AAV
380 IA2=L(6)*AAV
390 IB=L(11)*BAV
400 IS1=L(12)*SAV
410 IS2=L(13)*SAV
420 RATIO1=IB/(IB+IA2)
```

```
430 RATIO2=IS1/(IS1+IA1)
440 RATIO3=IS2/(IS2+IA2)
450 PRINT"R1 = ";RATIO1
460 PRINT"R2 = ";RATIO2
470 PRINT"R3 = ";RATIO3
500WTFRACBETA=0.40556*(RATIO1^2)+(0.59444*RATIO1)
510PRINT"CORRECTED WEIGHT PERCENTAGE USING QUADRATIC FIT IS ";WTFRACBETA
600 PRINT"MORE (Y/N)"
610 INPUT A$
620 IF A$="Y"THEN RUN
630 END
```